The Texas Medical Center Library

DigitalCommons@TMC

The University of Texas MD Anderson Cancer Center UTHealth Graduate School of Biomedical Sciences Dissertations and Theses (Open Access)

The University of Texas MD Anderson Cancer Center UTHealth Graduate School of Biomedical Sciences

5-2021

The Functional Contribution Of Adaptive Immunity In The Biology Of Pancreatic Cancer And Therapeutic Targeting Of Oncogenic Kras

Krishnan Mahadevan

Follow this and additional works at: https://digitalcommons.library.tmc.edu/utgsbs_dissertations

Part of the Medicine and Health Sciences Commons

Recommended Citation

Mahadevan, Krishnan, "The Functional Contribution Of Adaptive Immunity In The Biology Of Pancreatic Cancer And Therapeutic Targeting Of Oncogenic Kras" (2021). *The University of Texas MD Anderson Cancer Center UTHealth Graduate School of Biomedical Sciences Dissertations and Theses (Open Access)*. 1101.
https://digitalcommons.library.tmc.edu/utgsbs_dissertations/1101

This Dissertation (PhD) is brought to you for free and open access by the The University of Texas MD Anderson Cancer Center UTHealth Graduate School of Biomedical Sciences at DigitalCommons@TMC. It has been accepted for inclusion in The University of Texas MD Anderson Cancer Center UTHealth Graduate School of Biomedical Sciences Dissertations and Theses (Open Access) by an authorized administrator of DigitalCommons@TMC. For more information, please contact digitalcommons@library.tmc.edu.

The Functional Contribution Of Adaptive Immunity In The Biology Of Pancreatic Cancer And Therapeutic Targeting Of Oncogenic Kras

By
Krishnan K. Mahadevan, M.B.B.S*

APPROVED:

_____
Raghu Kalluri, M.D., Ph.D.
Advisory Professor

_____
Huamin Wang, M.D., Ph.D.

_____
Florencia McAllister, M.D.

_____
Jennifer Wargo, M.D.

_____
Robert R. Jenq, M.D.

APPROVED:

_____
Dean, The University of Texas
MD Anderson Cancer Center UTHealth Graduate School of Biomedical Sciences

THE FUNCTIONAL CONTRIBUTION OF ADAPTIVE IMMUNITY IN THE BIOLOGY OF PANCREATIC CANCER AND THERAPEUTIC TARGETING OF ONCOGENIC KRAS

A

DISSERTATION

Presented to Faculty of

The University of Texas

MD Anderson Cancer Center UT Health

Graduate School of Biomedical Sciences

in Partial Fulfillment

of the Requirements

for the Degree of

DOCTOR OF PHILOSOPHY

By

Krishnan K. Mahadevan, M.B.B.S
Houston, Texas

May 2021

Dedication

This thesis work is dedicated to the memory of my late grandfather, Kalyana Sundaram, who always inspires me and believed in my ability to be successful in the academic arena.

Acknowledgements

I feel deeply thankful for the guidance and support of several people throughout my graduate study. First, I am very grateful and lucky to be mentored by Dr. Raghu Kalluri. Dr. Kalluri has been a tremendous source of inspiration to me as a scientist, innovator and entrepreneur. When I joined the Kalluri lab family in March 2016, he put me under rigorous training with the most productive members of his scientific team. The amount of resources that he spent on my projects were staggeringly colossal, without which such elaborate disease models would have been impossible to generate and maintain. The patience and support that I received from him during failed experiments and negative results is something that I will never forget. Despite his busy schedule, I am also extremely appreciative of the time Dr. Kalluri invested in me for review of experiments, data analysis and mentoring me to scientifically think to develop experiments that would take the project to new heights. These years under his mentorship have not only made me a better scientist, but also instilled in me team-spirit, the importance of dedicated effort and collaboration.

Next, I would like to thank Dr. Hikaru Sugimoto for his invaluable help with animal experiments, histological analysis and data interpretation. I am extremely grateful to Dr. Valerie LeBleu for her encouragement and mentoring me with data review, manuscript writing and intellectual inputs for my project. The scientific rigor and dedication to precision are qualities in her that I would like to emulate as a scientist.

My advisory committee, consisting of Dr. Huamin Wang, Dr. Andrew Rhim, Dr. Jennifer Wargo, Dr. Florencia McAllister and Dr. Robert Jenq has constantly been a source of support, information and inspiration. Their ability to propose innovative ideas, and vett my research during committee meetings is a major reason for the progression of my project. Despite incredibly busy schedules, they always set aside time to talk with me and guide me, something that I consider extremely valuable. The variety of fields they specialize in, has helped me develop into the all-round scientist. I am also extremely appreciative of Dr. Robert Jenq and his lab members, Dr. Chia-Chi Chang and Dr. Mohammad Jamal in particular for collaboration with microbiome project.

I would like to thank Dr. Elena Ramirez in particular, from the LeBleu lab and Kalluri lab for her collaboration and help with flow cytometry and data analysis. I'm also extremely appreciative of all the people that have helped me with my PhD project, in particular Sujuan Yang, Dr. Xiaofeng Zheng, Dr. Yang Chen, Dr. Julienne Carstens, Lisa Becker, Dr. Sushrut Kamekar, Lisa Norberg, Michelle Kirtley, Dr. Mayela Mendt, Dr. Olga Volpert and Patricia Philip. I would also like to thank Dr. Adrienne Duran, Martha Taghavi and Vivien Tran for help with *in vivo* imaging and animal care.

My friends, Alex Li, Deevakar and Rumi Lee have always been a source of immense support throughout these years of my graduate study. Finally, I thank my loving wife and parents for their caring support, encouragement and motivation. Without them, it would not have been possible to overcome the challenges of the graduate school experience.

Table of contents

Approvals page i

Title page ii

Dedication iii

Acknowledgements iv

Table of contents vi

Abstract 1

Chapter 1: **Background and significance** 4

Pancreatic cancer disease burden and mortality 5

Pancreatic cancer - risk factors and disease staging 7

Genetic alterations in pancreatic cancer 9

Acinar to ductal metaplasia and pancreatic intraepithelial neoplasia 12

Current therapies in pancreatic cancer 12

T cells and myeloid cells in the pancreatic tumor microenvironment 14

Kras* in the pancreatic tumor microenvironment 18

Kras* targeting using iExosomes 18

Factors affecting T cell function in the pancreatic tumor

Microenvironment i) Microbiome 19

ii) Pancreatitis 21

Chapter 2: **Material and methods** 23

Animal studies i) PiKP and PiKT mice 24

ii) KPC CD4$^{-/-}$ and KPC CD8$^{-/-}$ mice _____24

iii) Microbiome experiments _____25

Tissue processing _____26

Immunotyping _____26

Immunofluorescence _____30

Immunohistochemistry_____32

Cell lines_____34

Pancreatic enzyme assays_____34

16S rRNA gene sequencing and bioinformatics analysis_____34

Statistics _____35

Results_____36

Chapter 3: **Kras* drives a T cell deficient and myeloproliferative PDAC TME** _____37

i) Kras* is required for progression and maintenance of PDAC tumors _____37

ii) Kras* represses T cells and promotes myeloid infiltration in PiKP mice _____41

iii) Kras* represses T cells and promotes myeloid infiltration in PiKT mice _____43

Chapter 4: **CD4$^+$ T cells impede the therapeutic efficacy of Kras* targeting in PDAC** _____45

i) CD4$^+$ and CD8$^+$ T cells do not alter primary tumor growth or survival, but CD4$^+$T cells promote metastasis in PDAC _____45

ii) iExosomes targeting Kras* increase T cell infiltration in PDAC _____48

iii) CD4$^+$ T cells impede the therapeutic efficacy of

iExosomes in PDAC _____49

Chapter 5: **The gut microbiome co-operates with CD4$^+$ T cells to impede Kras* targeting in PDAC** _____53

Chapter 6: **CD4$^+$ T cells promote tumorigenesis in KC mice with pancreatitis but has not impact on spontaneously developing tumors**_____57

i) CD4$^+$ T cells promote tumorigenesis in KC mice with acute pancreatitis_____57

ii) CD4$^+$ T cells promote tumorigenesis in KC mice with chronic pancreatitis_____60

iii) Kras* protects the pancreas against acute pancreatic injury_____61

Chapter 7: **CD4$^+$ T cells regulate dendritic cells to facilitate pancreatic tumorigenesis in mice with pancreatitis**_____64

1. i) Pancreatitis recruits CD11c$^+$ dendritic cells to the PDAC TME _____64

2. ii) CD4$^+$ T cells regulate dendritic cells to drive tumor initiation in mice with acute pancreatitis _____66

3. iii) Pancreatitis renders the pancreatic TME sensitive to Checkpoint blockade_____67

Summary of results _____69

Chapter 8: **Discussion** _____71

Role of Kras in shaping the PDAC TME* _____71

*Role of CD4$^+$ T cells in PDAC progression*_____72

Adaptive immune response and gut microbiome in Kras targeting therapy* _____74

Impact of pancreatitis on adaptive immune response in PDAC _____75

*Role of dendritic cells in sensitizing the PDAC TME to immunotherapy*____77

Conclusion _____77

Bibliography _____78

VITA_____91

List of Illustrations

Fig. 1: Pancreatic cancer – Disease burden and mortality_____6

Fig. 2: Pancreatic cancer – risk factors and disease staging_____8

Fig. 3: Principle genetic alterations in pancreatic ductal adenocarcinoma _____11

Fig. 4: Current therapies in pancreatic cancer _____14

Fig. 5: T cells and myeloid cells in the pancreatic tumor microenvironment_____17

Table 1a: Antibodies used for flow cytometry _____27

Table 1b: Phenotyping of cells in flow cytometry analysis_____29

Table 2a: T cell panel TSA staining _____31

Table 2b: Phenotyping of cells in TSA analysis_____31

Table 3: Immunohistochemistry_____33

R Fig. 1: Kras* is required for progression and maintenance of PDAC tumors ____38

R Fig. 2: Histopathology of PiKT and PiKP GEMMs _____40

R Fig. 3: Kras* represses T cells and promotes myeloid infiltration in PiKP tumors __42

R Fig. 4: Kras* represses T cells and promotes myeloid infiltration in PiKT tumors __44

R Fig. 5: KPC CD4$^{-/-}$ and KPC CD8$^{-/-}$ mice lack respective T cell populations in

the tumor and lymphoid organs _____46

R Fig. 6: $CD4^+$ and $CD8^+$ T cells do not alter primary tumor growth or survival, but $CD4^+$ T cells promote metastasis in PDAC _____47

R Fig. 7: iExosomes targeting Kras* increases T cell infiltration in PDAC _____49

R Fig. 8: $CD4^+$ T cells impede the therapeutic effects of iExosomes in PDAC _____51

R Fig. 9. Kaplan-Meier survival curves of KPC, KPC $CD4^{-/-}$ and KPC $CD8^{-/-}$ mice treated with iExosomes _____52

R Fig. 10: The gut microbiome co-operates with $CD4^+$ T cells to impede Kras* targeting in PDAC _____55

R Fig. 11: Baseline radiance and microbiome composition of B6 and $CD4^{-/-}$ mice treated with antibiotics _____56

R Fig. 12: $CD4^+$ T cells promote tumorigenesis in KC mice with acute pancreatitis _____59

R Fig. 13: $CD4^+$ T cells promote tumorigenesis in KC mice with chronic pancreatitis _____61

R Fig. 14: Kras* protects the pancreas against acute pancreatic injury _____63

R Fig. 15: Pancreatitis recruits activated dendritic cells to the tumor microenvironment _____65

R Fig. 16: $CD4^+$ T cells regulate dendritic cells to drive tumor initiation in mice with underlying pancreatitis _____67

R Fig. 17: Pancreatitis renders the pancreatic TME sensitive to checkpoint blockade. _____68

The Functional Contribution Of Adaptive Immunity In The Biology Of Pancreatic Cancer And Therapeutic Targeting Of Oncogenic Kras

Krishnan K. Mahadevan M.B.B.S*

Advisory professor: Dr. Raghu Kalluri

Pancreatic ductal adenocarcinoma (PDAC) is the third leading cause of cancer related deaths in the USA(https://seer.cancer.gov/statfacts/html/pancreas.html), whereby survival remains poor despite advances in surgical technique and new combination chemotherapies. Immune checkpoint blockade has revolutionized the treatment of cancers such as melanoma, bladder cancer and non-small cell lung carcinomas. Unfortunately, PDAC is among the tumor types that remain refractory to checkpoint immunotherapy(Royal et al., 2010, Le et al., 2013), with no survival benefits in clinical trials and pre-clinical animal models of PDAC(Winograd et al., 2015). Failure to respond to checkpoint blockade is frequently attributed to an immunosuppressive tumor microenvironment (TME), low neo-epitope burden and lack of tumor infiltrating T cells resulting from a desmoplastic stroma(McAllister et al., 2014, Zhang et al., 2014). However, the molecular underpinnings of immunosuppression in PDAC remain poorly understood.

Oncogenic Kras (Kras*, $Kras^{G12D}$ and other mutations), a key driver of PDAC is thought to play an important role in creating an immunosuppressive TME(Zhang et al., 2014, McAllister et al., 2014); however, its precise function in shaping the immune landscape of PDAC remains elusive. There is no clear understanding of the functional contribution of T cells and the nodes of regulation of immune infiltration in PDAC. In order to exploit the full potential of the immune system to treat PDAC, it is urgent to generate *in vivo* models that enables us functionally probe the role of oncogenic Kras in shaping

the TME with an inducible and pancreas specific model expressing Kras*. We demonstrate that Kras* contributed to a T cell deficient and myeloprofilerative TME in PDAC. Next, we generate models that closely mimic human PDAC and allow depletion of specific T cell subsets (CD4 and $CD8^+$ T cells). Such models offer a unique modality to interrogate the role of specific T cell subsets in PDAC progression and inform the development of effective immunotherapy approaches for PDAC. We employ a Kras* targeting agent (iExosomes) in the T cell depletion models to demonstrate that combination of Kras* and $CD4^+$ T cell targeting strategies resulted in robust tumor growth inhibitory response. Further, we show how the gut microbiome modulates T cell responses in the context of Kras* targeting in PDAC.

In the second part of our study, we determine how the presence of pancreatitis alters the TME and the course of progression of PDAC. A significant portion of PDAC patients have been reported to present with underlying chronic pancreatitis and bile duct obstruction. However, current therapeutic strategies do not consider the influence of chronic pancreatitis while stratifying PDAC patients in clinical trials. The presence of chronic inflammation in a cancer setting could recruit a unique immune signature to the TME and open new possibilities for immune modulation in these PDAC patients. Therefore, we investigate how pancreatitis impacts tumor progression and modulates the immune landscape of the PDAC microenvironment. We demonstrate that pancreatitis accelerates tumorigenesis in mice with Kras* mutant pancreas and recruits activated dendritic cells to the tumor microenvironment. However, $CD4^+$ T cells promote pancreatic tumorigenesis in mice with pancreatitis by regulating dendritic cells in the TME. Further, we demonstrate that presence of pancreatitis sensitizes the pancreatic immune microenvironment to checkpoint blockade.

Overall, our study offers novel mechanistic insights into how Kras* modulates the immune microenvironment and unravels potential therapeutic windows to synergize Kras* and $CD4^+$ T cell targeting approaches. Further, our study offers insights into how presence of pancreatitis alters immune microenvironment, suggesting stratification of a cohort of patients in clinical trials that could potentially benefit from immunotherapy approaches.

Chapter 1

Background and significance

Pancreatic cancer – Disease burden and mortality

Pancreatic cancer has surpassed colorectal cancer and is the third leading cause of cancer related deaths in the USA. Survival remains poor despite advances in surgical technique and new combination chemotherapies. Over the past 25 years (1992-2017), while the incidence and death rate of cancers overall have plummeted, pancreatic cancer continues to be on the rise despite progresses made in early detection and prevention of pancreatic cancer. While the incidence of cancers overall decreased by 84.5 persons per 100,000, pancreatic cancer incidence has increased by 1.3 persons per 100,000 over 25 years **(Fig. 1a)**. Similarly, the death rate due to cancers overall decreased by 60.9 persons per 100,000, whereas in pancreatic cancers the death rate has marginally increased by 0.4 persons per 100,000 people during the same period **(Fig. 1a)**. Pancreatic cancer is usually a disease of the elderly with maximum number of patients diagnosed between 65-74 years of age, with a median age of 70 years. At diagnosis, more than half of the patients (52%) have advanced metastatic disease and 30% of patients have regional spread to lymph nodes **(Fig. 1b**), indicating the aggressive and highly metastatic nature of the disease. Therefore, the five- year survival rate in pancreatic cancer remains at a dismal 10%.

Histologically, the pancreas is composed of an exocrine part with acinar cells secreting digestive enzymes and an endocrine part which secretes hormones such as insulin and glucagon. Most of the cancers arise from the exocrine pancreas (nearly 85%)(Hruban and Fukushima, 2007). Pancreatic ductal adenocarcinoma (PDAC) represent the majority of the tumors arising from the pancreatic acini **(Fig. 1c)**. This is the form of cancer that is commonly referred to as ‘Pancreatic cancer’ ubiquitously and henceforth in this manuscript. Other common exocrine pancreatic tumors include, acinar

cell carcinomas, colloid carcinomas, serous cystadenomas and undifferentiated carcinomas(Hruban and Fukushima, 2007). Tumors arising from the pancreatic islets are referred to as neuro-endocrine tumors, which account for 1-5% of the total pancreatic neoplasms.

Figure 1

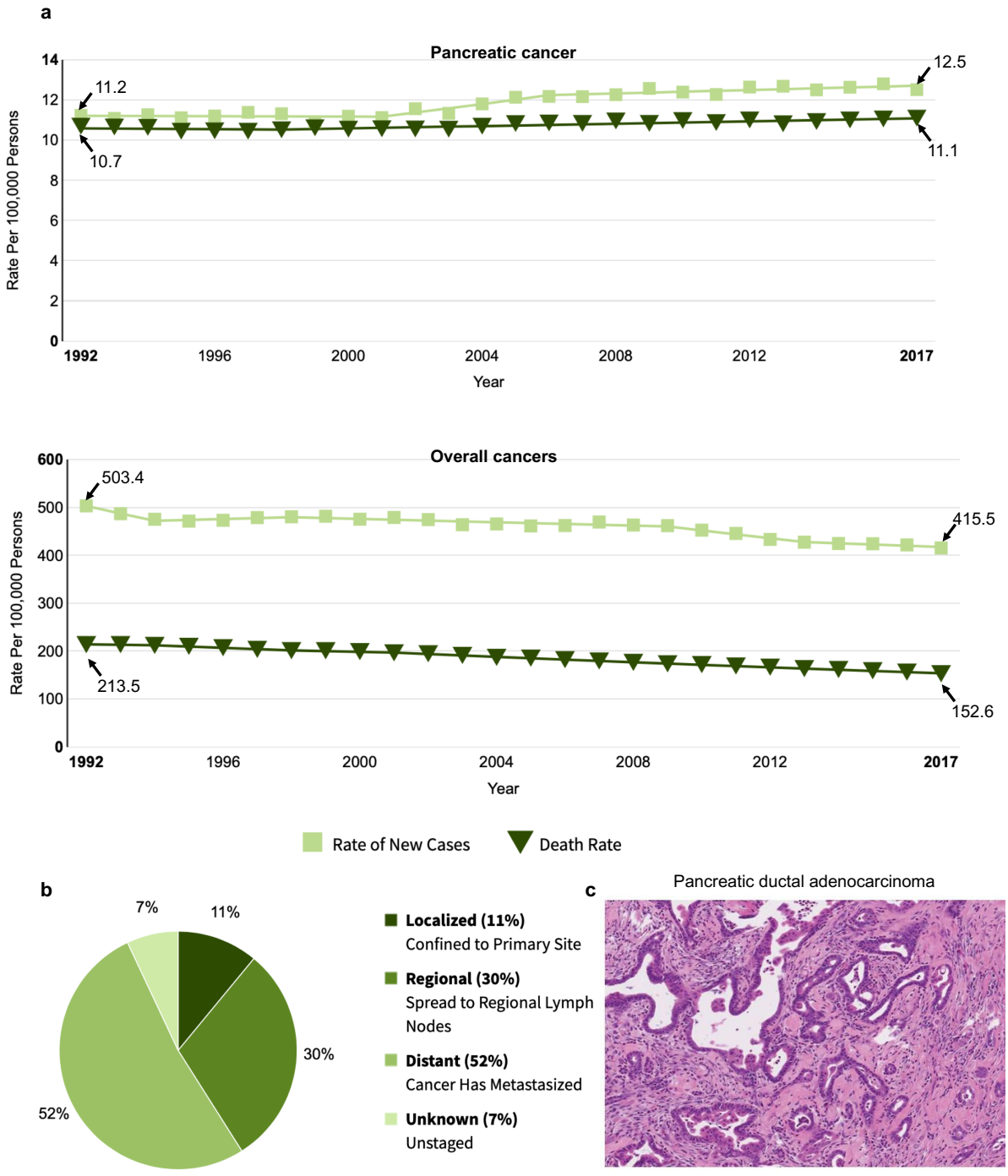

Fig. 1: Pancreatic cancer – Disease burden and mortality
(a) Overall cancers Vs. pancreatic cancer incidence and death rate; 25 year statistics. **(b)** PDAC disease spread and metastasis at diagnosis. **(c)** Representative hematoxylin and eosin (H&E) stained micrograph of PDAC. Fig. 1 - *Reproduced with permission from* https://seer.cancer.gov).

Pancreatic cancer – risk factors and disease staging

Among the various known risk factors for PDAC, patients with a known family history of PDAC with germline mutations such as Familial atypical multiple mole melanoma (FAMM) and Peutz Jeghers syndrome carry the highest risk for PDAC(Stoffel et al., 2019) **(Fig. 2a)**. Other familial diseases that increase the risk of PDAC are tabulated in Fig. 2a. Tobacco use and smoking are associated with a higher risk of PDAC (2.5 to 3.6 times more that in non-smokers)(Ryan et al., 2014, Stoffel et al., 2019). Obesity, underlying pancreatitis and diabetes mellitus are other important morbidities that are associated with an increased risk of developing PDAC(Ryan et al., 2014). The other factors that do not have a clear association with increased risk of developing PDAC include high-fat diet intake, coffee intake, alcohol consumption, H.pylori and Hepatitis B infections. According to the modified 8th edition of the American Joint Committee of Cancer (AJCC), TNM (Tumor-Node-Metastasis) staging classification has staged pancreatic cancer into four main stages(Allen et al., 2017), based on tumor size, resectability, loco-regional spread to lymph nodes, superior mesenteric artery or celiac axis and distant metastasis to the liver or lungs **(Fig. 2b-c)**.

Figure 2

a

TABLE 1. Genes Associated With Increased Risk for Pancreatic Cancer

Gene	Syndrome	Pancreatic Cancer Risk (%)	Other Associated Cancers*
APC	Familial adenomatous polyposis	1-5	Colorectal, upper GI, thyroid, brain
ATM	Ataxia telangiectasia (biallelic)†	1-5	Breast, prostate, gastric
BRCA2	Hereditary breast ovarian cancer syndrome	5-10	Breast, ovary, prostate, melanoma
BRCA1	Hereditary breast ovarian cancer syndrome	2	Breast, ovary, prostate, melanoma
CDKN2A	Familial atypical multiple mole melanoma (FAMMM)	10-30	Melanoma
MLH1, MSH2, MSH6, PMS2, EPCAM	Lynch syndrome	5-10	Colorectal, uterine, upper GI, ovary, urinary tract, brain, sebaceous neoplasms
PALB2		5-10	Breast, prostate
STK11	Peutz Jeghers syndrome	10-30	Breast, colorectal, upper GI, lung, reproductive tract
TP53	Li Fraumeni syndrome	Not defined	Breast, brain, sarcoma, adrenocortical carcinoma

b

TNM stage	Description
T-stage	
Tis	Carcinoma in situ
T1	Tumour <2 cm and limited to pancreas
T2	Tumour >2 cm and limited to pancreas
T3	Tumour extends beyond pancreas but no involvement of coeliac axis or SMA
T4	Tumour involves the coeliac axis or SMA
N-stage	
N0	Regional lymph nodes not involved
N1	Regional lymph nodes involved
M-stage	
M0	No distant metastases
M1	Distant metastases present

M, metastases; N, nodes; SMA, superior mesenteric artery; T, tumour.

STAGE			
Stage IA	T1	N0	M0
Stage IB	T2	N0	M0
Stage IIA	T3	N0	M0
Stage IIB	T1–T3	N1	M0
Stage 3	Any T	N2	M0
	T4	Any N	M0
Stage 4	Any T	Any N	M1

c

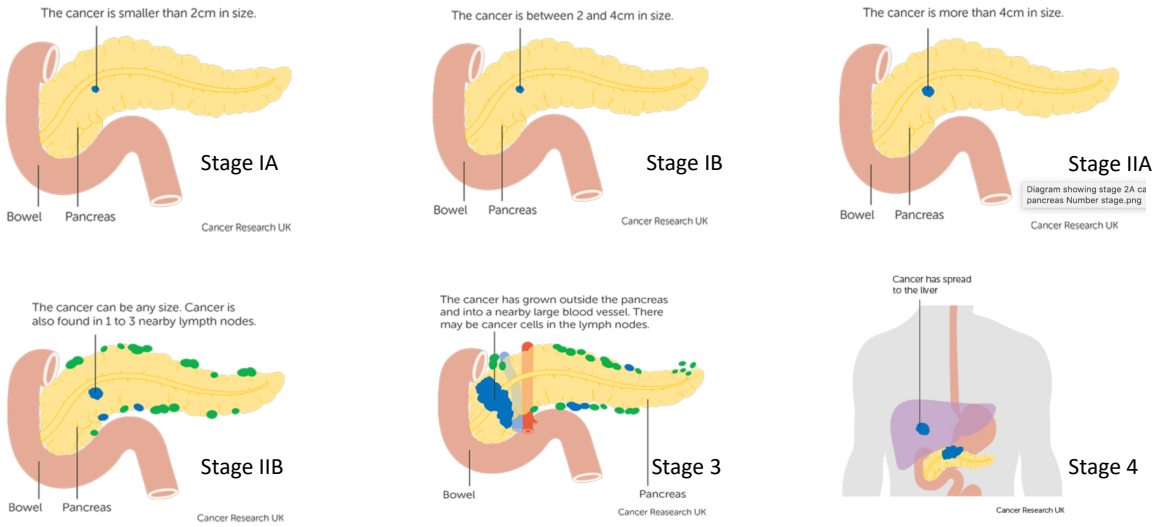

Fig. 2: Pancreatic cancer – risk factors and disease staging

(a) Genes associated with increased risk for developing PDAC - *Reproduced with permission from (Stoffel EM, McKernin SE, Brand R, Canto M, Goggins M, Moravek C, et al. Evaluating Susceptibility to Pancreatic Cancer: ASCO Provisional Clinical Opinion. J Clin Oncol 2019;37(2):153-64 doi 10.1200/JCO.18.01489)*. **(b)** AJCC modifed 8th edition for staging of PDAC – *Reproduced with permission from (Allen PJ, Kuk D, Castillo CF, Basturk O, Wolfgang CL, Cameron JL, et al. Multi-institutional Validation Study of the American Joint Commission on Cancer (8th Edition) Changes for T and N Staging in Patients With Pancreatic Adenocarcinoma. Ann Surg 2017;265(1):185-91 doi 10.1097/SLA.0000000000001763).* **(c)** Schematic representation of stages of spread of PDAC – *Reproduced with permission from (https://www.cancerresearchuk.org/about-cancer/pancreatic-cancer/stages-types-grades/tnm-staging)*

Genetic alterations in pancreatic cancer

Sequencing for genetic alterations from TCGA database revealed that PDAC is invariably associated with mutations in Kras, $Kras^{G12D}$ mutation being the most common (83% of PDACs, **Fig. 3**). Other genes in PDAC that are mutated include TP53, SMAD4, TTN, CDKN2A and MUC16 in decreasing order of their frequencies (Fig. 3). $Kras^{G12D}$ (Kras* or oncogenic Kras) mutation, which represents the principle driver mutation, is required for both the initiation and maintenance of PDAC(Collins et al., 2012). Multiple studies in PDAC have demonstrated that PDAC that developed in the presence of Kras* regress completely when the oncogenic signal is extinguished, suggesting that Kras* is critical for the survival of the cancer cells(Collins et al., 2012, Ying et al., 2012). In multiple murine studies, mutations in tumor suppressors such as TP53, SMAD4 and CDKN2A have shown to accelerate pancreatic carcinogenesis but were unable to initiate or maintain tumors in the absence of Kras* (Bardeesy et al., 2006, Hingorani et al., 2005, Aguirre et al., 2003). Kras* signaling reprograms pancreatic acinar cells into ductal lineage and progresses through pre-neoplastic and invasive PDAC stages (Bardeesy et al., 2006, Hingorani et al., 2005, Aguirre et al., 2003). Pancreatic cancer in humans progresses through two stages; an initial preinvasive phase and subsequently into invasive PDAC phase. The preinvasive lesions of pancreatic cancer include mucinous cystic neoplasms (MCNs), intraductal papillary mucinous neoplasms (IPMNs) and

pancreatic intraepithelial neoplasia (PanINs). Although Kras* is indispensable for tumor initiation, tumor latency and differentiation depend on mutations in tumor suppressor genes, suggesting that the evolution of PDAC is predicated on alterations in signaling pathways.

Figure 3

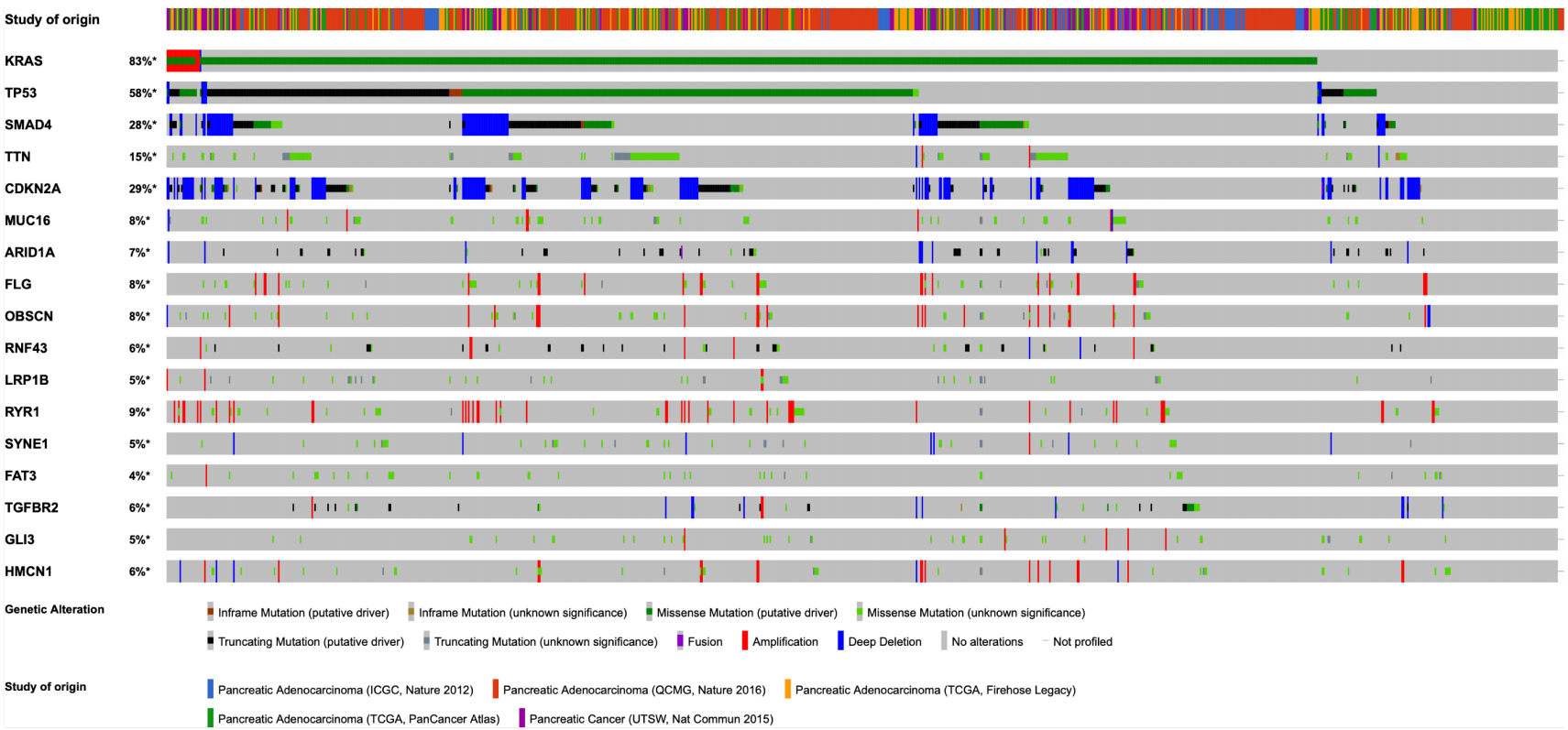

Fig.3: Principle genetic alterations in pancreatic ductal adenocarcinoma. *Analysis of key genetic mutations, mutational type and significance from* https://www.cbioportal.org. Patients from five datasets (*Pancreatic ductal adenocarcinoma – ICGC-Nature 2012, QCMG-Nature 2016, TCGA Firehose Legacy, TCGA PanCancer Atlas and UTSW-Nat Commun 2015*) were analyzed.

Acinar-Ductal metaplasia and Pancreatic intra-epithelial neoplasia: Pancreatic acini differentiate into ductal lineage and transform into duct like cells under environmental and genetic pressures(Takaori et al., 2004). This is a reversible process and the pancreatic epithelium returns to its normal, functional state when the factors causing injury to the pancreatic epithelium are removed(Pour et al., 2003). The process where one epithelial cell type changes to another as an adaptive response to injury is known as metaplasia. In the pancreas, injury to the pancreatic epithelium usually results from alcohol intake, smoking, obstruction of the hepato-pancreatic duct due to gallstones, all of these result in pancreatitis (an inflammatory condition of the pancreatic acini). To escape, the pancreatic acini differentiate into duct like cells and become resistant to the agents causing injury, a process known as acinar-ductal metaplasia (ADM)(Pour et al., 2003). However, in the face of sustained insult to the pancreatic acini, ADM progresses to pancreatic intra-epithelial neoplasia. Chronic pancreatitis is frequently associated with ADM and poses a significant risk factor for the development of PDAC(Wei et al., 2016). Murine pancreatic cancer studies demonstrate that although chronic pancreatitis accelerates the development of PDAC(Wei et al., 2016), concomitant pancreatitis was not required for the development of PanINs or PDAC(Habbe et al., 2008). One study that analyzed the role of inflammation in PDAC demonstrated that in the absence of TP53, chronic pancreatitis led to development of other lineages of pancreatic tumors such as acinar cell carcinoma, neuro-endocrine tumors and rarely PDAC(Swidnicka-Siergiejko et al., 2017).

Current therapies in pancreatic cancer:

Among patients diagnosed with pancreatic cancer, ~20% of the patients are eligible for surgical resection as many of the patients are at an advanced stage at the time of

diagnosis(Kamerkar et al., 2017). The common surgeries for pancreatic cancer include Whipple procedure (pancreaticoduodenctomy), distal pancreatectomy or complete pancreatectomy (all of which involve removing some or all portions of the pancreas). In many cases, pancreatic cancer surgeries are palliative in nature, which relieve symptoms such as pain, nausea/vomiting and jaundice due to PDAC obstructing the surrounding structures such as the duodenum or bile duct(Kamerkar et al., 2017). Among the chemotherapeutic agents used in the treatment of PDAC, 5-Fluorouracil (5-FU) was one of the early reagents used along with radiation therapy in patients that underwent resection(Neoptolemos et al., 2004). 5-Fluorouracil as a single agent improved the overall survival (median) of resected PDAC patients from 15.5 months (No chemotherapy group) to 20.1 months (with 5-FU) **(Fig. 4a)** (Neoptolemos et al., 2004). Further studies in pancreatic cancer demonstrate that in resectable PDAC, Gemcitabine (35 months) and FOLFIRINOX (54.4 months) (5-FU, Irinotecan, oxaliplatin and folinic acid) remain the standard for treatment of PDAC **(Fig. 4b)**(Conroy et al., 2018). In metastatic pancreatic cancer, Gemcitabine with nab-Paclitaxel improved overall survival of PDAC by 1.8 months, whereas FOLFIRINOX regimen improved the overall survival by 4.3 months **(Fig. 4c-d)** (Von Hoff et al., 2013, Conroy et al., 2018, Conroy et al., 2011). Overall, gemcitabine and FOLFIRINOX regimens only marginally improves survival of metastatic adenocarcinomas, which constitute the majority of the PDAC (> 52% of cancers at presentation).

Figure 4

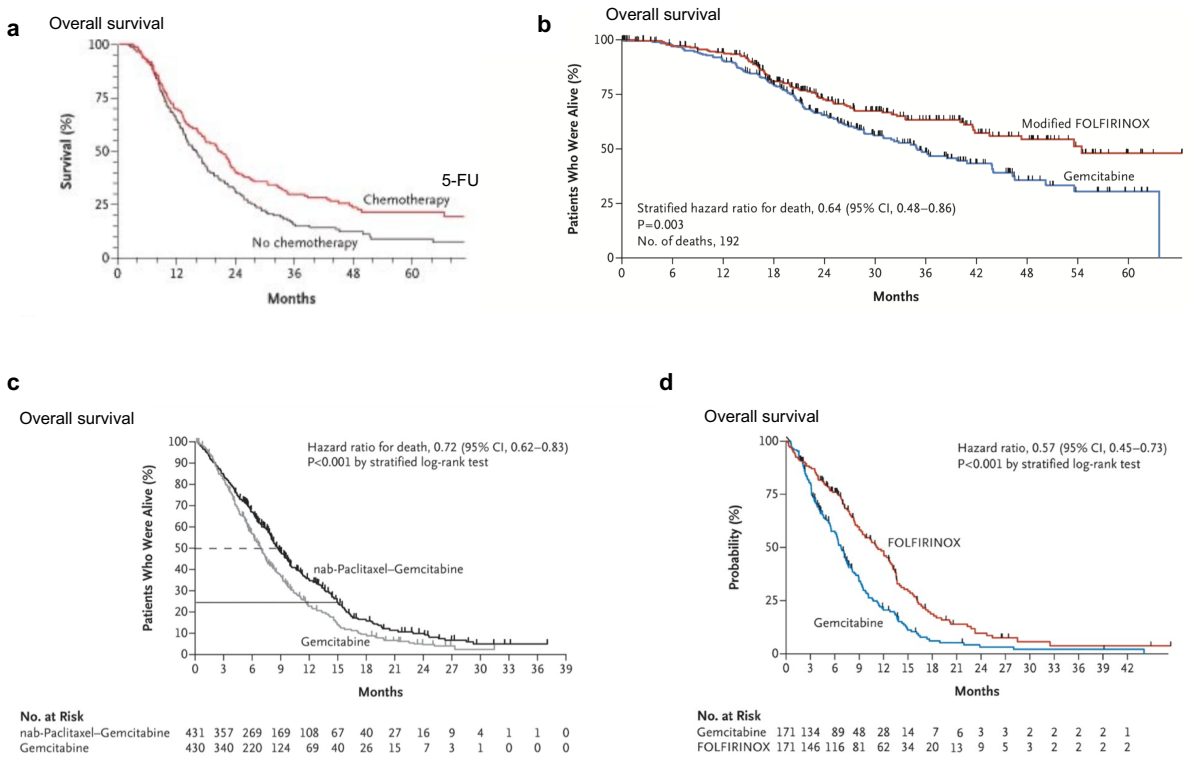

Fig. 4: Current therapies in pancreatic cancer. (a-d) Kaplan-Meier survival curves depicting overall survival of PDAC patients in clinical trials. **(a-b)** Overall survival of resectable PDAC patients – Reproduced with permission from **(a)** *(Neoptolemos JP, Stocken DD, Friess H, Bassi C, Dunn JA, Hickey H, et al. A randomized trial of chemoradiotherapy and chemotherapy after resection of pancreatic cancer. N Engl J Med 2004;350(12):1200-10 doi 10.1056/NEJMoa032295).* **(b)** *(Conroy T, Hammel P, Hebbar M, Ben Abdelghani M, Wei AC, Raoul JL, et al. FOLFIRINOX or Gemcitabine as Adjuvant Therapy for Pancreatic Cancer. N Engl J Med 2018;379(25):2395-406 doi 10.1056/NEJMoa1809775).* **(c-d)** Overall survival of metastatic PDAC patients – Reproduced with permission from **(c)***(Von Hoff DD, Ervin T, Arena FP, Chiorean EG, Infante J, Moore M, et al. Increased survival in pancreatic cancer with nab-paclitaxel plus gemcitabine. N Engl J Med 2013;369(18):1691-703 doi 10.1056/NEJMoa1304369).* **(d)** *(Conroy T, Desseigne F, Ychou M, Bouche O, Guimbaud R, Becouarn Y, et al. FOLFIRINOX versus gemcitabine for metastatic pancreatic cancer. N Engl J Med 2011;364(19):1817-25 doi 10.1056/NEJMoa1011923).*

T cells and myeloid cells in the pancreatic tumor microenvironment

Checkpoint immunotherapy has revolutionized the treatment of cancers such as melanoma, bladder cancer and lymphomas(Hodi et al., 2010, Lamm et al., 1991). However, PDAC remains refractory to checkpoint immunotherapy(Royal et al., 2010, Le

et al., 2013), with no survival benefits in clinical trials and pre-clinical animal models(Winograd et al., 2015). This prompted a comparison of immune infiltrates in the TME of PDAC and melanoma. One study found that the pancreatic TME had minimal to moderate infiltration of T cells and that these infiltrates were primarily in the stromal area and excluded from the tumoral area compared with melanoma, where the T cells were predominantly in the tumoral area(Blando et al., 2019). Failure to respond to immune checkpoint blockade has also been attributed to an immunosuppressive tumor microenvironment (TME), low neo-epitope burden, and lack of tumor infiltrating T cells resulting from a desmoplastic stroma(Evans et al., 2016, Olive et al., 2009). Although PDAC is considered an immunologically 'cold' tumor with minimal T cell infiltration(Evans et al., 2016), spatial distribution analyses of T cells within human PDAC tumors reveal that proximity of $CD8^+$ cytotoxic lymphocytes (CTLs) to the tumor cells correlate with improved patient survival(Carstens et al., 2017, Blando et al., 2019).

T- cells in PDAC can be broadly divided into either pro-tumorigenic or anti-tumorigenic T cells based on their functional role in the progression of PDAC. Studies on the role of innate T cells in PDAC demonstrate that $\gamma\delta$ T cells support pancreatic oncogenesis and tumor progression by restraining the adaptive $\alpha\beta$ T cell response(Daley et al., 2016). The authors further show that the $\gamma\delta$ T cells create an immune suppressive TME by checkpoint receptor (PDL-1) ligation in tumor infiltrating $\alpha\beta$ T cells(Daley et al., 2016). Subsequently, a study that explored the role of $CD4^+$ T cells in PDAC initiation demonstrated that ablation of $CD4^+$ lymphocytes prevents the pancreatic carcinogenesis in caerulein-induced PDAC models **(Fig. 5a)**(Zhang et al., 2014, McAllister et al., 2014). In another study that utilize orthotopic pancreatic cancer model, T regs, a subset of $CD4^+$ T cells have been shown to promote tumor progression by suppressing the function of

antigen presenting dendritic cells in pancreatic cancer(Jang et al., 2017). While these studies support a tumor-promoting role of $CD4^+$ and $\gamma\delta$ T cells in PDAC, ablation of specific T cell populations in mice also showed to have no impact on PDAC progression(Evans et al., 2016). The myeloid cells constitute a substantial portion of the dense, fibrotic stroma in PDAC. Depletion of myeloid cells resulted in an anti-tumor T cell response and inhibition of pancreatic tumorigenesis **(Fig. 5b)**(Zhang et al., 2017). Myeloid cells inhibit cytotoxic lymphocytes by inducing the expression of PD-L1 on cancer cells thereby masking anti-tumor immune response. Another study specifically probing the role of myeloid derived suppressor cells (MDSCs) in PDAC demonstrated that a specific subset of myeloid cells viz. Gr- MDSCs inhibit cytotoxic lymphocytes in

these mice(Zhang et al., 2017).

Figure 5

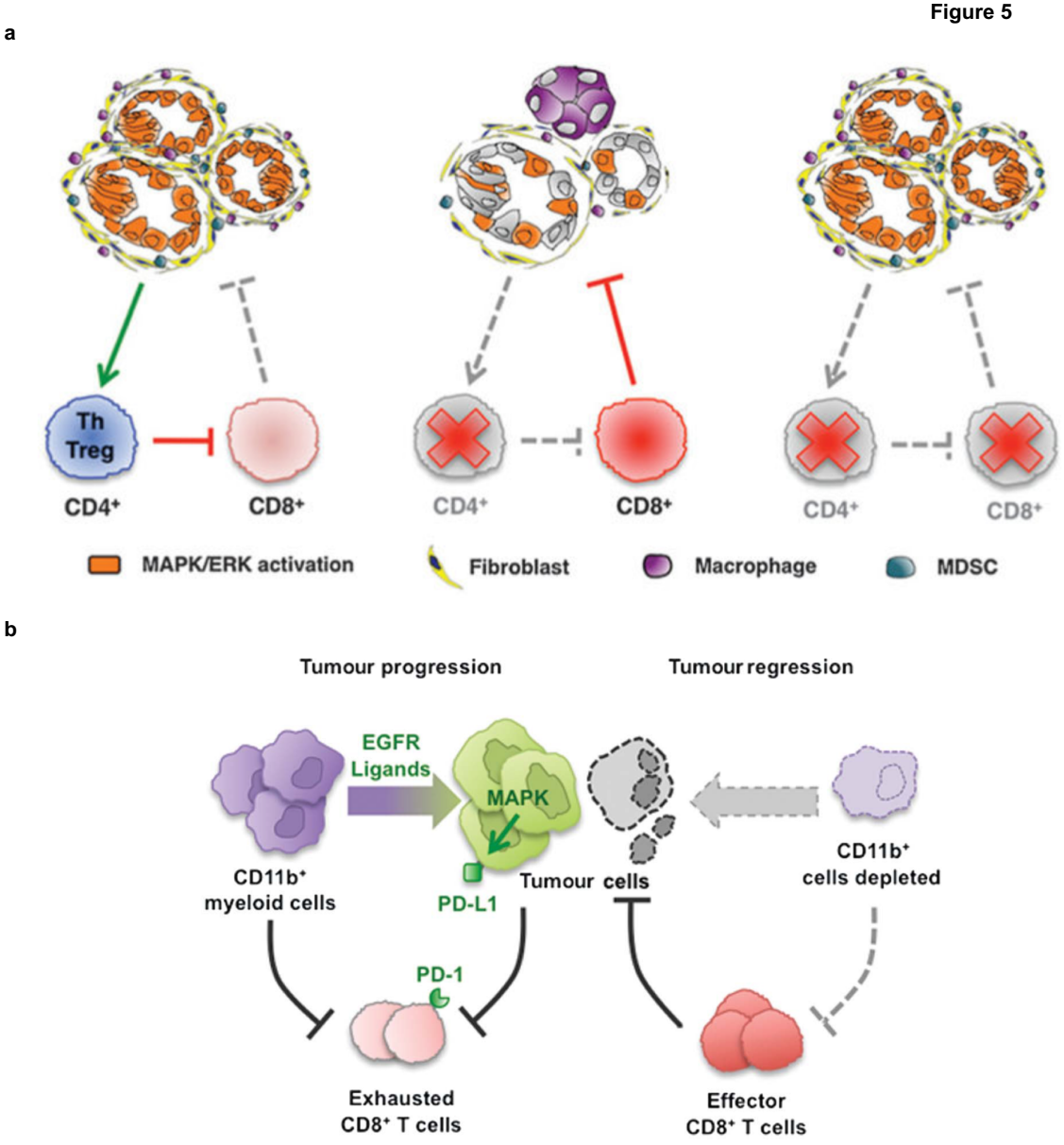

Fig. 5: **T cells and myeloid cells in the pancreatic tumor microenvironment**
(a) Schematic indicating the tumor promoting role of $CD4^+$ T lymphocytes in PanIN lesions. $CD4^+$ T cells inhibit $CD8^+$ T cells, preventing their anti-tumor activity. Depletion of both $CD8^+$ and $CD4^+$ T cells rescue the tumorigenesis in Kras* driven PDAC model. *Reproduced with permission from (Zhang Y, Yan W, Mathew E, Bednar F, Wan S, Collins MA, et al. $CD4^+$ T lymphocyte ablation prevents pancreatic carcinogenesis in mice. Cancer Immunol Res 2014;2(5):423-35 doi 10.1158/2326-6066.CIR-14-0016-T)*. **(b)** Schematic depicting that $CD11b^+$ myeloid cells protect tumour cell viability by inhibiting $CD8^+$ T-cell mediated anti-tumor immune response in PDAC. *Reproduced with permission from (Zhang Y, Velez-Delgado A, Mathew E, Li D, Mendez FM, Flannagan K, et al. Myeloid cells are required for PD-1/PD-L1 checkpoint activation and the*

establishment of an immunosuppressive environment in pancreatic cancer. Gut 2017;66(1):124-36 doi 10.1136/gutjnl-2016-312078).

Kras* in pancreatic tumor microenvironment

Kras* not only promotes cancer cell survival and proliferation, but also plays an important role in supporting an immunosuppressive tumor microenvironment (TME)(Zhang et al., 2014, Zhang et al., 2017, Liao et al., 2019). Murine PDAC models using an inducible Kras* suggest that activation of Kras* decreases T cells and increases macrophage infiltration in the tumor microenvironment (Zhang et al., 2014). Therefore, PDAC is considered an immunologically 'cold' tumor with minimal T cell infiltration(Evans et al., 2016). Another study in a colorectal cancer model with inducible Kras* mutation demonstrated that Kras*- IRF2 signaling axis promoted a T cell deficient and myeloproliferative tumor micro-environment. Further, the authors demonstrate that Kras* inhibition rendered the colorectal cancers sensitive to checkpoint immunotherapy (Liao et al., 2019). These findings thus support a role for intratumoral T cells in PDAC progression, and intersection of cancer-cell autonomous programs with compositional changes of the immune TME may uniquely position PDAC to escape immune surveillance and response to immune checkpoint therapy. Critical knowledge gaps persist in our evolving understanding of the complex desmoplastic reaction associated with PDAC; and the precise role of Kras* in shaping the immune landscape of PDAC remains elusive. The molecular underpinnings of immunosuppression in PDAC also remains poorly understood. Deciphering the functional contribution of the immune microenvironment and the nodes of regulation governing immune infiltration and anti-tumor immune responses in PDAC is critically needed to impact disease progression.

Kras* targeting using iExosomes:

Kras* mutation, although ubiquitous in PDAC represents a poorly druggable target(Cox et al., 2014). Although small molecules have been developed to target the oncogenic $Kras^{G12C}$ mutation in lung cancers, the $Kras^{G12D}$ mutation has been practically undruggable(Ostrem et al., 2013). The Kalluri laboratory recently developed a novel approach to target oncogenic Kras using engineered exosomes (iExosomes) with siRNA and validated this strategy in multiple preclinical PDAC models(Kamerkar et al., 2017, Mendt et al., 2018). Exosomes are endogenous membranous vesicles, 50-150 nm in diameter excreted by all cell types into body fluids and tissues. Their functions include transfer of molecular cargo, proteins, lipids and nucleic acids, between cells facilitating long-distance intercellular communication. Efficient siRNA transfer by exosomes(El-Andaloussi et al., 2012) inspired the generation of iExosomes for Kras*-siRNA delivery. iExosomes combine two important characteristics that enable efficient Kras* targeting. First, they avoid immune clearance by monocytes as they present “self” CD47 signal (Kamerkar et al., 2017, Chao et al., 2012), and thereby circumvent antigen presentation and escape an immune response. Second, the iExosomes strategy exploits micropinocytosis in Kras* mutant cells that facilitate uptake of exosomes loaded with Kras*- siRNA into cancer cells (Kamerkar et al., 2017, Commisso et al., 2013). In our study, we use this treatment modality, that efficiently targets Kras* is used to determine the effect of distinct T cell subsets on the outcome of Kras*-targeting therapies.

Factors affecting T cell function in the pancreatic tumor microenvironment

i) Microbiome

The gut microbiome has been implicated as one of the critical modulators of immune response in multiple cancer models. In melanoma mouse tumor models, it was found that ablation of the gut microbiome led to deterioration of immune response to checkpoint immunotherapy (Sivan et al., 2015, Routy et al., 2018). Similar findings were replicated

in non-small cell lung cancer and sarcoma murine models(Routy et al., 2018). Further analysis implicated Bifidobacterium as the critical mediator of anti-tumor response in these studies(Sivan et al., 2015). In melanoma patients, however the response to checkpoint immunotherapy correlated with presence of Ruminococcaceae bacteria in the gut microbiome(Gopalakrishnan et al., 2018). Increased alpha diversity, relative abundance of certain bacterial taxa and presence of T cells in the TME positively correlated with a response to checkpoint immunotherapy, whereas a lack of diversity in the microbial flora, antibiotic treatment and T cell deficient TME correlated negatively.

Novel regulatory networks of PDAC immune TME have also implicated the microbiome. Ablation of the microbiome with broad spectrum antibiotics (Abx) protects against preinvasive PDAC by reducing myeloid derived suppressor cells (MDSCs), and increasing M1 macrophages and T_H1 differentiation in the pancreas(Pushalkar et al., 2018). Bacterial ablation using broad spectrum antibiotics also increased efficacy of checkpoint immunotherapy in an orthotopic KPC model(Pushalkar et al., 2018). A comparison of microbiome diversity in humans indicated that long term survivors of PDAC display a high microbial alpha diversity. Human to mice fecal microbiome transplantation with fecal microbiota from long term survivors suppressed PDAC tumor growth, showed increased intratumoral $CD8^+$ T lymphocyte, enhanced Granzyme B and IFN-γ expression, and decreased Tregs, MDSCs and IL-2 compared to fecal microbiota transfer from short term survivors and untreated mice(Riquelme et al., 2019). These studies also indicate that anti-tumor immune response implicate systemic control exerted by the gut microbiome. The impact of Kras* in pancreas neoplasia, immune cells and the microbiome is unknown. To determine if such cooperation exists in PDAC, we utilize genetically engineered mouse models (GEMMs) with inducible Kras* in a conditional P53

or Tgfbr2 null background to identify the functional role of Kras* in modulating the immune TME. This was also studied in the context of a recently developed therapeutic strategy to target Kras* with exosomes(Kamerkar et al., 2017, Mendt et al., 2018) in spontaneous PDAC mice with conditional $Kras^{G12D/+}$ and $P53^{R172H/+}$ mutations(Hingorani et al., 2005). Subsequently, we analyze the impact of the gut microbiome on T cell responses using orthotopic implanted tumors in GEMMs with depletion of specific T cell populations.

ii) Pancreatitis

Frequently, patients with pancreatic cancer develop bile duct obstruction due to tumors impinging on the bile duct leading to chronic pancreatitis. In the clinical setting, chronic pancreatitis is usually a result of multiple acute insults to the pancreas. In addition, radiation and chemotherapeutic agents are known to induce pancreatitis in PDAC patients(Stromnes et al., 2014). However, chronic pancreatitis by itself was insufficient to induce PDAC(Swidnicka-Siergiejko et al., 2017). In pancreas specific Kras mutant mice, pancreatitis has shown to accelerate pancreatic tumorigenesis. Although pancreatitis has been associated with an increased risk of PDAC, the causal link remains weak. Several studies indicate that Treg and T_H17 subsets of $CD4^+$T cells promote pancreatic tumorigenesis in PDAC models in a background of pancreatitis(Zhang et al., 2014, McAllister et al., 2014). However, depletion of CD4 and $CD8^+$ T cells in a spontaneously developing PDAC model did not result in any difference in tumorigenesis and survival. The precise changes that underlying pancreatitis induce in the tumor microenvironment remains unclear. Understanding the differences in the biology of spontaneously developing PDAC and PDAC developing in a setting of chronic pancreatitis are critical if we are to unleash the immune system to treat PDAC associated with pancreatitis.

In this study, we first determine how Kras* modulates the immune microenvironment using a pancreas specific inducible Kras* allele in a P53 or Tgfbr2 mutant background. We identify the critical nodes of immune regulation in PDAC that are controlled by Kras* in the TME. Subsequently, we deplete these specific immune populations in the context of Kras* targeting therapy to understand the relevance of combining Kras* and T cell targeting therapies. In the second part of my project, we probe the functional differences in the immune microenvironment of spontaneously progressing PDAC and PDAC in the context of underlying pancreatitis. We analyze how the presence of inflammation transforms the fundamental nature of tumor microenvironment and explore potential ways to exploit the inflammatory TME to treat pancreatic cancer.

Chapter 2

Material and methods

Animal studies

i) PiKP and PiKT mice

The genotyping and tumor kinetics of the *Ptf1α$^{cre/+}$*, *tetO/CMV-LSL_Kras$^{G12D/+}$, P53$^{f/f}$, LSL-rtTA-EGFP* (PiKP) model used in this study has been described previously(Ying et al., 2012). To generate *Ptf1α$^{cre/+}$*, *tetO/CMV-LSL_Kras$^{G12D/+}$, Tgfbr2$^{f/f}$, LSL-rtTA-EGFP* (PiKT) model, P53$^{f/f}$ allele was bred out of the PiKP colony and replaced with Tgfbr2$^{f/f}$ mice (Chytil et al., 2002). Schematic of the mouse genetics is shown in (**R Fig. 1a**). For Kras* induction, mice were fed Doxycycline (Dox) water (Dox 2g/L, sucrose 20 g/L) starting at 18 weeks of age. 'Kras* On' cohort mice were maintained on Dox water until they were euthanized when mice reached moribundcy. Mice in the 'Kras* off' cohort were maintained on Dox until tumors had progressed to advanced stage (on average 6 weeks), following which mice were fed regular water without Dox and euthanized at 5 days, 2 weeks, 4 weeks or ≥21 weeks after Dox withdrawal.

ii) KPC CD4$^{-/-}$ and KPC CD8$^{-/-}$ mice

Pdx1-Cre; LSL-Kras$^{G12D/+}$; P53$^{R172H/+}$ (referred to as KPC) mice have been described previously(Hingorani et al., 2005). These mice were bred to CD4$^{-/-}$ (*Cd4^{tm1Mak}*) and CD8$^{-/-}$ (*Cd8^{tm1Mak}*) mice (both kindly provided by Dr. Tak Mak, University Health Network- University of Toronto) to obtain KC, KC CD4$^{-/-}$, KC CD8$^{-/-}$, KPC, KPC CD4$^{-/-}$ and KPC CD8$^{-/-}$ mice. All these mice were interbred and maintained on FVB/ C57Bl6/ BALB/c mixed background. iExo treatment was started on at 14 weeks following baseline MRI measurements in KPC, KPC CD4$^{-/-}$ and KPC CD8$^{-/-}$ tumor bearing mice as described earlier. GMP-compliant iExosomes from bone marrow derived mesenchymal stem cells, electroporated with siKras* were used as previously described in (Mendt et al., 2018). MRI imaging was performed using Bruker 7.0T MRI prior to start of iexosome therapy

and 2 and 4 weeks post start of iExosomes therapy. iExosomes were injected intra-peritoneal (i.p.) every 48 hours following baseline MRI till the endpoint or moribundcy in these mice as described earlier(Kamerkar et al., 2017).

We use an analogue of cholecystokinin (caerulein) to induce pancreatitis in mice. Caerulein treatment (individual dose: 50 μg/ Kg, i.p.) was started at 6 weeks of age in KC, KC $CD4^{-/-}$ and KC $CD8^{-/-}$ mice to induce acute or chronic pancreatitis. For acute pancreatitis experiments, the mice were given 6 hourly caerulein injections (4 times a day) on two alternative days, 24 hours apart (Zhang et al., 2014). The acute pancreatitis mice were sacrificed for histology and tumor comparisons 21 days following the start of caerulein injections. For chronic pancreatitis experiments, the mice were similarly injected 3 times a week for 3 consecutive weeks as described earlier(McAllister et al., 2014). Blood was collected by retro-orbital bleeding (50 μL each time) on days 3, 12, 18 and 22 for measurement of pancreatic enzymes. The chronic pancreatitis mice were sacrificed on day 53 following start of caerulein injections as described earlier(McAllister et al., 2014). For checkpoint blockade, an initial 200 μg αCTLA-4 (BioXCell, clone 9H10, BE0131), αPD-1 (RMP1-14, BE0146) antibody followed by two injection of 100 μg of αCTLA-4, αPD-1 antibodies were administered i.p.. For depletion of dendritic cells, four doses of 500 μg of anti-mouse CD11c (ThermoFischer scientific, Clone N418, C11538) were administered 5 days apart. Corresponding isotype controls - Syrian Hamster IgG (BioXcell, BE0087), Rat IgG2a (BioXcell, clone 2A3, BE0089) and Armenian hamster IgG (BioXcell, BE0091) were administered in the same route, dose and frequency as the antibody.

iii) Microbiome experiments:

For microbiome studies, 8-16 weeks old C57Bl6 mice and $CD4^{-/-}$ (bred in C57Bl6

background) were co-housed for 2 weeks and subsequently given 2 treatments of fecal microbiota transplant (FMT) 1 week apart. For microbiome ablation, these mice were treated with broad spectrum antibiotics by oral gavage three days a week (2 doses, 12h apart each day). The oral gavage contained an antibiotic cocktail with vancomycin (50 mg/mL; Sigma-Aldrich), neomycin (10 mg/mL; Sigma-Aldrich), metronidazole (100 mg/mL; Santa Cruz Biotech), and amphotericin (1 mg/mL; MP Biomedicals). In addition, ampicillin (1 mg/mL; Santa Cruz Biotech) was added to drinking water of mice. Under general anesthesia, 1 x 10^6 KPC 689 cells (with GFP-Luc) were injected orthotopically into the pancreas of mice using Hamilton 81000 syringe. Measurements for radiance (photons s^{-1} cm^{-2} sr^{-1}) were obtained by IVIS imaging (Xenogen spectrum) under uniform conditions across all experimental groups. iExo treatment was started on day14 following baseline IVIS imaging in KPC 689 orthotopic tumor bearing mice as described earlier(Kamerkar et al., 2017). All the mice were housed in MDACC animal facility under pathogen-free conditions and animal procedures were approved by MDACC institutional animal care and use committee.

Tissue processing

Blood was collected via retro-orbital vein and transferred into EDTA-tubes (BD 365974). Tumor, healthy pancreas, spleen and mesenteric lymph node were collected and placed into RPMI (Corning™, 10041CM) with 10% fetal bovine serum (FBS) on ice. The tumor was divided in three parts: one part of tumor was embedded in OCT compound, one part was formalin-fixed for histological analysis, and one part was processed for immunotyping or T cell isolation.

Immunotyping

Single cell suspensions were prepared from tumor, spleen and lymph node. Tumors were minced and digested in 5-10 mL of 0.1 mg/mL Liberase TL (Roche, 05401020001) and 0.2 mg/mL DNaseI (Roche, 10104159001) in RPMI-1640 for 30 min at 37 °C with gentle mixing. The digestion was stopped with equal volume of stop mixture (RPMI-1640, 10% FBS, 10 mM EDTA). Cells were filtered through 100 μm cell strainer (Corning 352350), washed 3 times with FACS buffer (PBS, 2% FBS). Spleens and lymph nodes were mashed through 100-um cell strainer and washed once with FACS buffer. Subsequently, ACK Lysing Buffer (Quality Biological, 118-156-101) was added to blood to lyse red blood cells. After a 5 min incubation at RT, the cell pellet was washed twice with PBS. Cells were stained with 100-μL surface antibody cocktail diluted in [FACS buffer, 20% Brilliant Stain Buffer (BD Bioscience, 566349), 50 μg/mL anti-mouse CD16/CD32 (2.4G2) block (TONBO biosciences, 40-0161), Fixable Viability Dye eFluor780 (eBioscience, 65-0865-14)] for 30 min on ice. Cells were washed twice with FACS buffer, fixed-permeabilized with Foxp3/Transcription Factor Staining Buffer Set (eBioscience, 00-5523-00) and stained for 30 min with intracellular antibody cocktail diluted in Fixation/Permeabilization diluent (eBioscience, 00-5223) on ice. Cells were washed twice with Fixation/Permeabilization diluent, fixed in Fixation buffer (BD Bioscience 554655), and washed with FACS buffer. Antibodies used in surface and intracellular staining cocktails are described in **Table 1a**. Data were acquired on Fortessa-X20 (BD Bioscience) and analyzed with FlowJo V10. Immune populations were gated on single live $CD45^+$ cells. Different immune cell populations were determined using gating strategies shown in **Table 1b**.

Table 1a. Antibodies used for flow cytometry

Antibody	Surface/	Dilution	Vendor, catalogue #

	Intracellular		
Anti-mouse CD45-Pacific Blue (Clone 30-F11)	Surface	1:100	Bio Legend, 103126
Anti-mouse CD45-PE-Cy7 (Clone 30-F11)	Surface	1:200	BD Bioscience, 552848
Anti-mouse CD3-PE-Cy7 (Clone 145-2C11)	Intracellular	1:200	eBioscience, 25-0031-82
Anti-mouse CD3-Alexa700 (Clone 17A2)	Intracellular	1:50	eBioscience, 56-0032-82
Anti-mouse CD4-BV605 (Clone RM4-5)	Surface	1:200	BioLegend, 100548
Anti-mouse CD8-BV650 (Clone 53-6.7)	Surface	1:200	BioLegend, 100742
Anti-mouse CD11b-BV711 (Clone M1/70)	Surface	1:400	BD Bioscience, 563168
Anti-mouse CD11b-BV786 (Clone M1/70)	Surface	1:100	BD Bioscience, 740861
Anti-mouse PD1 PerCP-Cy5.5 (Clone 29F.1A12)	Surface	1:100	BioLegend, 135208
Anti-mouse PDL1-APC (Clone F.9G2)	Surface	1:100	BioLegend, 124312
Anti-mouse PDL1- PE (Clone MIH5)	Surface	1:100	eBioscience, 12-5982-83
Anti-mouse CD49b-PE (Clone Dx5)	Surface	1:100	eBioscience, 12-5971-81
Anti-mouse NK1.1 (Clone PK136)	Surface	1:200	eBioscience, 12-5941-83
Anti-mouse Ki67-Alexa 488 (Clone B56)	Intracellular	1:100	BD Bioscience, 558616
Anti-mouse FoxP3 (Clone FJK-16s)	Intracellular	1:50	eBioscience, 56-5773-82
Anti-mouse F4/80-PE (Clone Cl:A3-1)	Surface	1:10	BioRad, MCA497PE
Anti-mouse Ly6C-APC (Clone AL-21)	Surface	1:200	BD Bioscience, 560595
Anti-mouse Ly6G-PE-Cy7 (Clone 1A8)	Surface	1:200	BD Bioscience, 560601
Anti-mouse CD19-BV650 (Clone 6D5)	Surface	1:100	BioLegend, 115541
Anti-mouse CD19-PerCP-Cy5.5 (Clone 1D3)	Surface	1:100	BD Bioscience, 561113
Anti-mouse CD11c-eFluor615 (Clone N418)	Surface	1:50	eBioscience, 42-0114-82

Anti-mouse CD11c-PE-CF594 (Clone HL3)	Surface	1:100	BD Bioscience, 562454
Anti-mouse MHCII eFluor450 (Clone M5/114.15.2)	Surface	1: 300	eBioscience, 48-5321-80
Anti-mouse MHCII-BV510 (Clone M5/114.15.2)	Surface	1:100	BioLegend, 107635
Anti-mouse CD40-BV650 (Clone 3/23)	Surface	1:100	BD Bioscience, 740492
Anti-mouse CD86-BV605 (Clone GL1)	Surface	1:100	BD Bioscience, 563055
Anti-mouse CD45RB-APC (Clone C363.16A)	Surface	1:100	eBioscience, 17-0455-81
Anti-mouse CD45RB-FITC (Clone C363.16A)	Surface	1:100	eBioscience, 11-0455-82
Anti-mouse TIM3-PE/Dizzle (Clone B8.2C12)	Surface	1:100	BioLegend, 134013
Anti-mouse TIM3-BV711 (Clone RMT3-23)	Surface	1:100	eBioscience, 119727
Anti-mouse T-bet-PE-Cy7 (Clone eBio4B10)	Intracellular	1:100	eBioscience, 25-5825-80
Anti-mouse GranzB-APC (Clone GB11)	Intracellular	1:100	Invitrogen, GRB05
Anti-mouse CD44-PE-Cy7 (Clone IM7)	Surface	1:100	BD Bioscience, 560569
Anti-mouse CD62L-APC (Clone MEL-14)	Surface	1:100	BD Bioscience, 561919
Anti-mouse CD25-APC-Cy7 (Clone PC61)	Surface	1:100	BD Bioscience, 561038
Anti-mouse CD25-APC_R700 (Clone PC61)	Surface	1:100	BD Bioscience, 565135
Anti-mouse CD69-PE-CF594 (Clone H1.2F3)	Surface	1:100	BD Bioscience, 562455

Table 1b. Phenotyping of cells in flow cytometry analysis

Cell	Phenotype
T cells	Live/CD45$^+$/CD3$^+$
CD4$^+$ T cell	Live/CD45$^+$/CD3$^+$/CD4$^+$
CD8$^+$ T cell	Live/CD45$^+$/CD3$^+$/CD8$^+$
Treg	Live/CD45$^+$/CD3$^+$/CD4$^+$/FoxP3$^+$
Myeloid cells	Live/CD45$^+$/CD11b$^+$

Mo-MDSC	Live/CD45$^+$/CD11b$^+$/Ly6C$^+$/ Ly6G $^{low/-}$
Gr-MDSC	Live/CD45$^+$/CD11b$^+$/Ly6G$^+$/Ly6C $^{low/-}$
Ly6C$^-$ Ly6G$^-$	Live/CD45$^+$/CD11b$^+$/Ly6C$^-$Ly6G$^-$
B cells	Live/CD45$^+$/CD19$^+$
NK cells	Live/CD45$^+$/CD3$^-$/NK1.1$^+$ or Live/CD45$^+$/CD3$^-$/CD49b$^+$

Immunofluorescence

Immunofluorescence staining was performed using Tyramide Signal Amplification (TSA) technology as described earlier (Carstens et al., 2017). In short, 5μm formalin fixed paraffin embedded (FFPE) sections were deparaffinized and fixed in formaldehyde: methanol (1: 10). Antigen retrieval was performed in Tris-EDTA (TE) buffer (pH 9.0) at 95^{0}C for 15 min, following which the slides were blocked in 4% Cold water fish gelatin (CWFG) (Sigma-Aldrich, GL7765) for 10 min, stained with primary antibody (1h at RT) and secondary antibody (10 min at RT), followed by incubation with TSA fluorophore (10 min at RT). In between steps, tissues were washed with tris buffered saline with 0.1% tween-20 (TBST) 3 times x 2 min each wash. Subsequently, another round of antigen retrieval is performed and the staining for the next antibody ensues. The details of antibodies, dilution, vendor information, TSA reagents, polymers and buffers used are detailed in **Table 2a**. After the last round of antigen retrieval, slides were cover slipped with mounting media containing DAPI (Fluoroshield^{TM} with DAPI – F6057). The phenotyping of cells for CD4, CD8, Foxp3 and CD11b staining in PiKP and PiKT tumors were performed as described in **Table 2b.** Multiple representative images (at 20X magnification) were obtained from the tumor containing areas in the PiKP (Kras* On, Kras* 5d off, Kras* 2w off and Kras* 4w off) and PiKT mice (Kras* On, Kras* 2w off and Kras*4w off). Uninvolved pancreatic tissue, associated adipose tissue and intra tumor lymphoid

follicle were not included for the analysis. Number of $CD4^+$, $CD8^+$, $CD11b^+$, $CD4^+$ $Foxp3^+$ and $CD4^+$ $Foxp3^-$ per 20x field were counted and the mean number of each cell type was tabulated. The average numbers of each of these cell types were compared between groups.

For the thymus and spleens of KPC, KPC $CD4^{-/-}$ and KPC $CD8^{-/-}$ mice, 5μm cryostat OCT sections were fixed in acetone at 4^0 C for 5 min, blocked in 1% BSA in PBS for 30 mins, stained with primary antibodies - CD4 (Abcam, Ab183685, 1:400) or CD8 (Abdserotec, MCA1767T, 1:100) in 1% BSA in PBS (1h at RT) and secondary antibodies (Goat anti-rabbit (H+L), Alexa Fluor Plus 488, ThermoFischer, A32731, 1:250 for CD4 primary or Goat anti-rat IgG (H+L), Alexa Fluor 400, 1:250 for CD8 primary) (30 min at RT). Subsequently, slides were cover slipped as described earlier.

Table 2a. T cell panel TSA staining

Antigen	Primary antibody			Secondary antibody		TSA fluorophore
	Vendor	Catalogue #	Conc.	Vendor	Polymer	
CD8	Cell signaling technology	98941s	1:250	BioCare	Rabbit-on-Rodent HRP	Opal 650
CD4	Abcam	Ab183685	1:400	BioCare	Rabbit-on-Rodent HRP	Opal 520
Foxp3	ThermoFischer Scientific	14-4771-80	1:50	BioCare	Rat HRP	Opal 650
CD11b	Abcam	Ab133357	1:500	BioCare	Rabbit-on-Rodent HRP	Opal 650
GATA3	Cell signaling technology	5852S	1:1500	BioCare	Rabbit-on-Rodent HRP	Opal 650
Rorγt	Abcam	Ab207082	1:1000	BioCare	Rabbit-on-Rodent HRP	Opal 650
T-bet	Abcam	Ab91109	1:100	Vector Laborotaries	M.O.M. Immunodetection kit	Opal 650

Table 2b. Phenotyping of cells in TSA analysis

Cell type	Phenotype
$CD8^+$ T cells	$CD8^+$
$CD4^+$ T cells	$CD4^+$
Treg	$CD4^+$ $Foxp3^+$
Teff	$CD4^+$ $Foxp3^-$
Myeloid cells	$CD11b^+$
T_H1	$CD4^+$ $T\text{-}bet^+$
T_H2	$CD4^+$ $GATA3^+$
T_H17	$CD4^+$ $Ror\gamma t^+$

Immunohistochemistry

FFPE sections were deparaffinized, antigen retrieval was performed in the respective buffers mentioned in Table 3 for 15 min at 95^0 C, endogenous peroxide was neutralized by treatment with 3% H_20_2 in PBS for 15 min at RT. Subsequently, 4% CWFG in phosphate buffered saline, 0.1% Tween-20 (PBST) was used for blocking and staining with primary antibodies listed below (1h at RT), followed by incubation with secondary antibody (Horse Anti-Rabbit IgG Antibody (H+L), Biotinylated, BA-1100, 1: 200, 1h at RT). Next, the slides were stained using Vectastatin ABC kit, PK 6100 as per the manufacturer's instructions. The sections were incubated in DAB and counter-stained with hematoxylin. In between steps, tissues were washed with PBST 3 times x 2 min each wash. The buffers used, the antibodies with dilution and vendor information for IHC are tabulated in Table 3. For analysis of IHC, multiple random images (at 40x magnification) were selected for scoring $CD4^+$, $CD8^+$ T cells. We observed that majority of the pancreatic tumor tissue did not show any $CD4^+$ or $CD8^+$ T cells. The corresponding spleen tissue was used as controls for staining. On average, one in every 10 fields (40x) had positive staining for $CD4^+$ and $CD8^+$ T cells. Representative images containing positive staining were quantified and the mean number of each cell

type was tabulated. The average number of $CD4^+$ and $CD8^+$ T cells were compared between groups.

For analysis of IHC, multiple random images (at 40x magnification) were selected for scoring $CD4^+$, $CD8^+$ T cells. We observed that majority of the pancreatic tumor tissue did not show any $CD4^+$ or $CD8^+$ T cells. The corresponding spleen tissue was used as controls for staining. On average, one in every 10 fields (40x) had positive staining for $CD4^+$ and $CD8^+$ T cells. Representative images containing positive staining were quantified and the mean number of each cell type was tabulated. The average number of $CD4^+$ and $CD8^+$ T cells were compared between groups. Ki67 proliferation index was calculated on multiple random images from tumors using the formula: number of Ki67 positive nuclei divided by total number of nuclei in a given field of vision. Human tonsil tissue was used as positive control for Ki67 staining. For quantification of CD11b and CD11c staining, total number of positive staining cells per HPF were calculated from all the PanIN containing area in different groups. For quantification of CK19, images that cover the whole of PanIN and uninvolved pancreatic tissue were obtained at low power magnification (10x). Images were uploaded to Image J software and RGB stack images were obtained. Average percentage of $CK19^+$ area per 10x field was calculated in the total pancreas.

Table3. Immunohistochemistry

Antigen	Antigen retrieval buffer	Primary antibody		
		Vendor	Catalogue #	Conc.
CD8	TE, pH 9.0	Cell signaling technology	98941s	1:250
CD4	TE, pH 9.0	Abcam	Ab183685	1:400
Ki67	TE, pH 9.0	Abcam	Ab15580	1:100
CD11b	Citrate, pH 6.0	Abcam	Ab133357	1:500
CK19	Citrate, pH 6.0	Abcam	Ab52625	1:200

CD11c	Citrate, pH 6.0	Cell signaling technology	97585	1:300

Cell lines

KPC-689 cells (with GFP-Luc) used for orthotopic injections were cultured and maintained in RPMI-1640 (Corning 10-040-CV) with 10% FBS (Gemini Fetal Plex 100-602) and Penicillin-Streptomycin (Corning 30-002-CI).

Pancreatic enzyme assays

Pancreatic amylase and lipase in the plasma (Blood collected with Heparin sodium, Sigma-Aldrich, 2106-10VL) were measured by - Section of Veterinary Laboratory Medicine, DVMS, MD Anderson cancer center. For measurement of fecal elastase, fresh fecal samples were collected, weighed using pre-weighted barcoded tubes and processed by manual disruption in the assay buffer recommended. Fecal elastase measurements (Enzchek, ThermoFischer) were performed as per the vendor's instructions.

16S rRNA gene sequencing and bioinformatics analysis

Fecal pellets from mice with and without treatment with broad spectrum antibiotics were snap frozen. Briefly, the bacterial genomic DNA was extracted from fecal pellets using QIAamp fast DNA stool kit (Qiagen), with the addition of an intensive bead-beating lysis step. The V4 hypervariable region of 16S rRNA was amplified and sequenced with a 2 x 250 bp paired-end protocol on the Illumina Miseq platform, as described earlier (Shono et al., 2016, Caporaso et al., 2012). Sequencing data from the paired-end reads were de-multiplexed by QIIME. All identified operational taxonomic units (OUTs) were

assigned using Mothur method with the Silva database. The relative abundance of each OTU was determined for all samples. The detailed pipeline of analysis has been previously described (Wang et al., 2018). For 16S rRNA qPCR, copy numbers of 16S rRNA was estimated with the following primers – 16S rRNA Forward: 5′-ACT CCT ACG GGA GGC AGC AGT-3′ AND Reverse: 5′-TAT TAC CGC GGC TGC TGG C −3′.

Statistics

Statistical tests were performed using GraphPad Prism 8 and reported alongside figure legends. Shapiro- Wilk test was used to assess normality of distribution of samples to select the statistical test for comparison of means and variance. For samples with normal distribution, parametric, unpaired T-test and one-way ANOVA were used for comparison of means and variance respectively. For non-normal distribution of samples, non-parametric T-test (Mann- Whitney test) and Kruskal-Wallis test were used. Log-rank test was used to compare Kaplan-Meier survival curves. P values are reported as *P<0.05, **P<0.01, ***P<0.001, **** P<0.0001, *ns*: not significant.

Chapters 3 – 7: **Results**

PiKP and PiKT GEM models and immunotyping results experiments described from R.

Fig1-4 in this manuscript were generated by Dr. Elena Ramirez (LeBleu & Kalluri lab)

Chapter 3: **Kras* drives a T cell deficient and myeloproliferative PDAC TME.**

i) Kras* is required for progression and maintenance of PDAC tumors

To analyze the effects of Kras* in shaping the TME, we utilize inducible Kras mice on conditional TP53 or Tgfbr2 null backgrounds, by generating the PiKP (*P48-Cre; R26-rtTa-IRES-EGFP*; *tetO-LSL-Kras$^{G12D/+}$; P53$^{L/L}$*) and PiKT (*P48-Cre; R26-rtTa-IRES-EGFP*; *tetO-LSL-Kras$^{G12D/+}$; Tgfbr2$^{L/L}$*) genetically engineered mouse models (GEMMs) (**R Fig. 1a**). In both GEMMs, Kras* induction by continuous doxycycline (Dox) administration in the drinking water starting at 18 weeks of age resulted in rapid development of pancreatic tumors, with similar median survival of ~7 weeks following Dox administration (**R Fig. 1b–c**). We also evaluated disease progression in a distinct cohort of mice wherein Dox was administered to 18 weeks old PiKP and PiKT mice (activating Kras*), and subsequently withdrawn 6 weeks later (**R Fig.1b**). Both PiKP and PiKT mice show a complete regression of tumors following Kras* extinction, and cancer regression translated into long term survival following Kras* suppression (**R Fig. 1d–e**).

Next, to understand the effects of Kras* suppression in the TME, we evaluated the immune composition of PDAC tumors with Kras* and compared it to PDAC tumors in which Kras* expression was suppressed. We employed the previously described 'on and off' doxycycline-inducible Kras* genetic system(Ying et al., 2012). At the time of Dox withdrawal, all mice presented with significant, palpable tumors. These mice were euthanized at 5 days, 4 weeks, and $\geq$21 weeks following Dox withdrawal, effectively evaluating tumors at multiple time points following Kras* suppression (**R Fig. 2a**). Histological analysis of the pancreas tissue revealed that healthy pancreatic acini is replaced by invasive PDAC when mice were on Dox, as previously reported(Ying et al., 2012). When Dox was withdrawn from mice on Dox, invasive PDAC was replaced by

normal pancreatic tissue, decrease in tumor weights, PanIN lesions, ADMs (Acinar-ductal metaplasia), adipose and fibrotic tissue after 4 weeks and 21 weeks of Kras* ablation (**R Fig. 2b–g**). Although no changes in tumor histology were observed immediately after 5days of Dox withdrawal, complete suppression of invasive PDAC was observed at later time points. Interestingly, much of the invasive PDAC tissue was replaced with adipose tissue in mice that were off Dox for 4 and 21 weeks (**R Fig. 2b**).

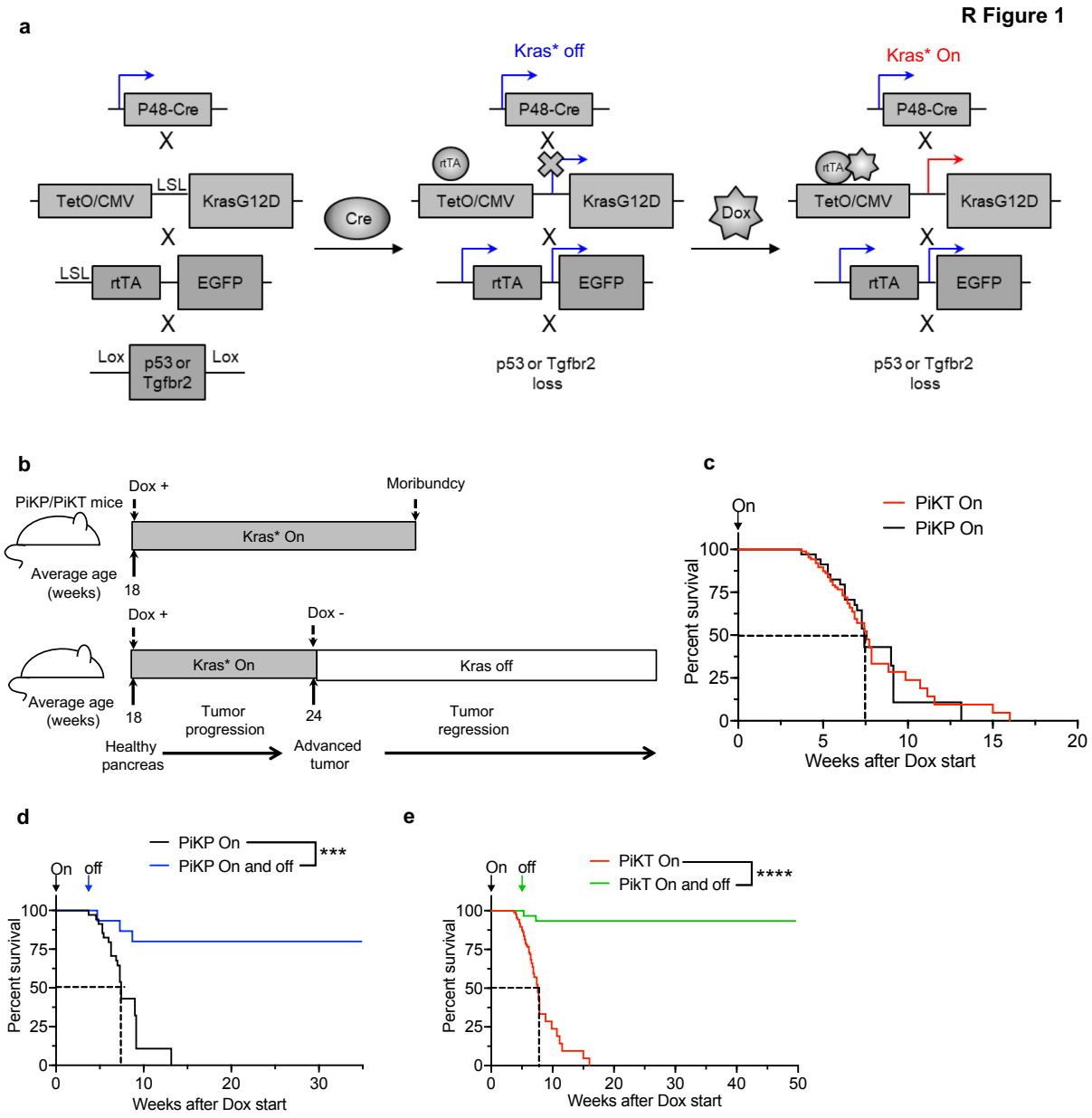

R Fig. 1: Kras* is required for progression and maintenance of PDAC tumors

(a) Genotypes of PiKT and PiKP mouse models: Cre-mediated recombination enables pancreas specific homozygous loss of Tgfbr2 (PiKT) or p53 (PiKP) and rtTA/tetO controlled $Kras^{G12D}$ (Kras*) expression and extinction (Kras*off). Kras* expression is induced in the pancreas with Doxycycline (Dox) administration in the drinking water (Kras* on). Once tumors are formed, Kras* expression is extinguished with withdrawal of Dox (Kras* off). **(b)** Timeline of the experiment. Kras* was induced in PiKP and PiKT mice starting at 18 weeks of age. In one cohort of mice, Kras* was turned off after 6 weeks. The other cohort was Kras* on until end point. **(c)** Kaplan Meier survival curves of PiKT and PiKP mice on Dox. PiKT (n=87), PiKP (n=35) mice. **(d, e)** Kaplan Meier survival curves of PiKT and PiKP mice with Kras* on and Kras* off after 6 weeks of Kras* induction with Dox. PiKP Kras* On (n=35), PiKP Kras* On and Off (n=15). PiKT Kras* On (n=87), PiKT Kras* On and Off (n=30). Significance was determined by log rank test, ***P<0.001, **** P < 0.0001, *ns*: not significant. This work was done with the help and collaboration of Dr. Elena Ramirez.

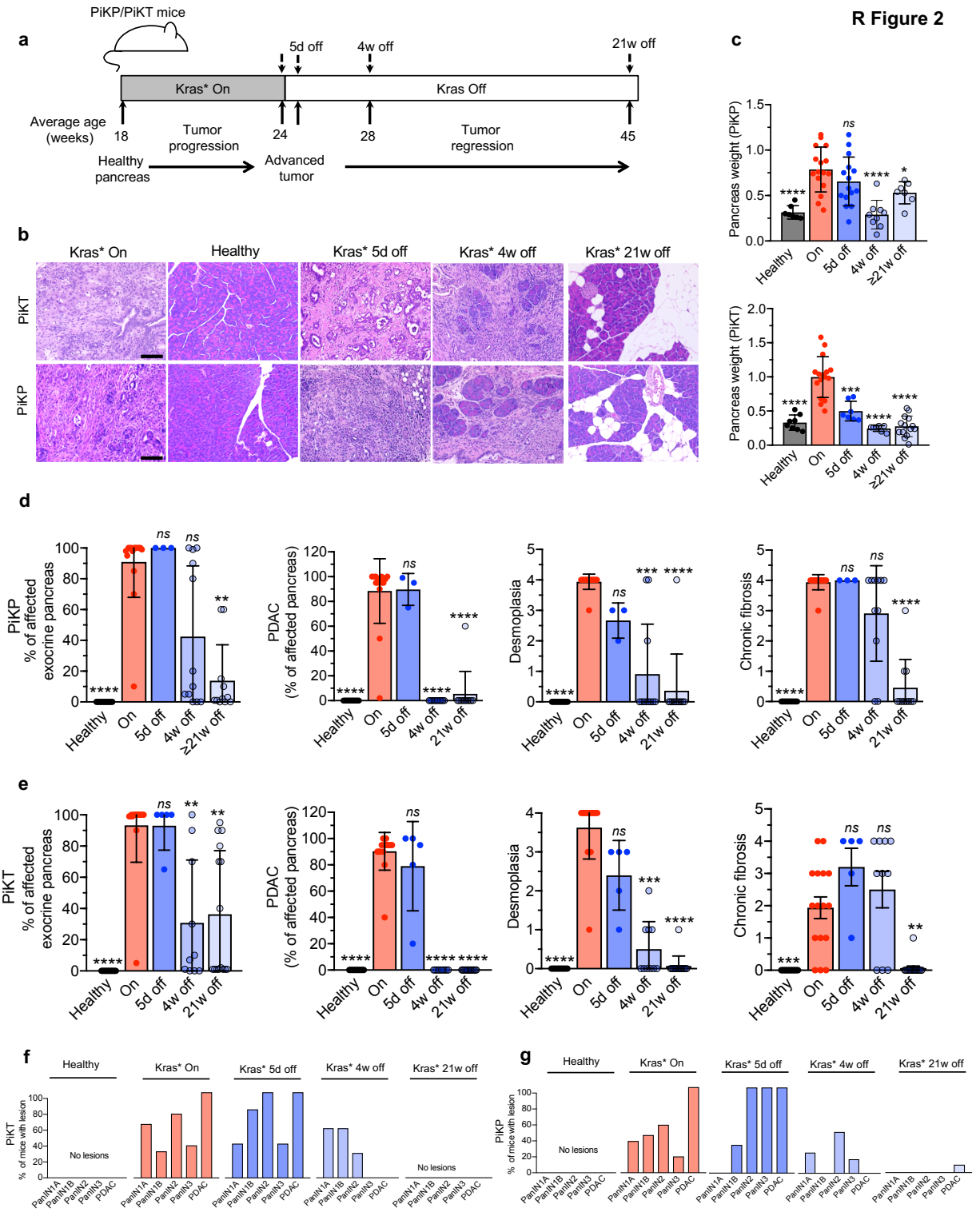

R Fig. 2: Histopathology of PiKT and PiKP GEMMs

(a) Timeline of the experiment. Kras* was induced in PiKP and PiKT mice at 18 weeks of age. After 6 weeks of induction, Kras* was turned off and tumors were analyzed at 5 days, 4 weeks and ≥ 21 weeks. **(b)** Histopathological analyses of H&E pancreas sections of mice in the indicated groups and time points described in **(a)**. **(c)** Pancreas or tumor weights of PiKP and PiKT mice at different time points mentioned in **(a)**. **(d, e)** Percentage

of PDAC out of affected pancreas, percentage of affected exocrine pancreatic acini, score of desmoplasia (active fibrosis) and chronic fibrosis of PiKP **(c)** and PiKT **(d)** tumors. **(f, g)** Percent of mice with PanIN 1A, PanIN 1B, PanIN2, PanIN3 lesions and PDAC in Kras* On, 5d off, 4w off and 21w off PiKP **(f)**, and PiKT **(g)** mice. In **(b-g)** PiKT: healthy (n=14), Kras* on (n=16), Kras* 5d off (n=5), Kras* 4w off (n=10), Kras* ≥21w off (n=15). PiKP: healthy (n=13), Kras* on (n=16), Kras* 5d off (n=3), Kras* 4w off (n=11), Kras* ≥21w off (n=11) mice. Data are presented as the mean ± SD. Significance was determined by Unpaired T-test (parametric or non-parametric) in **(c)** and using Kruskal-Wallis test in **(d and e)**. *P<0.05, **P<0.01, ***P<0.001, **** P<0.0001, *ns*: not significant. This work was done with the help and collaboration of Dr. Elena Ramirez.

ii) Kras* represses T cells and promotes myeloid infiltration in PiKP tumors

To determine the functional contribution of Kras* in modulating the immune infiltrates in the PDAC TME, we performed comprehensive flow cytometry immunophenotyping analyses of the tumors of PikP mice on Dox (on) and 5 days following Kras* suppression (5d off). The immunophenotyping analysis demonstrated that Kras* suppression resulted in an increase in the fraction of T cells and a decrease in the fraction of myeloid cells (**R Fig. 3a-c**). Subtyping analyses indicated a significant increase in T cell fractions [T cells ($CD3^+$), Treg ($CD4^+$ $Foxp3^+$), Teff ($CD4^+$ $Foxp3^-$)] in the PiKP tumors following Kras* suppression (**R Fig. 3b-c**). The changes in the frequencies of T cells and myeloid cells in Kras* mice were not as pronounced in the spleen of these mice (**R Fig. 3c**), supporting that the impact of suppressing Kras* was mostly realized in the tumor immune microenvironment. In addition to the increase in T cell frequencies following Kras* suppression, tumors were also immunolabeled for immune markers, and quantitative analyses revealed an influx of Treg, Teff, and $CD8^+$ T cells in Kras* suppressed tumors (**R Fig. 3d**). A decrease in myeloid immune infiltration was also observed after 2 weeks of Kras* suppression (**R Fig. 3d**).

R Figure 3

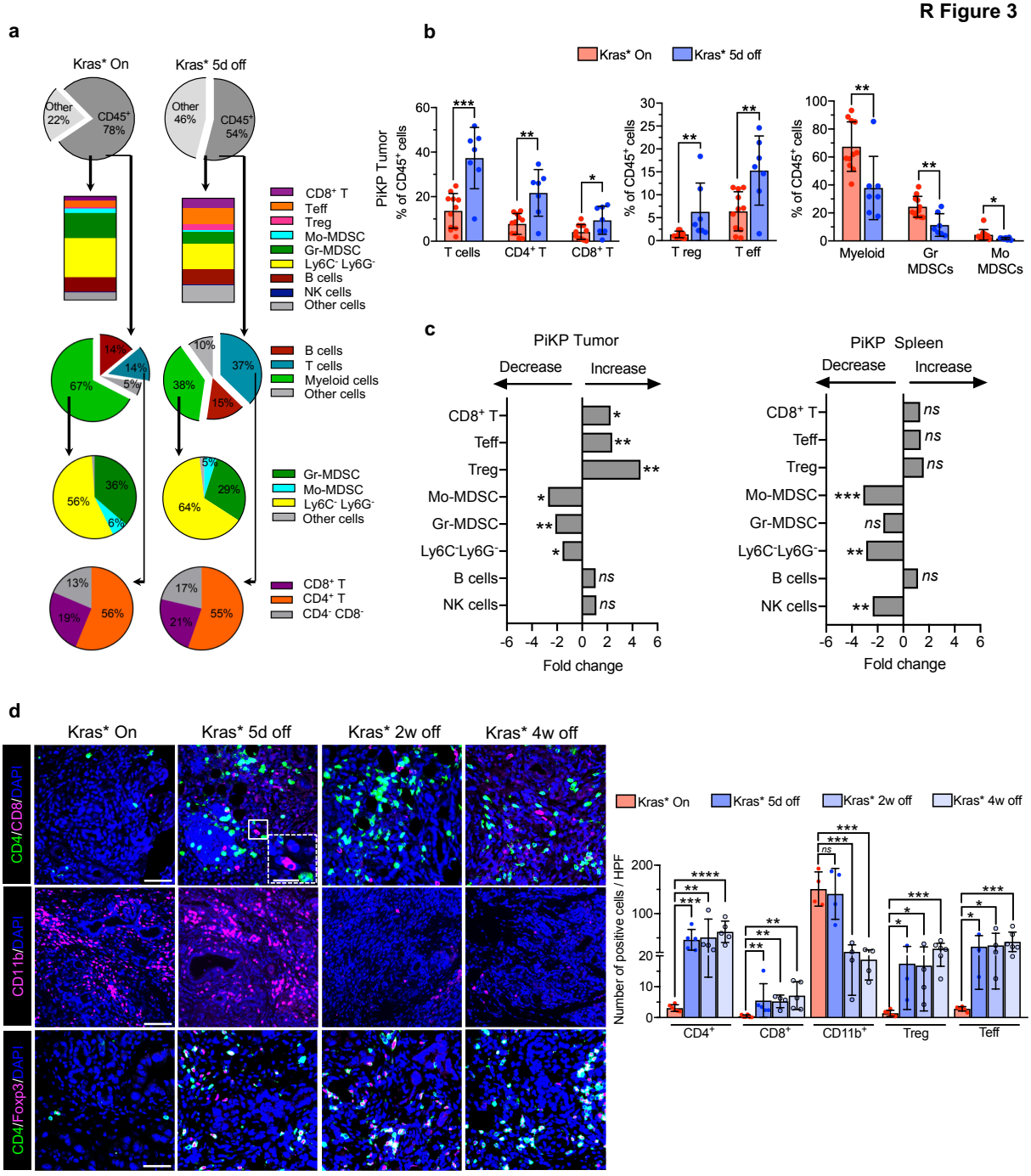

R Fig. 3: Kras* represses T cells and promotes myeloid infiltration in PiKP tumors. **(a)** Intra-tumoral immune composition of PiKP mice with 'Kras* on' (n=11 mice) and 'Kras* 5 days off' (n=7 mice) determined as % of CD45$^+$ cells by flow cytometry. **(b)** Quantification of tumor infiltrating CD45$^+$ cells in 'Kras* on' and 'Kras 5 days off' mice analyzed by FlowJo. Cell populations were defined as T cells (CD45$^+$ CD3$^+$), CD4$^+$ T cells (CD45$^+$ CD3$^+$ CD4$^+$), CD8$^+$ T cells (CD45$^+$ CD3$^+$ CD8$^+$), Treg (CD4$^+$ Foxp3$^+$), Teff (CD4$^+$ Foxp3$^-$), myeloid cells (CD45+ CD11b+), Gr-MDSC (CD11b+ Ly6G+) and Mo-MDSC (CD11b+ Ly6C+) populations in PiKP tumors. **(c)** Fold change of immune cells in

Kras* 5 days off mice in PiKP tumors and spleens, increase or decrease is indicated by arrows. **(d)** Immunolabeling and quantification of $CD4^+$ T cells (CD4), $CD8^+$ T cells (CD8), myeloid cells (CD11b), Tregs ($CD4^+$ $Foxp3^+$) and Teff ($CD4^+$ $Foxp3^-$) in Kras* On and Kras* off (5 days, 2 weeks and 4 weeks) PiKP mice (n = 3-6). Scale bars, 100µm. In **(b)** and **(d)**, data are presented as the mean ± SD. Significance was determined by Unpaired T-test (parametric or non-parametric). *P<0.05, **P<0.01, ***P<0.001, **** P<0.0001, *ns*: not significant. This work was done with the help and collaboration of Dr. Elena Ramirez.

iii) Kras* represses T cells and promotes myeloid infiltration in PiKT tumors

To confirm that our findings from our PiKP model was Kras* driven and were not influenced by the interposition of TP53 mutation in our model, we analyze the effects of Kras* suppression in a second PiKT model. We performed comprehensive flow cytometry immunophenotyping analyses of the tumors of PikT mice on Dox (on) and 5 days following Kras* suppression (5d off). The immunophenotyping analysis demonstrated that Kras* suppression resulted in an increase in the fraction of T cells and a decrease in the fraction of myeloid cells (**R Fig. 4a-c**). Subtyping analyses indicated a significant increase in T cell fractions [T cells ($CD3^+$), Treg ($CD4^+$ $Foxp3^+$), Teff ($CD4^+$ $Foxp3^-$) in the PiKT tumors following Kras* suppression (**R Fig. 4b-c**). The changes in the frequencies of T cells and myeloid cells in Kras* mice were not as pronounced in the spleen of these mice (**R Fig. 4c**), supporting that the impact of suppressing Kras* was mostly realized in the tumor immune microenvironment. In addition to the increase in T cell frequencies following Kras* suppression, tumors were also immunolabeled for immune markers, and quantitative analyses revealed an influx of Treg, Teff, and $CD8^+$ T cells in Kras* suppressed tumors (**R Fig. 4d**). A decrease in myeloid immune infiltration was also observed after 2 weeks of Kras* suppression (**R Fig. 4d**). The phenotype in the PiKT mice almost mirrored that of the PiKP mice following Kras* suppression indicating firmly that Kras* promotes the exclusion of T cells in PDAC tumors, and favors myeloid cells infiltration.

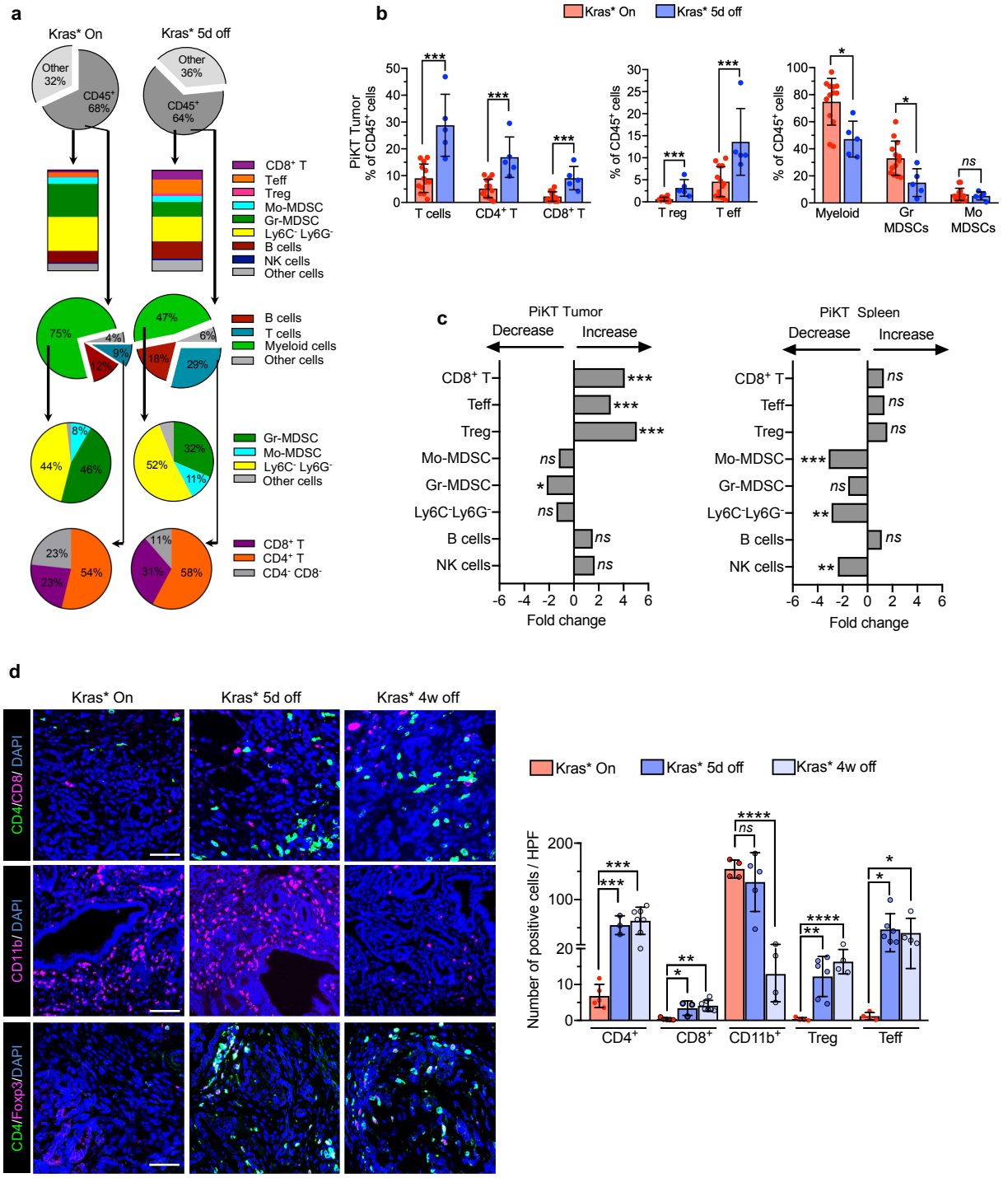

R Fig. 4: Kras* represses T cells and promotes myeloid infiltration in PiKT tumors: **a)** Intra-tumoral immune composition of PiKT mice with 'Kras* on' (n=11 mice) and 'Kras* 5 days off' (n=7 mice) determined as % of CD45$^+$ cells by flow cytometry. **(b)** Quantification of tumor infiltrating CD45$^+$ cells in 'Kras* on' and 'Kras 5 days off' mice analyzed by FlowJo. Cell populations were defined as T cells (CD45$^+$ CD3$^+$), CD4$^+$ T cells (CD45$^+$ CD3$^+$ CD4$^+$), CD8$^+$ T cells (CD45$^+$ CD3$^+$ CD8$^+$), Treg (CD4$^+$ Foxp3$^+$), Teff (CD4$^+$ Foxp3$^-$), myeloid cells (CD45+ CD11b+), Gr-MDSC (CD11b+ Ly6G+) and Mo-MDSC (CD11b+ Ly6C+) populations in PiKT tumors. **(c)** Fold change of immune cells in

Kras* 5 days off mice in PiKT tumors and spleens, increase or decrease is indicated by arrows. **(d)** Immunolabeling for $CD4^+$ T cells (CD4), $CD8^+$ T cells (CD8), myeloid cells (CD11b), Tregs ($CD4^+$ $Foxp3^+$) and Teff ($CD4^+$ $Foxp3^-$) in Kras* On and Kras* off (5 days and 4 weeks) PiKT mice (n=3-7 mice). Scale bars, 100μm. In **(b-d)**, data are presented as the mean ± SD. Significance was determined by Unpaired T-test (parametric or non-parametric). *P<0.05, **P<0.01, ***P<0.001, **** P<0.0001, *ns*: not significant. This work was done with the help and collaboration of Dr. Elena Ramirez.

Chapter 4: **$CD4^+$T cells impede the therapeutic efficacy of Kras* targeting in PDAC**

i) $CD4^+$ and $CD8^+$ T cells do not alter primary tumor growth or survival, but $CD4^+$ T cells promote metastasis in PDAC

Next, we functionally probed the role of distinct T cell populations noted to increase in the PDAC TME following Kras* suppression (**R Fig. 3-4**). We bred $CD4^{-/-}$ ($Cd4^{tm1Mak}$)(Rahemtulla et al., 1991) or $CD8^{-/-}$ ($Cd8a^{tm1Mak}$)(Fung-Leung et al., 1991) mice with *Pdx1-Cre; LSL-Kras$^{G12D/+}$; P53$^{R172H/+}$* (KPC) to generate *CD4$^{-/-}$; Pdx1-Cre; LSL-Kras$^{G12D/+}$; P53$^{R172H/+}$* (KPC $CD4^{-/-}$) and *CD8$^{-/-}$; Pdx1-Cre; LSL-Kras$^{G12D/+}$; P53$^{R172H/+}$* (KPC $CD8^{-/-}$) mice. Depletion of $CD4^+$ and $CD8^+$ T cells in the thymus and spleen of KPC $CD4^{-/-}$ and KPC $CD8^{-/-}$ mice was confirmed by immunofluorescence staining (**R Fig. 5a-b**). The depletion of $CD4^+$ and $CD8^+$ T cells in the tumor and intra-tumoral lymphoid follicle of the KPC $CD4^{-/-}$ and KPC $CD8^{-/-}$ mice were confirmed in the pancreatic TME (**R Fig. 5c-d**).

The KPC $CD4^{-/-}$ and KPC $CD8^{-/-}$ mice developed PDAC tumors with a similar latency and median survival as the control KPC strain (**R Fig. 6a**). All three mice cohorts succumb to similar tumor burden (**R Fig. 6b**). Analysis of primary tumor grade and proliferation in these mice showed no significant differences between the KPC, KPC $CD4^{-/-}$ and KPC $CD8^{-/-}$ mice (**R Fig. 6c-e**). Analysis of metastasis in these PDAC mice revealed decreased liver metastasis in the KPC $CD4^{-/-}$ mice compared to the KPC and KPC $CD8^{-/-}$ mice (**R Fig. 6f-g**). However, there was no significant difference in lung

metastasis between any of the groups (**R Fig. 6h**). Our results point to CD4⁺ T cells as a potential target to restrict liver metastases in PDAC patients.

R Figure 5

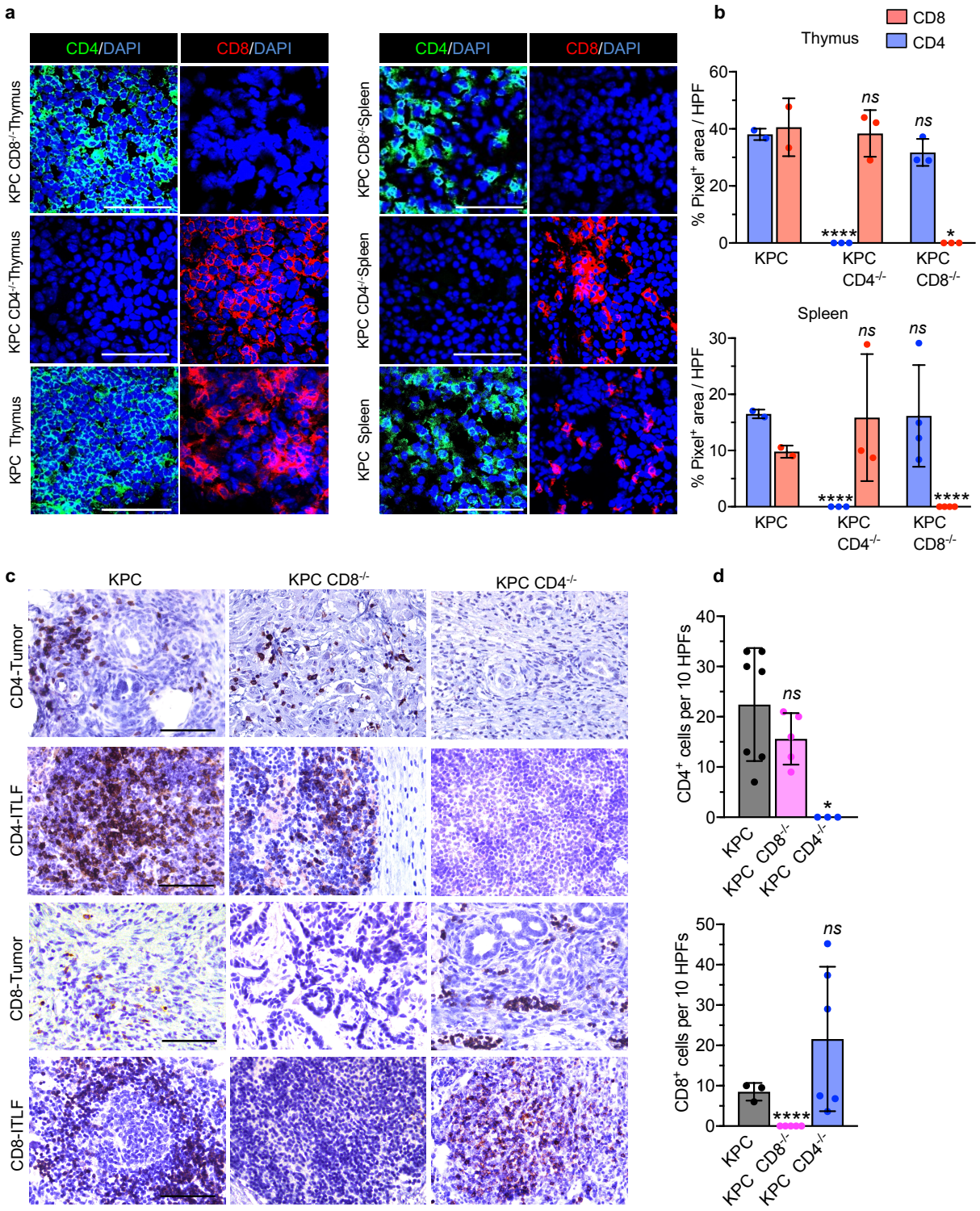

R Fig. 5: KPC CD4$^{-/-}$ and KPC CD8$^{-/-}$ mice lack respective T cell populations in the tumor and lymphoid organs. (a-b) CD4 and CD8 immunostaining **(a)** and corresponding quantification **(b)** of % of CD4^{+} or CD8^{+} area of thymus and spleen of KPC, KPC CD4$^{-/-}$ and KPC CD8$^{-/-}$ mice. n=2-4 mice in each group. **(c)** CD4 and CD8 immunostaining and corresponding quantification **(d)** of KPC, KPC CD4$^{-/-}$ and KPC CD8$^{-/-}$ mice tumors (also note staining in intra-tumoral lymphoid follicle- ITLF). n=3-7 mice in each group. Data are presented as the mean ± SD. Significance was determined by Unpaired T-Test (parametric or non-parametric). *P<0.05, **** P<0.0001, *ns*: not significant.

R. Figure 6

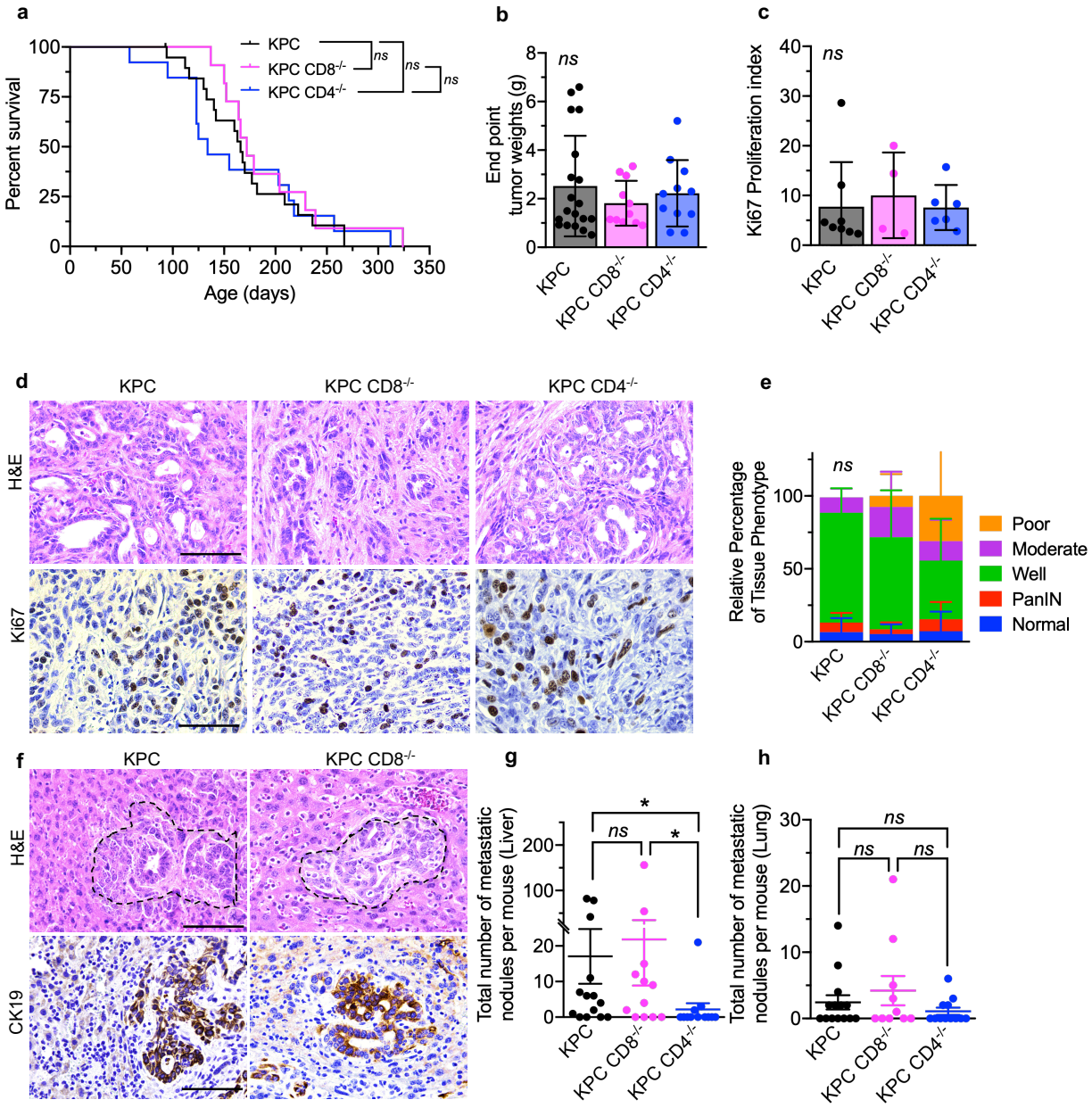

R Fig. 6: CD4^{+} and CD8^{+} T cells do not alter primary tumor growth or survival, but

CD4$^+$ T cells promote metastasis in PDAC. (a) Kaplan-Meier survival curve of baseline KPC (n = 19), KPC CD4$^{-/-}$ (n = 13) and KPC CD8$^{-/-}$ (n = 11) mice. P value by log rank test. **(b)** End point tumor weights of KPC, KPC CD4$^{-/-}$ and KPC CD8$^{-/-}$ mice. (**c-e**) Representative H&E images and Ki67 immunostaining of KPC, KPC CD4$^{-/-}$ and KPC CD8$^{-/-}$ tumors at end point, with quantification of Ki67 proliferation index, and relative percentage of histological phenotypes. **(f)** Representative H&E images and CK 19 immunostaining of liver metastasis of KPC and KPC CD8$^{-/-}$ mice. (**g-h**) Quantification of liver metastasis **g**), and lung metastasis **h**), of KPC, KPC CD4$^{-/-}$ and KPC CD8$^{-/-}$ mice. In (b), (c), (g), (e) and (h) data represents mean ± SD**.** Scale bars, 100um. In (b), (c), significance was determined by Unpaired (parametric) T test. In (e), significance was determined by two-way ANOVA. In (g) and (h), significance was determined by Unpaired (non-parametric) T test. *P<0.05, *ns* - not significant.

ii) iExosomes targeting Kras* increase T cell infiltration in PDAC.

Next, we examine if the immune changes observed in the PiKP and PiKT mice TME following Kras* extinction can be replicated by a Kras* targeting agent. To suppress Kras* in PDAC bearing mice, we employed a previously developed therapeutic strategy using iExosomes to deliver Kras^{G12D} siRNA to tumors(Kamerkar et al., 2017, Mendt et al., 2018). We analyze T cell infiltration in KTC tumors (*Ptf1a$^{cre/+}$; LSL-Kras$^{G12D/+}$; Tgfbr2$^{lox/lox}$*) at an age matched time point (day44) and mice bearing KPC689 orthotopic tumors (end point) treated with iExosomes from our previous studies(Kamerkar et al., 2017). The experimental scheme of start of iExosomes treatment and injection of orthotopic KPC 689 tumors are described in the figure below (**R. Fig. 7a-d**). The PDAC TME following iExo treatment showed increased infiltration of CD4$^+$ and CD8$^+$ T cells in both the KTC and KPC 689 tumor models compared to respective controls (**R. Fig. 7a-d**). These result support that the iExosomes therapy phenocopied the immune TME changes observed in genetic Kras* suppression (**R Fig. 3**).

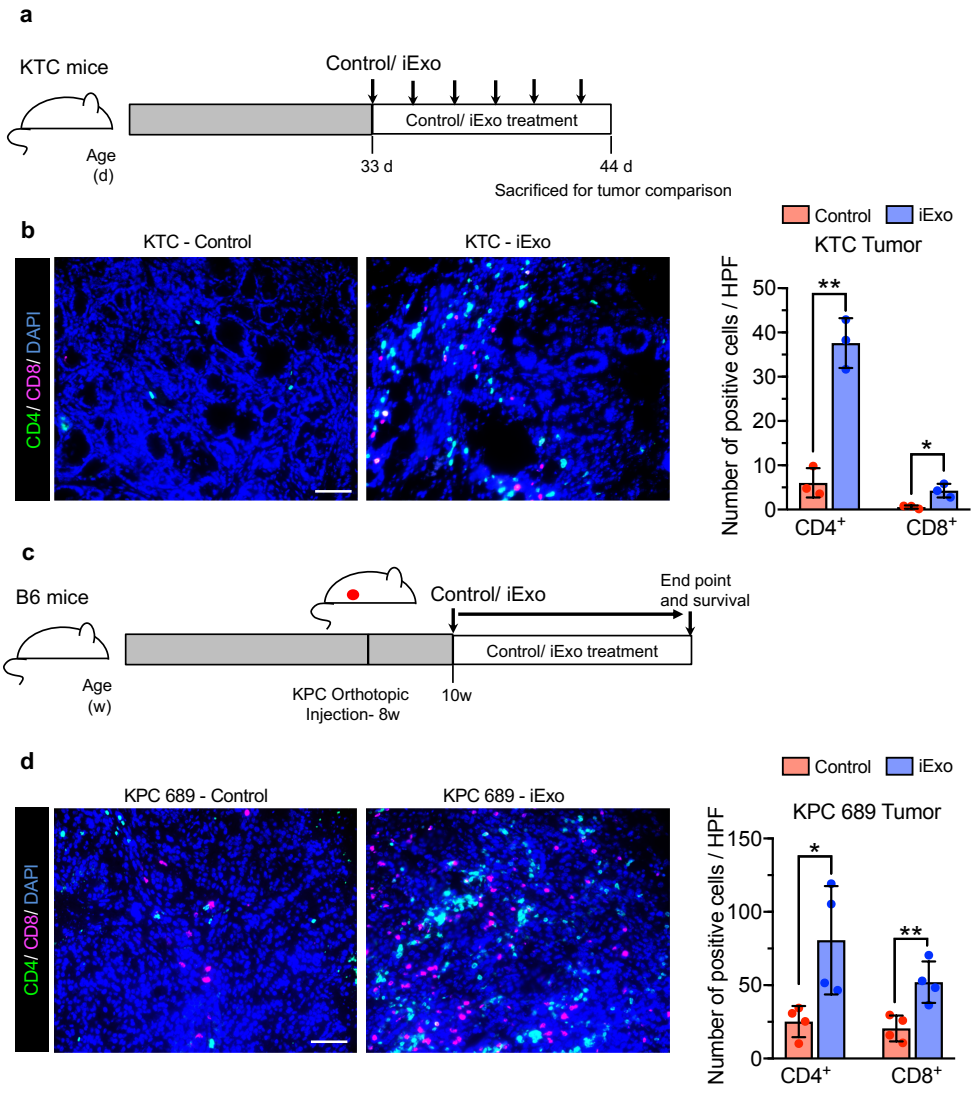

R Fig. 7: iExosomes targeting Kras* increase T cell infiltration in PDAC. a) Timeline of the experiment for KTC mice treated with iExosomes every 48h starting at 33days of age and sacrificed on day 44 for age matched tumor comparisons. **(b)** CD4 and CD8 immunolabeling and quantification of end point KPC 689 – control (n=4), KPC 689 – iExo (n=4) treated tumors. **(c)** Timeline of the experiment for B6 mice injected with KPC 689 cells into pancreas at 8 weeks of age. iExo treatment started at 10w, every 48h till end point. **(d)** CD4 and CD8 immunolabelling and quantification on end point KPC 689 – control (n = 4) and KPC 689 – iExo (n = 5) treated tumors. In (b), (d), Data represent mean ± SD. Significance was determined by Unpaired (parametric) T test *P<0.05, **P<0.01. This work was done on tissue sections from a previous study (39).

iii) CD4⁺ T cells impede the therapeutic efficacy of iExosomes in PDAC

Age-matched (14 weeks old) KPC, KPC-CD4$^{-/-}$ and KPC-CD8$^{-/-}$ mice with comparable tumor volumes (**R Fig. 8a-b**) were placed on iExosomes regimen (see Methods) and tumor progression was monitored by serial MRI measurements (**R Fig. 8c-d**). The assessment of tumor volumes by MRI showed tumor stasis in KPC mice treated with iExosomes, which was abolished by the depletion of CD8^{+} T cells (**R Fig. 8d-e**). However, in the KPC CD4$^{-/-}$ mice, the tumor volumes plateaued in the majority of the mice following iExosomes therapy (**R Fig. 8e**). The KPC CD4$^{-/-}$ mice demonstrated enhanced tumor growth inhibition compared to the KPC mice following iExosomes therapy. As previously reported(Kamerkar et al., 2017), iExosomes significantly improve the survival of KPC mice (**R Fig. 9a-d**). The survival of the control groups of KPC, KPC CD4-/- and KPC CD8-/- mice show no difference in survival although the KPC CD8-/- mice seem to have a marginally longer survival than the KPC mice cohort (**R Fig. 9e**).

The depletion of CD4^{+} T cells in KPC CD4$^{-/-}$ mice exaggerated the effects of Kras* blockade compared to the control KPC and KPC CD8$^{-/-}$ animals, supporting that CD4^{+} T cells restrained the impact of Kras* targeting (**R Fig. 9a, f, g**). However, depletion of CD8^{+} T cells in KPC CD8$^{-/-}$ eliminated the survival benefits offered by Kras* targeting with iExosomes, indicating CD8^{+} T cells play a role in tumor control by Kras* targeting in this model (**R Fig. 9a, d**). Collectively, the data suggests that tumor growth inhibition by Kras* targeting agent(s) is maximized in the absence of CD4^{+} T cells. These data support the view that CD4^{+}T cells in PDAC TME exert a pro-tumorigenic effect through its inhibitory subsets in Kras* suppressed tumors, further supporting the idea that Tregs, T_H2 and T_H17 cells are a critical mediator of PDAC progression.

R Figure 8

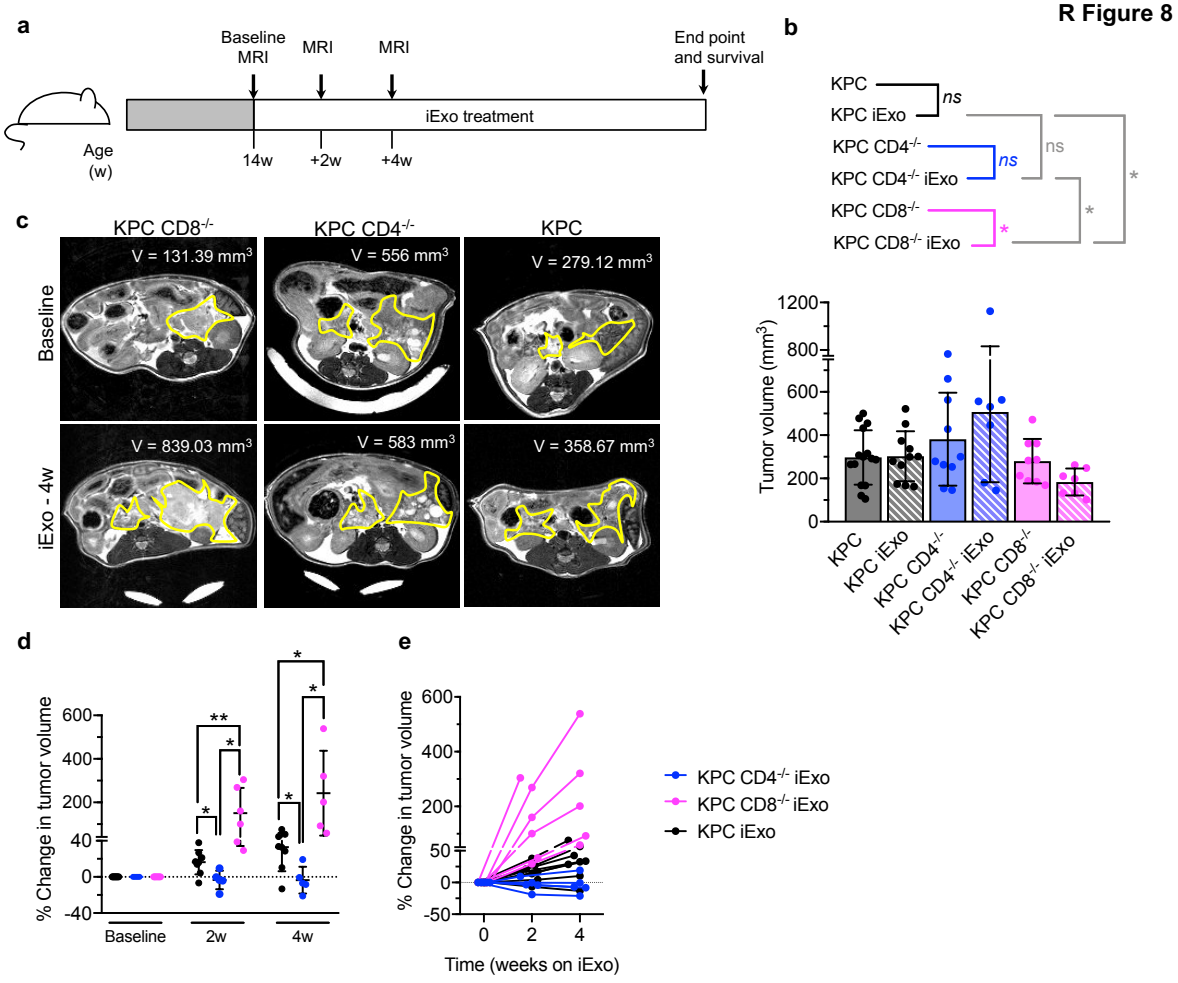

R Fig. 8: CD4⁺ T cells impede the therapeutic effects of iExosomes in PDAC. (a) Timeline of the experiment for KPC, KPC CD4$^{-/-}$, KPC CD8$^{-/-}$ mice treated with iExosomes every 48h starting at 14 weeks of age. Baseline MRI measurements were done prior to enrollment into iExosomes treatment groups. Mice were subsequently imaged by MRI at indicated time points. Untreated mice were also analyzed as control groups. **(b)** Baseline tumor volume at 14 weeks of age by MRI in KPC, KPC CD4$^{-/-}$, and KPC CD8$^{-/-}$ mice. Data are presented as the mean ± SD. n=7-14 mice in each group. **(c)** Baseline (top) and 4 weeks post iExo time point (bottom) MRI imaging of tumors following iExosomes treatment. **(d)** Change in tumor volumes (based on MRI measurements) of KPC, KPC CD8$^{-/-}$ and KPC CD4$^{-/-}$ at 2 weeks and 4 weeks following iExo treatment (n=5-8 mice in each group). **(e)** Spider plots representing percent increase in tumor volumes following iExosomes treatment in KPC, KPC CD4$^{-/-}$, and

KPC CD8$^{-/-}$ mice.

R Figure 9

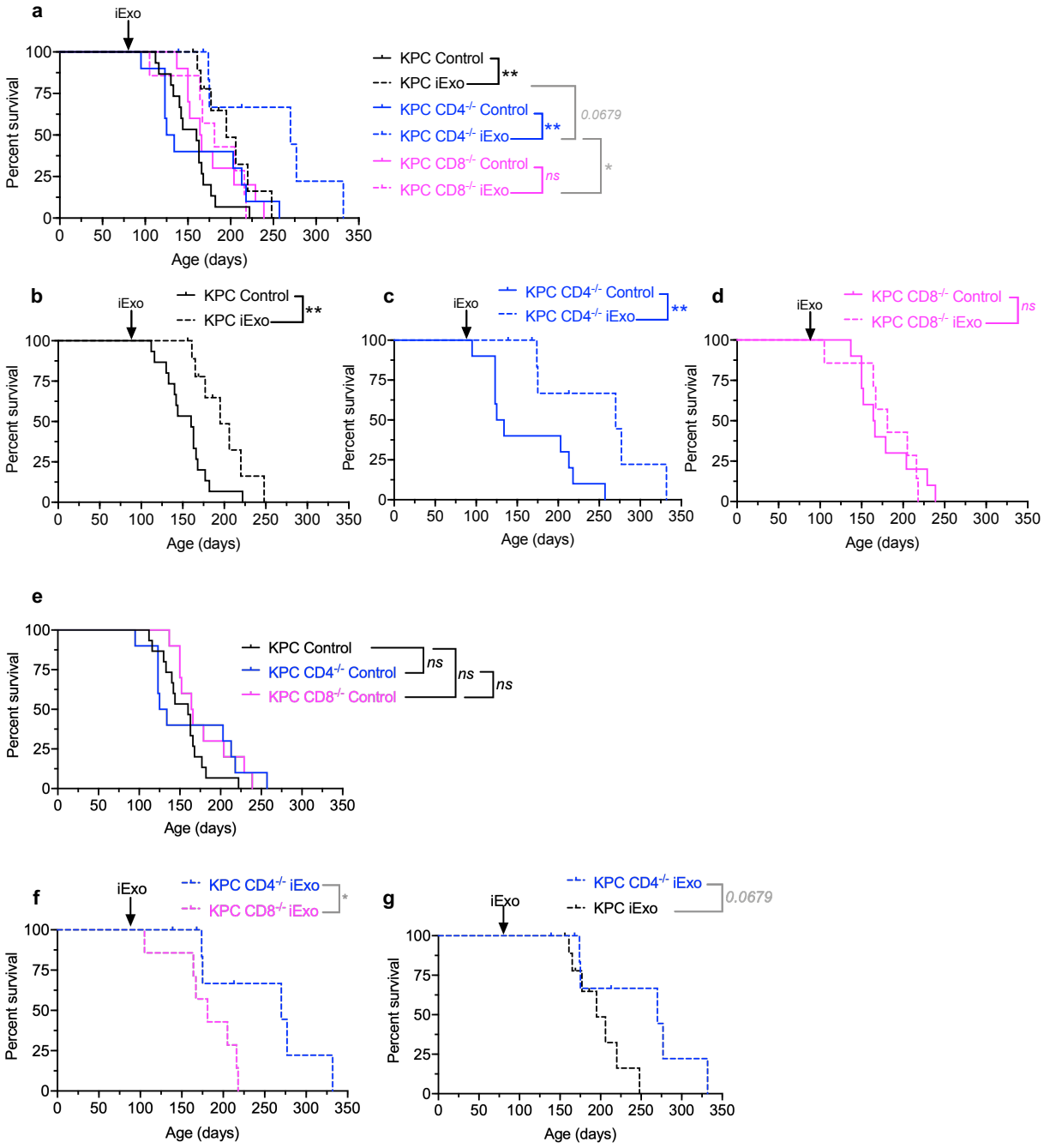

R Fig. 9. Kaplan-Meier survival curves of KPC, KPC CD4$^{-/-}$ and KPC CD8$^{-/-}$ mice treated with iExosomes. (a) Kaplan–Meier survival curves of the indicated groups. n=14 (KPC control), n=11 (KPC iExo); n=10 (KPC CD4$^{-/-}$ control), n=8 (KPC CD4$^{-/-}$ iExo); n=9 (KPC CD8$^{-/-}$ control), and n=7 (KPC CD8$^{-/-}$ iExo) mice. **(b-g)** Individual Kaplan–Meier survival curves from (a). Data are presented as the mean ± SD. Significance was determined by log rank test, *P<0.05, **P<0.01, *ns*: not significant

Chapter 5: **The gut microbiome co-operates with CD4$^+$ T cells to impede Kras* targeting in PDAC.**

Several clinical and pre-clinical studies that investigated the heterogeneity of responses to checkpoint immunotherapy in melanoma and PDAC demonstrated that host bacterial diversity play a critical role in modulating T cell response in immunotherapy(Gopalakrishnan et al., 2018, Riquelme et al., 2019). We investigated whether the gut microbiome modulates CD4$^+$ T cells in Kras* targeting therapy. Eight to sixteen weeks old C57Bl/6 wild type (B6) and CD4$^{-/-}$ (same genetic background) cohorts of mice were co-housed to normalize the gut microbial flora. In addition, two doses of fecal microbiota transfer (FMT) were performed one week apart to normalize the gut microbiome across different study groups (**R Fig.10a**). Two weeks later, two cohorts of B6 mice and one cohort of CD4$^{-/-}$ mice were administered broad spectrum antibiotics (Abx) till end point (see methods). Both antibiotics treated and untreated mice were orthotopically injected with 10^6 bioluminescent KPC689 cells (**R Fig.10a**). 16s rRNA quantitative PCR analysis of the bacterial DNA in the fecal pellets of Abx treated and untreated group showed a significant decrease in bacterial DNA in the gut of Abx treated mice (**R Fig.10b**). 16s rRNA sequencing revealed that Prevotellaceae, Bacteroidales, Erysipelotrichaceae, Bacteroidaceae, and Helicobacteraceae were the most abundant bacteria by family in the gut of untreated B6 and CD4$^{-/-}$ mice (**R Fig.10c**). As previously reported(Kamerkar et al., 2017), iExosomes significantly improve the survival of KPC689 tumor bearing (**R Fig.10d**). In contrast, the Abx treated B6 mice compared to untreated B6 mice did not show any difference in survival, and Abx treatment did not impact response to iExosomes therapy (**R Fig.10d**). However, when the CD4$^+$ T cells are depleted, microbiome ablation resulted in further increase in survival with iExosomes therapy than when the microbiome is kept intact (**R**

Fig.10e). Baseline IVIS imaging after two weeks following tumor injection did not show any significant differences in tumor growth in Abx treated compared to untreated mice (**R Fig.11a-b**). Following baseline IVIS imaging (**R Fig.11a-b**), iExosomes treatment was initiated and continued until experimental endpoints (**R Fig.10a**). Further analysis of bacterial populations at a species level resolution revealed that Muribaculum intestinale, Parabacteroides distasonis, Bacteroides acidifaciens, Bacteroides sartorii, and Bifidobacterium pseudolongum were among the most abundant bacteria classifiable at the species level (**R Fig.11c**).

Collectively these findings support that the impact of Kras* targeting in the context of impaired Tregs ($CD4^{-/-}$) is aided by suppression of the microbiome.

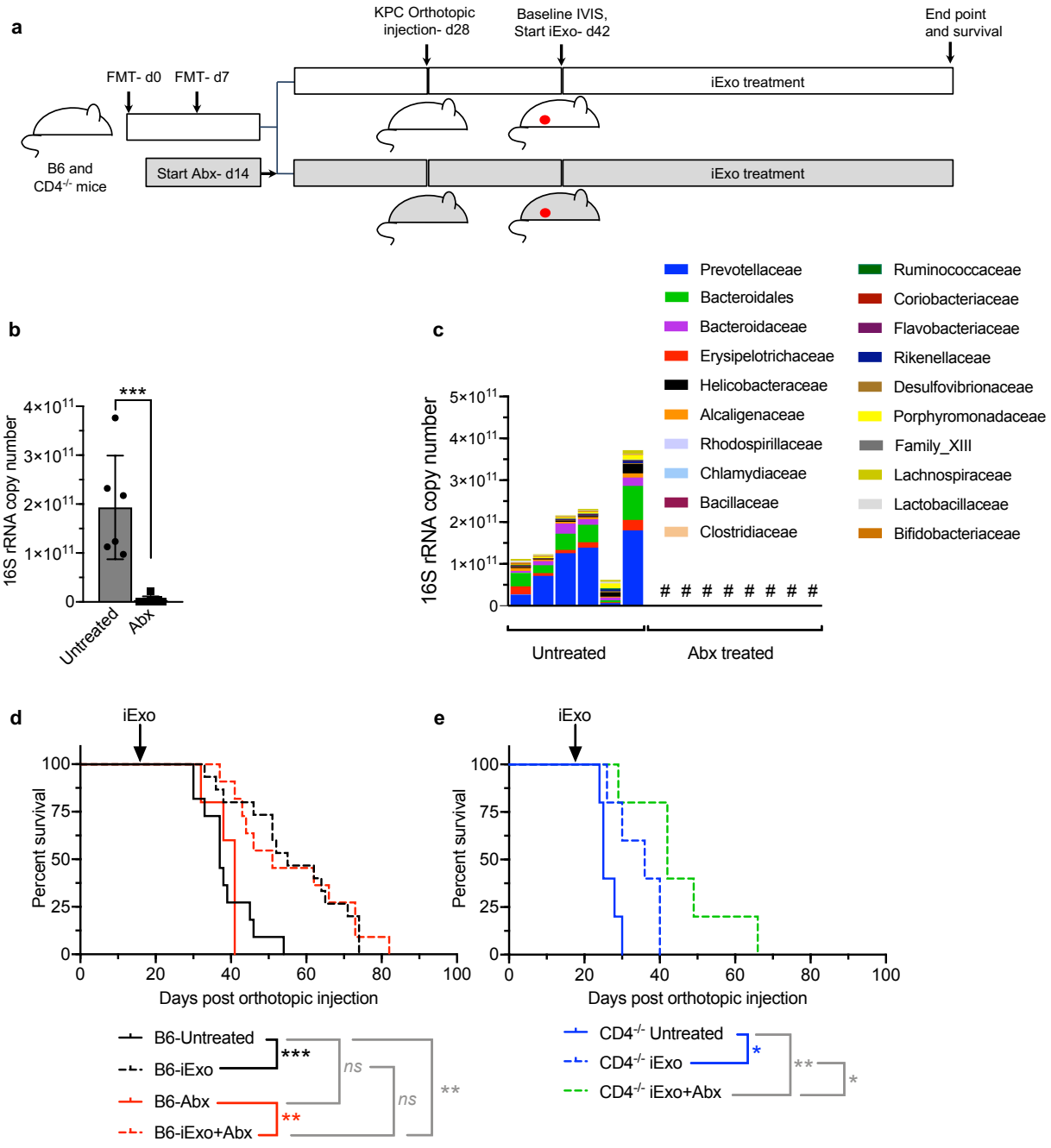

R Fig. 10: The gut microbiome co-operates with CD4⁺ T cells to impede Kras* targeting in PDAC. (a) Timeline of the experiment for B6 and CD4$^{-/-}$ mice treated with iExosomes and broad-spectrum antibiotics (Abx) **(b)** qPCR analysis for bacterial 16s rRNA copy number per fecal pellet of mice treated with broad spectrum antibiotics (Abx) vs. untreated control (d28). **(c)** Phylogenetic composition of fecal samples of untreated (n = 6) and Abx treated (n = 8) mice at the bacterial family level (>0.1% abundance). **(d)** Kaplan Meier survival curves of mice bearing orthotopic KPC 689 tumors with or without microbiome ablation. B6-untreated (n=11), B6-iExo (n=5), B6-Abx (n=15), B6-iExo+Abx

(n=11) mice. **(e)** Kaplan Meier survival curves of mice bearing orthotopic KPC 689 tumors, CD4$^{-/-}$ untreated (n=5), CD4$^{-/-}$ iExo (n=5), and CD4$^{-/-}$ iExo+Abx (n=5) mice. # denotes low amounts of 16s rRNA. Data are presented as the mean ± SD. Significance was determined by Unpaired T-test (parametric) **(b)**, and log rank test **(d, e).** *P<0.05, **P<0.01, ***P<0.001, *ns*: not significant. This work was done with the help and collaboration of Dr. Hikaru Sugimoto, Dr. Robert Jenq and Dr. Chia-Chi Chang.

R Figure 11

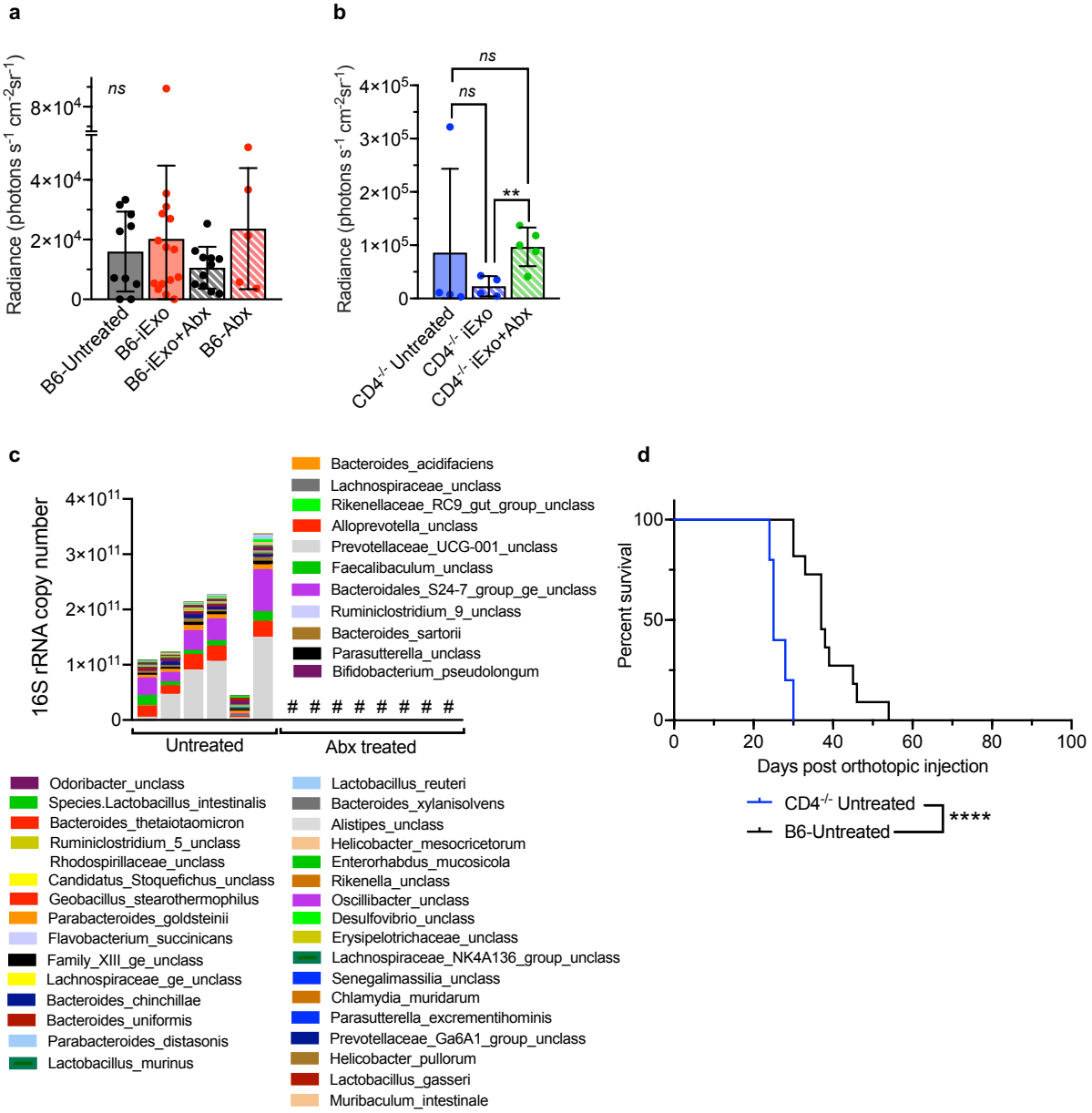

R Fig. 11: Baseline radiance and microbiome composition of B6 and CD4$^{-/-}$ mice treated with antibiotics. (a) Baseline IVIS imaging at day 42 as in **R Fig. 10a** of B6-Untreated (n=11), B6-iExo (n=15), B6- iExo+Abx (n=11), and B6-Abx (n=5) treated mice. **(b)** Baseline IVIS imaging at day 42 as in **R Fig. 10a** of CD4$^{-/-}$ untreated (n=4), CD4$^{-/-}$

iExo (n=4) and CD4$^{-/-}$ iExo+Abx (n=5) treated mice. **(c)** Detailed phylogenetic composition of fecal samples at species level resolution, related to **R Fig. 10c.** # denotes low amounts of 16s rRNA. **(d)** Kaplan Meier survival curves of mice bearing orthotopic KPC 689 tumors, B6- Untreated (n=15) Vs. CD4$^{-/-}$ untreated (n=5) mice, related to **R Fig. 10d-e**. Data are presented as the mean ± SD. Significance was determined by Unpaired T test (parametric or non- parametric) in (a) and (b), and log rank test in (d). **P<0.01, **** P<0.0001, *ns*: not significant. This work was done with the help and collaboration of Dr. Robert Jenq and Dr. Chia-Chi Chang

Chapter 6: **CD4^{+} T cells promote tumorigenesis in KC mice with pancreatitis but have no impact on spontaneously developing tumors.**

i) CD4^{+} T cells promote tumorigenesis in KC mice acute pancreatitis

To understand the distinct functions of T cells in spontaneously arising tumors and tumors with underlying pancreatitis, we analyzed tumor initiation in spontaneously developing PanIN lesions and pancreatitis induced mice. We crossed *CD4$^{-/-}$* or *CD8$^{-/-}$* mice with *Pdx1-Cre; LSL-Kras$^{G12D/+}$* (KC) and generated *CD4$^{-/-}$; Pdx1-Cre; LSL-Kras$^{G12D/+}$*(KC CD4$^{-/-}$) and *CD8$^{-/-}$; Pdx1-Cre; LSL-Kras$^{G12D/+}$* (KC CD8$^{-/-}$) mice. To assess spontaneous tumor initiation in KC, KC CD4$^{-/-}$ and KC CD8$^{-/-}$ mice, we compared age matched mice sacrificed at a mean age of 200 days. Analysis of PanIN lesions in these three cohort of mice showed no significant differences in tumor initiation as seen by histological phenotypes (**R Fig. 12a-b**) or CK19 immunostaining (**R Fig. 12a, c**). None of the KC mice had any evidence of invasive cancer in our cohort. To understand the influence of underlying pancreatitis on PDAC initiation, we treat 6w old KC, KC CD4$^{-/-}$ and KC CD8$^{-/-}$ mice with caerulein, an analogue of cholecystokinin which has been implicated in the pathogenesis of human pancreatitis. These mice were sacrificed 3 weeks later to assess tumor initiation (**R Fig. 12d**). We chose this time point for sacrifice as 3 weeks as it was optimal to assess adaptive immune response at this time point. Pancreatitis accelerated tumor initiation in KC mice (Compare PanINs in KC mice w/o caerulein Vs. KC acute pancreatitis (**R Fig. 12e-f**) as seen by histological

phenotypes and CK 19 immunostaining (**R Fig. 12e-g**). However, we observed that KC $CD4^{-/-}$ mice had relatively fewer PanIN lesions compared to KC and KC $CD8^{-/-}$ mice (**R Fig. 12e-g**). Thus, our results suggest that $CD4^{+}$ T cells promote tumor initiation in mice with underlying pancreatitis, whereas have no impact on tumor initiation in spontaneously developing PanINs.

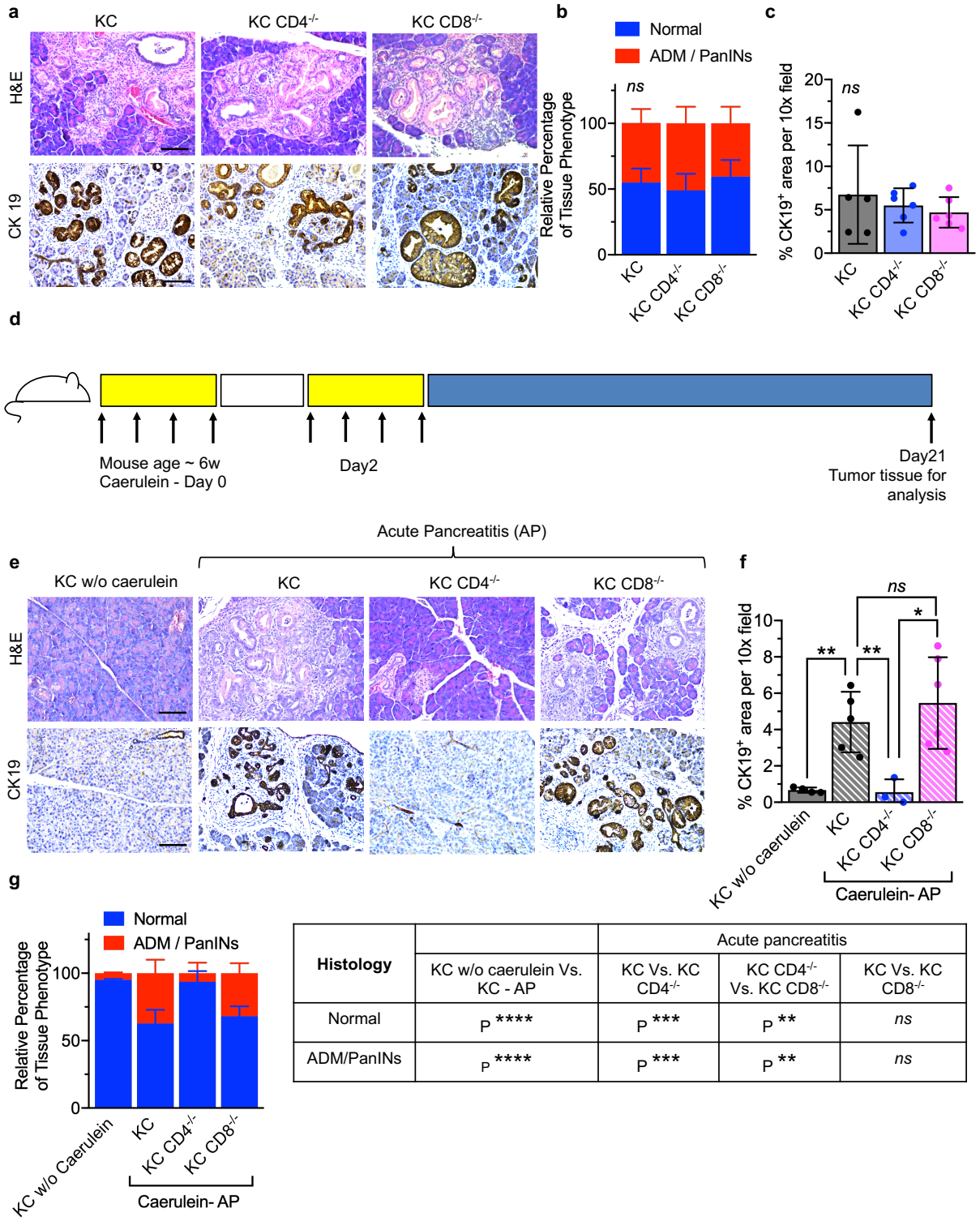

Histology		Acute pancreatitis		
	KC w/o caerulein Vs. KC - AP	KC Vs. KC CD4-/-	KC CD4-/- Vs. KC CD8-/-	KC Vs. KC CD8-/-
Normal	P ****	P ***	P **	*ns*
ADM/PanINs	P ****	P ***	P **	*ns*

R Fig. 12: CD4⁺ T cells promote tumorigenesis in KC mice with acute pancreatitis. (a) Representative H&E and CK19 immunostaining of PanIN lesions of spontaneously progressing KC mice (age matched sacrifice at ~ 200 d from birth). **(b)**

Relative percentages of histological phenotypes. **(c)** Quantification of CK19 positive area in the pancreas. In (a-c), KC (n= 5), KC $CD4^{-/-}$ (n=6) and KC $CD8^{-/-}$ (n=6). **(d)** Schematic representation of acute pancreatitis induction with experimental treatment time points. Caerulein administration induces pancreatitis in KC mice in contrast to spontaneously progressing PanINs. **(e)** Representative H&E and CK19 immunostaining of PanIN lesions of mice with and without caerulein treatment. **(f)** Quantification of CK19 positive area in the pancreas from (f). **(g)** Relative percentages of histological phenotypes. In (e-g), KC w/o caerulein (n=4), Acute pancreatitis- KC (n= 5), KC $CD8^{-/-}$ (n=6) and KC $CD4^{-/-}$ (n=3). In (b), (c), (f) and (g), data represents mean ± SD. In (b, g), significance was determined by two-way ANOVA and in (c, f) significance was determined by Unpaired (parametric) T test, * $P < 0.05$, ** $P < 0.01$, *** $P < 0.001$, **** $P < 0.0001$, *ns*- not significant.

ii) CD4+ T cells promote tumorigenesis in KC mice with chronic pancreatitis

Next, we probe the role of $CD4^+$ T cells in tumor initiation in a setting of underlying chronic pancreatitis. Chronic pancreatitis is observed in 10% of patients with PDAC (**R Fig. 13a**). Frequently, patients with pancreatic cancer develop bile duct obstruction due to tumors impinging on the bile duct leading to chronic pancreatitis. In the clinical setting, chronic pancreatitis is usually a result of multiple acute insults to the pancreas commonly due to repeated alcohol use and intermittent gallbladder obstruction due to tumor invading the bile duct. We probe whether depletion of $CD4^+$ T cells restrict tumor initiation in a chronic pancreatitis setting. To mimic the development of chronic pancreatitis in humans, we inject KC, KC $CD4^{-/-}$ and KC $CD8^{-/-}$ mice with caerulein 4 times a day, three times a week for 3 weeks (**R Fig. 13b**). These mice were sacrificed 8 weeks later to assess tumor histology. Consistent with our findings in KC mice with acute pancreatitis, $CD4^+$ T cells promote tumorigenesis in KC mice with chronic pancreatitis. KC $CD4^{-/-}$ mice had fewer PanIN lesions compared to KC and KC $CD8^{-/-}$ mice as seen by tumor histology and CK 19 immunostaining (**R Fig. 13c-e**).

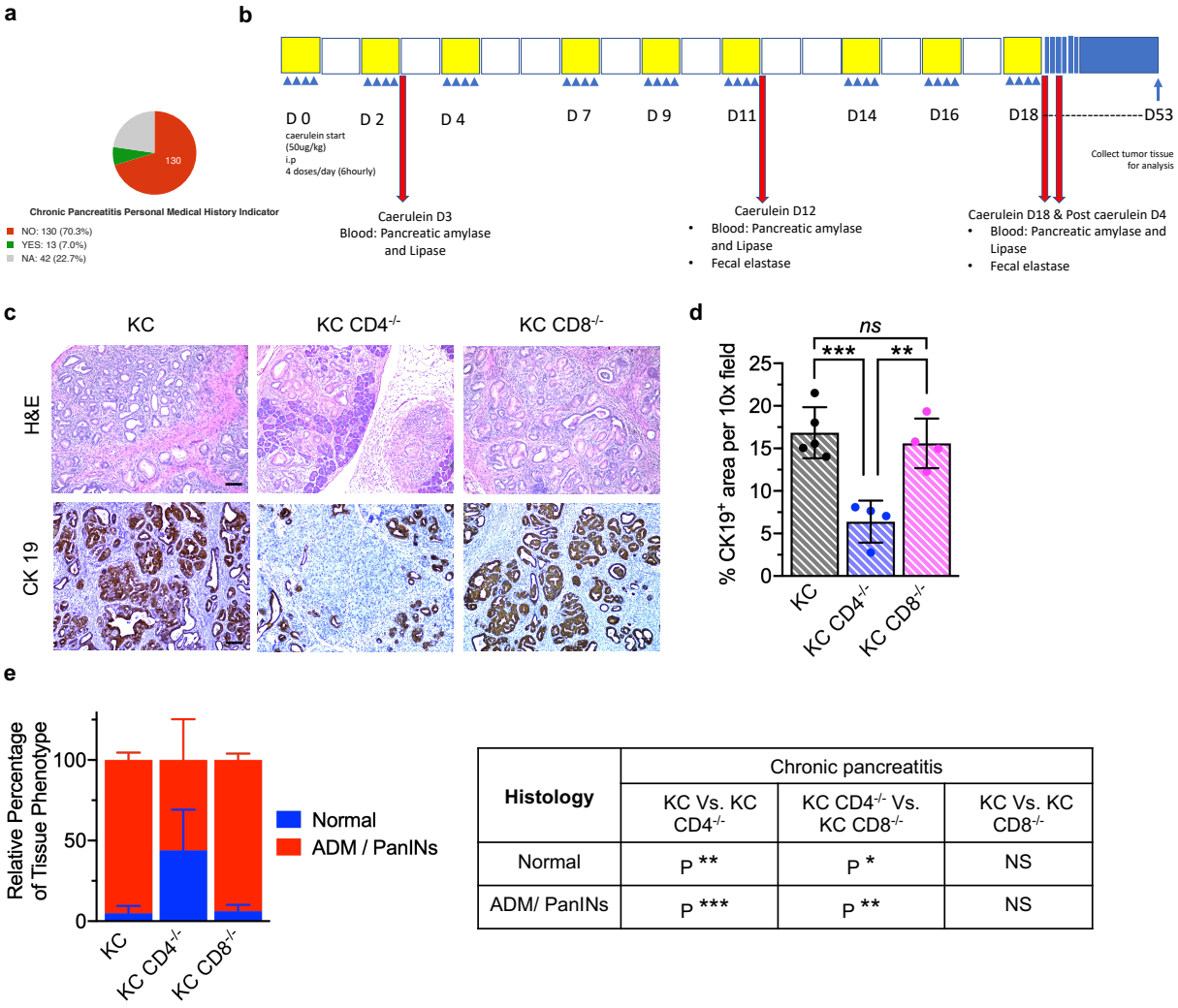

Histology	Chronic pancreatitis		
	KC Vs. KC CD4$^{-/-}$	KC CD4$^{-/-}$ Vs. KC CD8$^{-/-}$	KC Vs. KC CD8$^{-/-}$
Normal	P **	P *	NS
ADM/ PanINs	P ***	P **	NS

R Fig. 13: CD4^{+} T cells promote tumorigenesis in KC mice with chronic pancreatitis. (a) Analysis of number of PDAC patients with documented history of underlying chronic pancreatitis from the TCGA database. **(b)** Schematic representation of chronic pancreatitis induction with experimental treatment time points. Caerulein administration induces pancreatitis in KC mice in contrast to spontaneously progressing PanINs. **(c)** Representative H&E and CK19 immunostaining of PanIN lesions in experimental mice with chronic pancreatitis. **(d)** Quantification of CK19 positive area in the pancreas from (c). **(e)** Relative percentages in histological phenotypes from (c) and two-way ANOVA table comparing histological phenotypes in (c). In (c-e) Chronic pancreatitis- KC (n= 5), KC CD8$^{-/-}$ (n=4) and KC CD4$^{-/-}$ (n=4). In (d) and (e), data represents mean ± SD. In (e), significance was determined by two-way ANOVA and in (d) significance was determined by Unpaired (parametric) T tests, * P < 0.05, ** P < 0.01, *** P < 0.001, *ns*- not significant.

iii) Kras* protects the pancreas against acute pancreatic injury:

Metaplasia is frequently a response associated with infections and inflammation where one form of differentiated epithelium transforms into another. It is essentially a protective response which reverses once the inciting stimulus or inflammation subsides. When the injury to the tissue continues, the epithelium undergoes transformation resulting in intra-epithelial neoplasia (pre-malignant lesions). This is commonly observed in the gastro-esophageal (GE) junction where acid reflux commonly results in intestinal metaplasia and GE junction tumors. However, metaplasia and intra-epithelial neoplasia are replaced by the native functional epithelium once the injury to the tissue subsides. Here, we observe that Kras* accelerates ADM and PanIN formation (**R Fig. 12e-g**) and hypothesize that Kras* protects the pancreatic epithelium against pancreatitis by accelerating ADM/ PanIN formation. We induce pancreatitis in mice with and without Kras* expression in the pancreas and subsequently compare the levels of enzymes associated with pancreatic injury (**R Fig. 14a-d**). Increase in pancreatic amylase and lipase levels in the blood combined with a decrease in fecal elastase levels are hallmarks of clinical pancreatitis(Engle et al., 2019). We observed that both pancreatic amylase and lipase levels are elevated in both KC and Cre negative mice quickly after caerulein administration, continue to rise after day 3, and eventually fall by day18 and further lower on day 22 (4 days after last dose of caerulein – post caerulein D4) (**R Fig. 14a-b**). However, we observed that KC mice had 3 times lower amylase and 19 times lower lipase levels at the peak compared to their Cre negative counterparts (**R Fig. 14d**). We observed that KC mice and Cre negative mice show similar baseline levels of pancreatic amylase and lipase (**R Fig. 14d**). Fecal elastase levels in KC mice with pancreatitis is significantly reduced compared to age matched KC mice without pancreatitis (**R Fig. 14c**). These results suggest that Kras* protects the pancreas

against acute pancreatic injury, whereas the protective effect on the epithelium is lost in a setting of chronic pancreatitis. Our results suggest that the pancreatic acini eventually develop tolerance to repeated pancreatic injury and becomes unresponsive to cholecystokinin stimuli. Therefore, Kras* accelerates tumorigenesis, whereas offers little protection against chronic pancreatitis in our mouse model.

R Figure 14

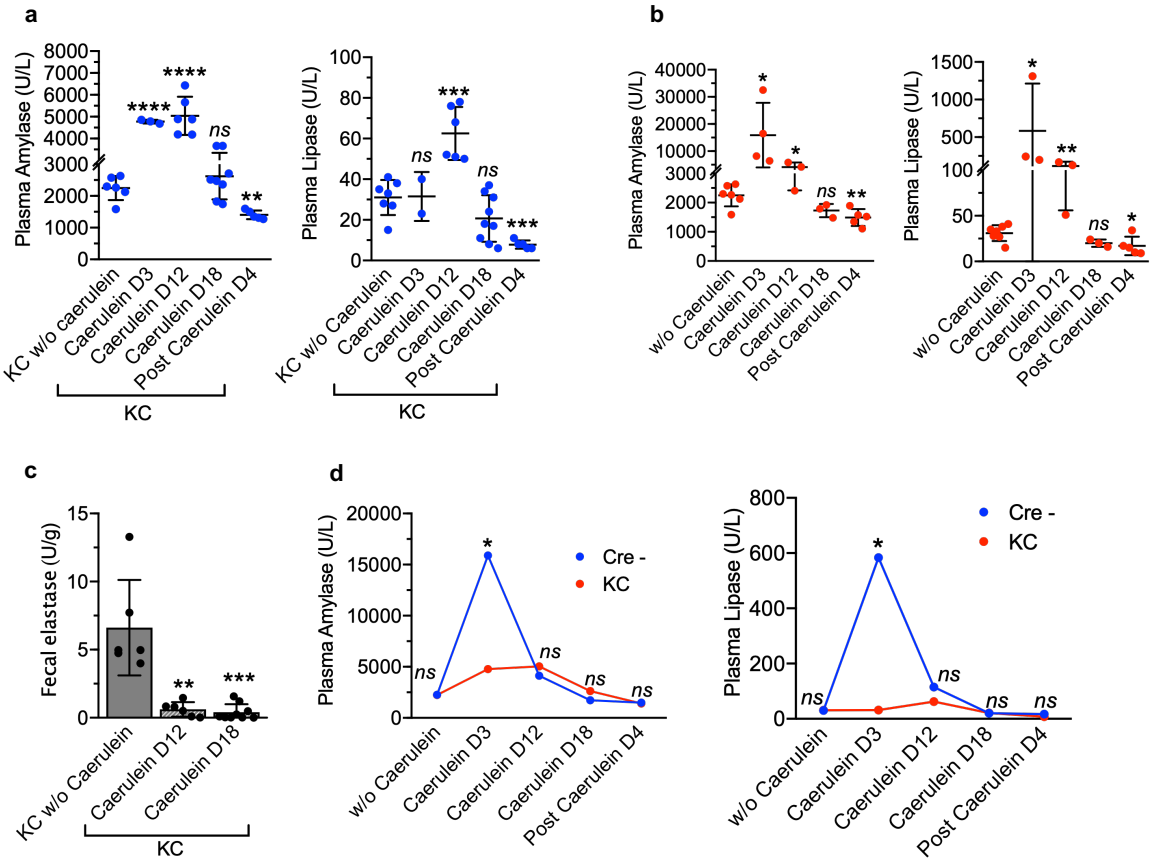

R Fig. 14: Kras* protects the pancreas against acute pancreatic injury. (a-b) Plasma amylase levels and lipase levels in KC mice **(a)**, and cre negative mice **(b)**, without caerulein Vs. caerulein treated mice at indicated experimental time points. **(c)** Fecal elastase levels in KC mice without caerulein Vs. caerulein treated mice. **(d)** Comparison of mean plasma amylase and lipase levels in Cre- Vs. KC mice with chronic pancreatitis. In (a-c), data represents mean ± SD. n = 2-9 mice in all cohorts. In (a), (b), (c) and (d), significance between groups was determined by Unpaired (parametric and non-parametric) T test. * P < 0.05, ** P < 0.01, *** P < 0.001, **** P < 0.0001, *ns*- not significant.

Chapter 7: **$CD4^+$ T cells regulate dendritic cells to facilitate pancreatic tumorigenesis in mice with underlying pancreatitis.**

i) Pancreatitis recruits $CD11c^+$ dendritic cells to the PDAC TME

Now that we established that T cells play distinct roles in spontaneously arising PDAC and PDAC arising in the setting of pancreatitis, we further probe the differences in the tumor microenvironment of the spontaneous and pancreatitis associated PDAC. Spontaneous KC mice and KC mice with acute pancreatitis had similar tumor stage as seen by tumor histology and CK19 immunostaining (**R Fig. 15a-b**). Analysis of different immune sub-populations from the TCGA datasets in PDAC patients with and without a history of chronic pancreatitis revealed a higher number of dendritic cells in patients with a history of chronic pancreatitis (**R Fig. 15c**). We used an online platform CIBERSORT to analyze relative abundances of a member cell type in a mixed population of bulk expression (RNA sequencing) data. Next, we analyzed if there were any differences in myeloid, macrophage and dendritic cell populations between spontaneous and pancreatitis associated PDAC in KC mice. There were no significant differences in $CD11b^+$ myeloid populations by CD11b by immunostaining between the two groups (**R Fig. 15d, e**), whereas there was a significantly higher infiltration of dendritic cells in pancreatitis associated PanINs (CD11c immunostaining, **R Fig. 15d, e**). Further, we compare the T cell infiltration in these stage-matched tumors. Among the $CD4^+$ T cells, there was no significant difference in the way the CD4+ T cells polarized [Spontaneous Vs. Pancreatitis associated PDAC: Tregs (44% Vs. 48%), T_H1(0.32% Vs. 0.4%), T_H2 (30% Vs. 23%), T_H17(21% Vs. 17%) (**R Fig.15f**).

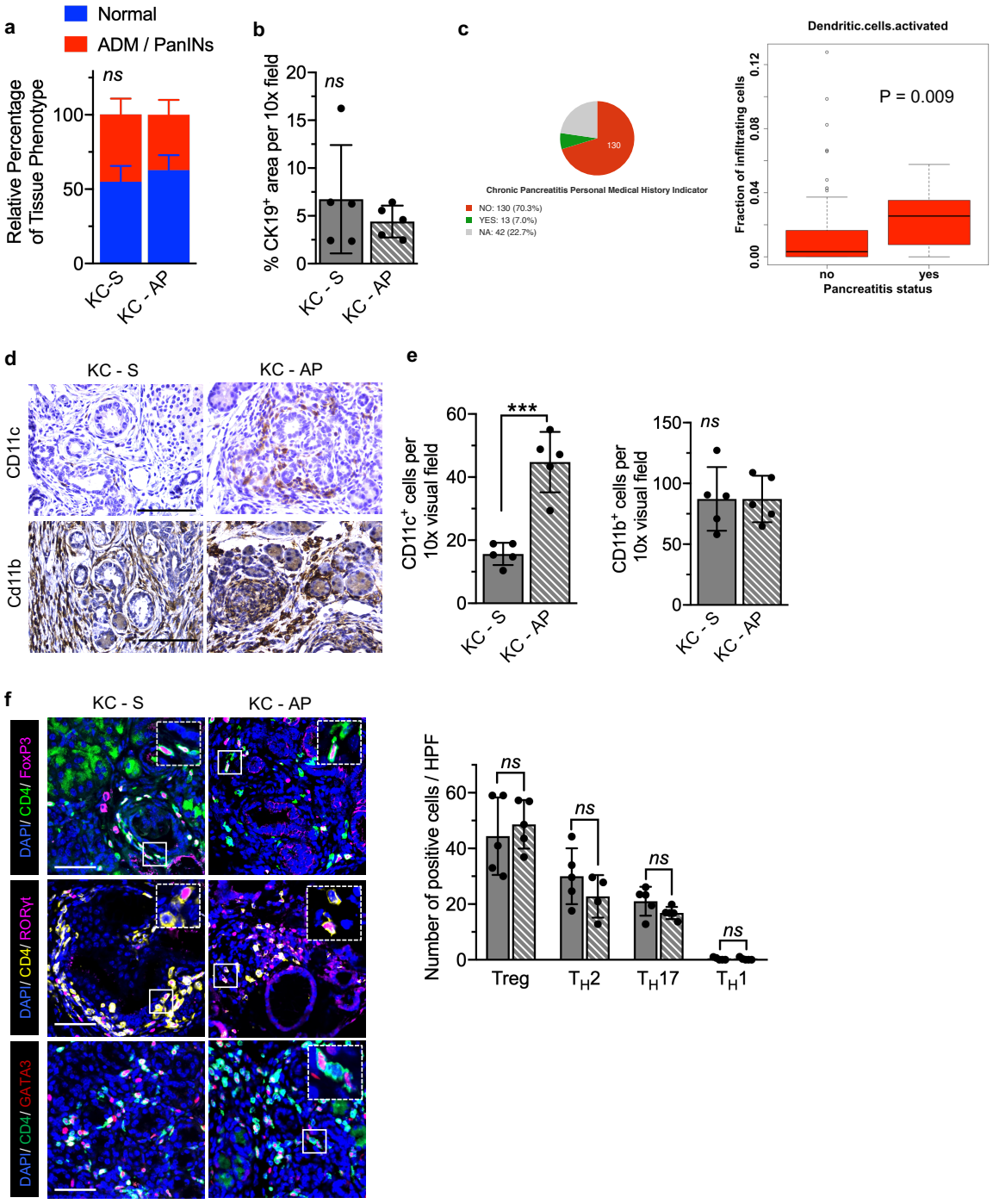

R Fig. 15: Pancreatitis recruits activated dendritic cells to the tumor microenvironment. (a) Relative percentages in histological phenotypes in spontaneous (KC-S) and acute pancreatitis (KC-AP) mice. **(b)** Quantification of CK19 positive area in the pancreas of KC-S and KC-AP mice. **(c)** Analyses of patients with known history of chronic pancreatitis from TCGA datasets. Dendritic cells as a fraction of tumor infiltrating cells from TCGA dataset (analyzed by CIBERSORT, P represents adjusted P value, FDR < 0.01). **(d-e)** Representative images of CD11c and CD11b

immunostaining in KC-S and KC-AP mice and quantification. **(f)** Representative images and quantification of CD4/FoxP3 (Treg), CD4/RoRγt (T_H17) and CD4/GATA3 (T_H2) immunolabelling in KC-S and KC-AP mice. In (a), (b), (e) and (f), data represents mean ± SD. In (a), significance was determined by two-way ANOVA and in (b), (e) and (f) significance was determined by Unpaired (parametric) T-test, *** P < 0.001, *ns*- not significant.

ii) $CD4^+$ T cells regulate dendritic cells to drive tumor initiation in mice with acute pancreatitis

Studies have shown that regulatory T cells inhibit tumor associated dendritic cells and restrain expression of co-stimulatory ligands necessary of activation of cytotoxic lymphocytes in PDAC(Jang et al., 2017). Therefore, we hypothesize that depletion of $CD4^+$ T lymphocytes removes the brakes on tumor associated dendritic cells in caerulein treated KC $CD4^{-/-}$ mice. In our spontaneous KC model of PDAC, the depletion of $CD4^+$ T cells did not result in restriction of tumor initiation due to lack of dendritic cells and antigen presentation in these tumors (**R Fig. 12a-c**). However, induction of pancreatitis resulting in accumulation of dendritic cells facilitate immune-modulation of these tumors. The depletion of the inhibitory $CD4^+$ cells in these KC mice with pancreatitis removes its inhibitory infiluence on the dendritic cells, enabling tumor growth inhibition in these mice. To establish that the activated dendritic cells restrict tumor initiation in the KC $CD4^{-/-}$ mice with pancreatitis, we deplete the dendritic cells in these mice with an inhibitory αCD11c antibody (**R Fig. 16a**). Depletion of $CD11c^+$ dendritic cells resulted in rescue of tumor initiation in the KC $CD4^{-/-}$ mice as seen by tumor histology and CK19 immunostaining (**R Fig. 16b-d**). In conclusion, $CD4^+$ T cells render dendritic cells tolerogenic in pancreatitis associated PDAC mice.

R Figure 16

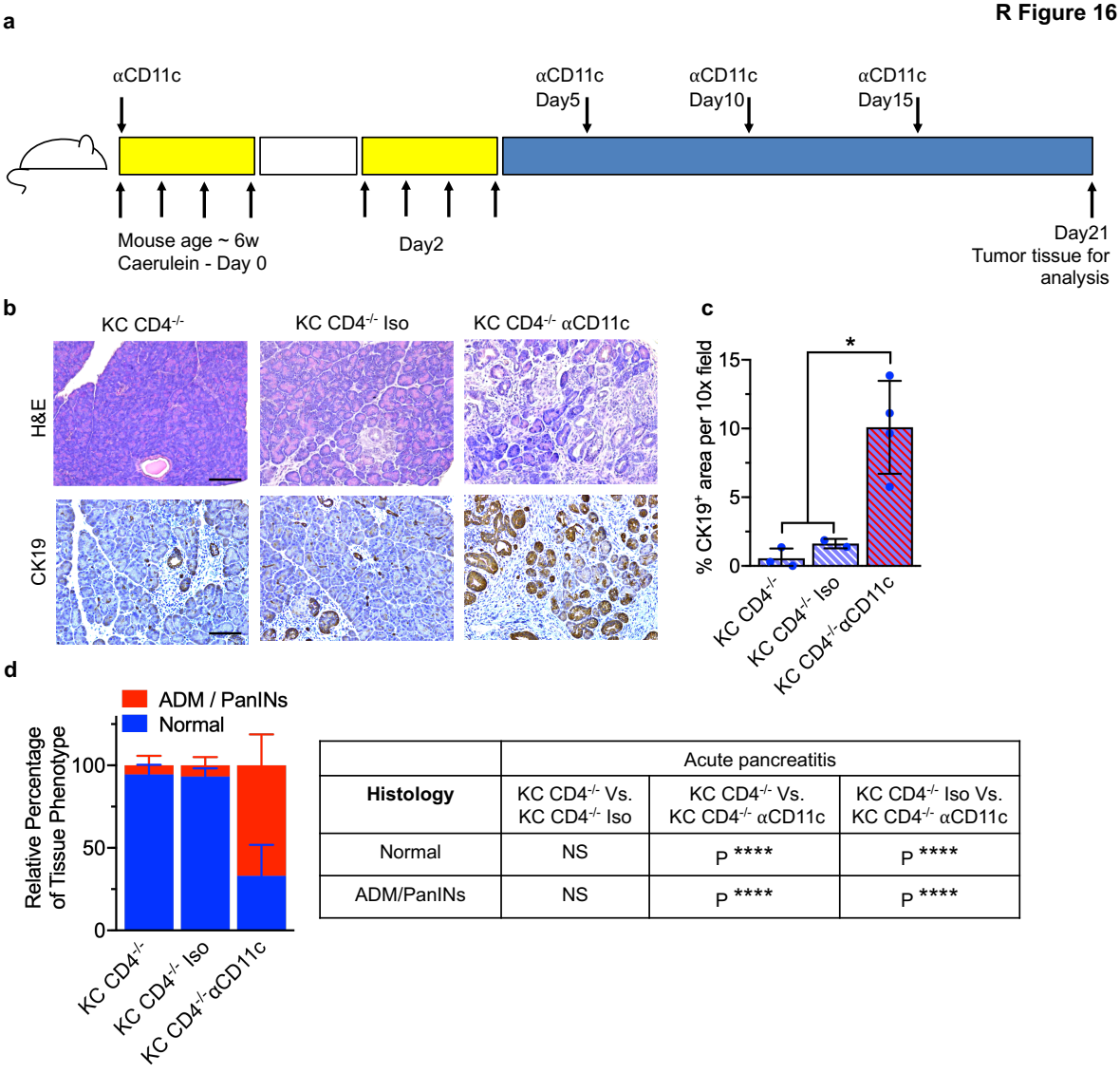

	Acute pancreatitis		
Histology	KC CD4$^{-/-}$ Vs. KC CD4$^{-/-}$ Iso	KC CD4$^{-/-}$ Vs. KC CD4$^{-/-}$ αCD11c	KC CD4$^{-/-}$ Iso Vs. KC CD4$^{-/-}$ αCD11c
Normal	NS	P ****	P ****
ADM/PanINs	NS	P ****	P ****

R Fig. 16: CD4^{+} T cells regulate dendritic cells to drive tumor initiation in mice with pancreatitis. (a) Schematic representation of acute pancreatitis induction with αCD11c or isotype treatment time points in KC CD4$^{-/-}$ mice. **(b)** Representative H&E and CK19 images of PanIN lesions of with αCD11c or isotype treated KC CD4$^{-/-}$ mice. **(c)** Quantification of CK19 positive area in the pancreas. **(d)** Relative percentages of histological phenotypes and two- way ANOVA table from (b). (KC CD4$^{-/-}$ (n = 5), KC CD4$^{-/-}$ Isotype (n = 4) and KC CD4$^{-/-}$ αCD11c (n = 4) mice. Data represents mean ± SD. In (c) significance was determined by Unpaired (parametric) T-test, * P < 0.05, **** P < 0.0001, *ns*- not significant.

iii) Pancreatitis renders the pancreatic TME sensitive to checkpoint blockade

Next, we question whether presence of underlying pancreatitis would render the pancreatic cancers sensitive to checkpoint blockade. Multiple studies in patients

and in pre-clinical models have established that checkpoint immunotherapy has failed to produce durable survival responses in PDAC. We investigate whether combination of αCTLA4/PD1 or αPD1 monotherapy would produce a tumor growth inhibitory response in KC mice in the presence of antigen presenting dendritic cells recruited during acute pancreatitis (**R Fig. 17a**). When the KC mice were sacrificed 3 weeks later for analysis of immunotherapy response, we observed that there was a decrease in PanINs in the αCTLA4/PD1 and αPD1 treated KC mice with pancreatitis compared to the Isotype and untreated KC mice with acute pancreatitis (**R Fig. 17b-c**). Therefore, we establish that presence of underlying pancreatitis sensitizes the tumor-microenvironment for checkpoint blockade in KC mice.

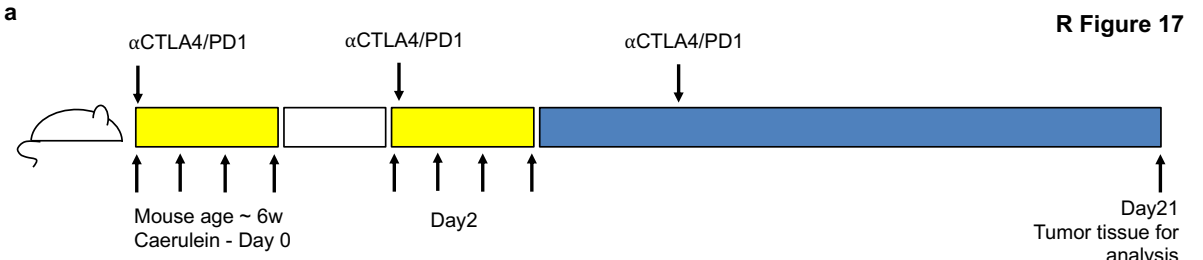

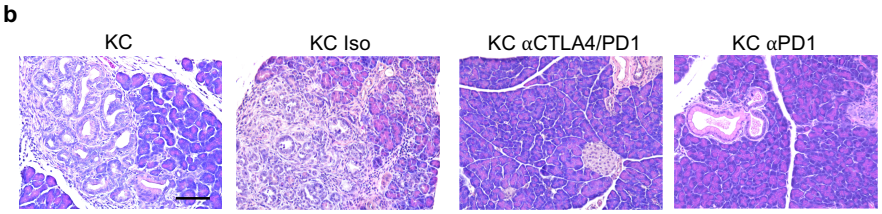

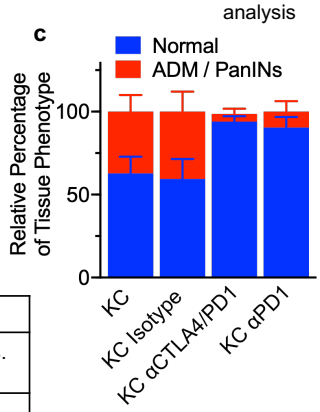

	Acute pancreatitis				
Histology	KC Vs. KC Iso	KC Vs. KC αCTLA4/PD1	KC Vs. KC αPD1	KC Iso Vs. KC αCTLA4/PD1	KC Iso Vs. KC αPD1
Normal	NS	P **	P *	P ***	P *
ADM/PanINs	NS	P ***	P *	P ***	P *

R Fig. 17: Pancreatitis renders the pancreatic TME sensitive to checkpoint blockade. **(a)** Schematic representation of acute pancreatitis induction with αCTLA4/PD1 or isotype treatment time points in KC mice. **(b)** Representative H&E images of PanIN lesions of with αCTLA4/PD1, αPD1 or isotype treated KC mice. **c**) Relative percentages in histological phenotypes and two-way ANOVA table from (b),

KC (n= 5), KC Isotype (n = 2), KC αPD1 (n = 2) and KC αCTLA4/PD1 (n=4). In (c), data represents mean ± SD. * P < 0.05, ** P < 0.01, *** P < 0.001.

Summary of results:

In this study, we first analyze how Kras* modulates the immune microenvironment in PDAC. We utilize an inducible and pancreas specific Kras* expressing murine model that can be manipulated by addition or withdrawal of doxycycline to control Kras expression. Extinction of Kras* led to global increases in T cell populations and reduction in the myeloid infiltrate in the TME. Although there was a reversal of immunosuppressive TME, we also found an increase in suppressor $CD4^+$ T lymphocyte population following Kras* extinction. Extinction of Kras* also resulted in improved survival of the PDAC mice, regression of established PDAC tumors, desmoplasia and chronic fibrosis. Next, we examine if the immune phenotype observed with the inducible murine model can be realized with a therapeutic agent targeting Kras*. Towards this end, we examine the impact of iExosomes targeting Kras* on the TME. We observed that following Kras* targeting therapy, multiple PDAC models demonstrate an increase in T cell population in the TME, mimicking the phenotype observed in the PiKP and PiKT mice. Next, we probe the functional contribution of distinct T cell populations that increase following iExosomes therapy in the TME. We crossed KPC with $CD4^{-/-}$ and $CD8^{-/-}$ mice to generate KPC, KPC $CD4^{-/-}$ and KPC $CD8^{-/-}$ mice cohorts.

Depletion of $CD4^+$ T lymphocytes enhanced the therapeutic efficacy of Kras* targeting compared to controls and CD8 knockout mice, whereas depletion of $CD8^+$ T lymphocytes diminished its therapeutic efficacy. Analysis of the role of $CD4^+$ and $CD8^+$ T cells in primary PDAC progression revealed similar tumor latency, median survival and proliferation in the KPC, KPC $CD4^{-/-}$ and KPC $CD8^{-/-}$ mice. However, the depletion

of $CD4^+$ T cells in a KPC model showed decreased liver metastasis compared to controls and CD8 knockout mice.

Next, we explore the differences between spontaneously arising PanINs and PanINs arising in a TME with underlying pancreatitis. We assess tumor initiation at an age matched time point (~200 days in all groups) between the KC, KC $CD4^{-/-}$ and KC $CD8^{-/-}$ mice. No differences in tumor initiation were observed between these groups in mice spontaneously developing tumors. However, in the setting of acute pancreatitis in these mice, KC $CD4^{-/-}$ mice did not develop PanIN lesions, suggesting that $CD4^+$ T cells promote tumorigenesis in mice with pancreatitis. Next, we confirmed our findings in KC $CD4^{-/-}$ mice with a chronic pancreatitis model. A phenotype similar to that observed in acute pancreatitis was observed in the chronic model. Further, we probe the differences in immune infiltrate between the spontaneous and pancreatitis driven KC mice cohorts. We observed an upregulation of $CD11c^+$ dendritic cells in the TME of KC mice with acute pancreatitis. In addition, a similar increase in dendritic cell population was also observed in the human PDAC patients with a known history of chronic pancreatitis. We probe the interactions between dendritic cells and $CD4^+$ T cells by depletion of $CD11c^+$ dendritic cells in the KC $CD4^{-/-}$ mice. Depletion of dendritic cells in KC $CD4^{-/-}$ mice rescued tumor initiation in the KC $CD4^{-/-}$ mice indicating that $CD4^+$ T cells inhibit dendritic cell populations, promoting tumorigenesis in KC mice with pancreatitis. Next, we assess if increased antigen presentation in KC mice with underlying pancreatitis render them sensitive to checkpoint blockade. Treatment of KC mice in a setting of acute pancreatitis with αCTLA4 and αPD1 antibody resulted in inhibition of tumorigenesis compared to the control and isotype treated KC mice.

However, treatment with αPD1 antibody alone resulted in a sub-optimal inhibition of tumorigenesis.

Chapter 8: **Discussion**

Role of Kras in shaping the PDAC TME*

Although mortality and disease outcomes of several cancers have improved substantially over the last decade, pancreatic cancer outcomes have only improved marginally (Fig. 1). One recent breakthrough that has improved disease outcomes in melanoma, non-small cell lung cancer and lymphomas is cancer immunotherapy. However, PDAC is among the cancers that is resistant to checkpoint immunotherapy (2, 3). The mechanisms behind a lack of response to immunotherapy remains poorly understood due to fundamental gaps in knowledge of understanding the immunobiology of PDAC.

One study that analyzed the fundamental differences in the tumor microenvironment of PDAC and melanoma attributed the lack of response to immunotherapy to a T cell deficient milieu and lack of T_H1 cells in PDAC (Blando et al., 2019). T cells function by cell-cell contact and hence proximity of the T cells to the tumor cells is an important predictor of T cell response in cancer(Carstens et al., 2017). Studies in murine colonic adenocarcinoma model with Kras* expression demonstrated that Kras* suppressed T cell infiltration, promotes MDSCs and rendered the Kras* mutant colonic adenocarcinomas resistant to checkpoint immunotherapy(Liao et al., 2019). However, clinical data in NSCLCs suggests that presence of mutant Kras rendered the lung cancers susceptible to checkpoint immunotherapy. The differences in disease phenotypes in these models most likely stem from the disparate roles of

Kras* in different tumor settings. While Kras* has been established to be a principle driver mutation in PDAC, Kras* mutation is not as ubiquitous in colonic adenocarcinoma or NSCLCs(Liu et al., 2020). A majority of NSCLCs do not have known driver mutations and mutations in Kras* might have varied roles in different tumor contexts in the presence of other passenger or co-existing driver mutations.

In our study, we use inducible iKras* GEMMs, with either P53 or Tgfbr2 conditional null alleles. Upon induction of Kras*, both the tumors exhibited similar dependency on Kras* for survival and growth, and enabled a comprehensive analysis of the role of Kras* on PDAC immune microenvironment. We probe the functional contribution of Kras* in shaping the TME by extinction of Kras* in mice with established PDAC. Our results suggest that Kras* plays an important role in creating a T cell deficient and myeloproliferative TME in PDAC that renders it resistant to T-cell targeting therapies. Genetic extinction of this oncogenic signal led to the recruitment of T cells, depletion of myeloid cells and transforms the immunologically 'cold' TME into a 'hot' one. Interestingly, Kras* extinction also increased the infiltration of immunosuppressive T regs in the TME in addition to reversing the T cell deficient and myeloproliferative TME. Further, consistency of the phenotype observed in two models with different co-existing mutations establishes that Kras* represents the principle driver in shaping the immune microenvironment in PDAC, and presence of other mutations did not affect the nature of the immune infiltrate. In addition to shaping the immune microenvironment, our results suggest that Kras* promotes desmoplasia and chronic fibrosis, two of which pose major challenges to delivery of drugs and T cell infiltration in PDAC(Provenzano et al., 2012).

Role of $CD4^+$ and $CD8^+$ T cells in PDAC progression

Next, we probe the role of $CD4^+$ and $CD8^+$ T cells in a spontaneously model of PDAC by depleting different T cell populations in KPC mice. Studies analyzing T cell infiltration in PDAC suggest that proximity of $CD8^+$ T cells to pancreatic cancer cells correlate with better survival outcomes(Carstens et al., 2017). T cells in PDAC can be classified as either pro-tumorigenic or anti-tumorigenic based on their specific roles in PDAC progression. Studies using murine PDAC models demonstrate that $\alpha\beta$ T cells(Daley et al., 2016), $CD4^+$ T cells(Zhang et al., 2014), T_H17 cells(McAllister et al., 2014), T_H2 cells(Dey et al., 2020) and $CD11b^+$(Zhang et al., 2017) myeloid cells promote tumorigenesis, whereas dendritic cells and $CD8^+$ T lymphocytes restrict PDAC progression(Jang et al., 2017, Pushalkar et al., 2018).

We utilize a murine PDAC (KPC model) that closely mimics the development of human pancreatic cancer to understand the effects of depletion of specific T cell populations. The KPC model represents a penetrant model for metastasis as more than half the mice develop liver metastasis and a small portion of the mice develop lung metastasis. However, unlike in humans, most mice in the KPC model die due to primary tumor burden rather than metastasis. In our KPC model, we found that depletion of $CD4^+$ T cells in PDAC, attenuated liver metastasis. Despite a trend towards decrease in lung metastasis, no significant differences were observed in lung metastasis with depletion of $CD4^+$ T cells as lung metastases were less frequent and not as robust as liver metastasis in the KPC model. However, depletion of $CD4^+$ or $CD8^+$ T cells did not alter primary tumor growth or survival. A similar murine breast cancer model that crossed the MMTV-PyMT model with the CD4 and CD8 knockout mice demonstrated decreased lung metastasis in the mice with depletion of $CD4^+$ T cells(DeNardo et al., 2009). The authors further demonstrate that $CD4^+$ T cells impact

metastasis by regulating Gr1- macrophages, which in turn promote metastasis in these murine breast cancer mice(DeNardo et al., 2009).

Adaptive immune response and gut microbiome in Kras targeting therapy:*

Next, we probe the specific roles of $CD4^+$ and $CD8^+$ T cells in the therapeutic targeting of $Kras^{G12D}$ mutation. We employed iExosomes to target Kras* in the context of $CD4^+$ and $CD8^+$ T cell depletion in the KPC model. We observed in our PiKP and PiKT models that Kras* extinction promotes T cell infiltration in the PDAC TME. Further, we question if such a dominant role of Kras* can be translated clinically using a therapeutic agent to target Kras*. iExosomes targeting Kras* demonstrated an increase in $CD4^+$ and $CD8^+$ T cell populations in the TME following Kras* targeting. Thus, the proof of concept studies firmly establish our hypothesis that Kras* predominantly drives T cell suppression, and that therapeutic Kras* targeting could potentially render the PDAC TME amenable to T cell targeting strategies. Depletion of $CD4^+$ T cells in the KPC model enhanced tumor growth inhibitory response following Kras targeting while depletion of $CD8^+$ T cells counteracted its benefits. Our results suggest that $CD4^+$ T cells are suppressive in nature (predominantly T regs, T_H2, T_H17 with minimal T_H1 infiltration) and constitute the majority of the T cell infiltrate in PDAC. Depletion of these immunosuppressive $CD4^+$ T cells facilitate the anti-tumor response of $CD8^+$ T cells in PDAC.

The gut microbiome has been demonstrated to exert a critical influence as an extrinsic modulator of T cell response in multiple studies of melanoma and NSCLCs(Gopalakrishnan et al., 2018, Sivan et al., 2015). Analysis of the intra-tumoral microbiome in human PDAC revealed that presence of Gammaproteobacteria in PDAC contributed to resistance to gemcitabine therapy(Geller et al., 2017).

Gammaproteobacteria degrades gemcitabine to its inactive form, 2′,2′-difluorodeoxyuridine. A murine study analyzing the impact of gut microbiome in PDAC demonstrated that the gut microbiome promotes tumorigenesis and tumor progression by restricting the $CD8^+$ T cell response(Pushalkar et al., 2018). Further, the authors demonstrate that the depletion of the gut microbiome renders PDAC tumors sensitive to checkpoint immunotherapy(Pushalkar et al., 2018). In contrast to the previously published data, our data suggests that depletion of the gut microbiome did not alter tumorigenesis or Kras* targeting response. However, the gut microbiome facilitates $CD4^+$ T cells and depletion of the gut microbiome together with $CD4^+$ T cells significantly improved the survival of pancreatic cancer mice following Kras* targeting therapy. The presence of $CD4^+$ T cells over-ride the effects of depletion of gut microbiome in our PDAC model.

Impact of pancreatitis on adaptive immune response in PDAC:

In the next part of our study, we question how underlying pancreatitis alters the tumor microenvironment and disease progression in PDAC. Analysis of TCGA datasets revealed that ~10% of PDAC patients have had a known history of chronic pancreatitis. Further analysis revealed that these patients had a higher proportion of dendritic cells in their TME, suggesting enhanced antigen presentation in the tumor microenvironment of these mice. In addition to patients with a known history of chronic pancreatitis, obstruction or invasion of the hepato-pancreatic duct during the course of pancreatic cancer can evoke pancreatitis in a substantial portion of patients. We hypothesize that presence of pancreatitis in PDAC functionally alters the nature of the TME and opens new opportunities for targeting the adoptive immune response in PDAC.

We observed no difference in tumorigenesis in our KC mice with depletion of $CD4^+$ and $CD8^+$ T cells. However, other studies that used murine models of PDAC to analyze the role of $CD4^+$ and $CD8^+$ T cells in PDAC demonstrated that $CD4^+$ T cells promotes tumorigenesis(McAllister et al., 2014, Zhang et al., 2014). When we probed the reasons for difference in phenotype between our model and that of others, we found that the other studies utilize a caerulein induced pancreatitis model, whereas our study analyzed the impact of T cells in a spontaneously progressing model of PDAC. Chronic pancreatitis poses a significant risk factor for the development of PDAC. Multiple murine models of PDAC have shown chronic pancreatitis to accelerate the progression of PDAC. Next, we see if we could replicate the findings from other studies in our murine models. Induction of pancreatitis altered the functional outcome of the $CD4^+$ T cells in our model. We observed that in the setting of both acute and chronic pancreatitis, $CD4^+$ T cells promote tumorigenesis. These findings led us to analyze the functional differences in the pancreatic immune microenvironment induced by the presence of underlying pancreatitis. We found no differences in myeloid, T_H1, T_H2, T_H17 and regulatory T cells between the spontaneous and the pancreatitis induced models of tumorigenesis. The pancreatitis induced KC mice, however demonstrated higher number of $CD11c^+$ dendritic cells compared to the spontaneously progressing PDAC mice. The similarities in the dendritic cell phenotypes induced by pancreatitis between the human datasets and our murine models prompted us to further explore the cross talk between dendritic cells and $CD4^+$ T cells in the KC models with pancreatitis. We hypothesize that the $CD4^+$ T cells exert inhibitory influence of dendritic cells thereby prevent the development of an anti-tumor response. Therefore, depletion of $CD4^+$ T cells in a pancreatitis setting that recruit dendritic cells to the TME prevent tumorigenesis. Further, depletion of dendritic cells in the $CD4^+$ T cell depleted mice

rescued tumor development in these mice highlighting the importance of dendritic cell-$CD4^+$ T cell axis in the TME.

Role of dendritic cells in sensitizing the PDAC TME to immunotherapy

Next, we examine if the dendritic cells recruited in the process of pancreatitis render the KC mice susceptible to checkpoint blockade. Several lines of studies demonstrate that checkpoint immunotherapies failed to produce tumor growth inhibition in clinical trial and preclinical models of PDAC (2,3). However, in the setting of acute pancreatitis, combination checkpoint blockade with αCTLA4 and αPD1 antibodies inhibit tumorigenesis, whereas monotherapy with αPD1 produced a partial tumor inhibitory response. Collectively, our findings suggest that presence of activated dendritic cells in the TME renders the KC mice sensitive to checkpoint blockade. Collectively, our results offer rationale for stratification of patients with underlying pancreatitis specifically for immunotherapy approaches in clinical trials.

Conclusion:

Our results offer mechanistic insights into the role of Kras* in shaping the immune microenvironment in PDAC. The study demonstrates the potential for combining Kras* and $CD4^+$ T cell targeting therapies in PDAC. Further, our study offers novel and systematic insights into how pancreatitis fundamentally alters the nature of the TME. This novel finding opened a whole new range of therapeutic opportunities from utilization of dendritic cell vaccines to stratifying patients for checkpoint immunotherapy in clinical trials.

Bibliography:

http://www.microbial-earth.org. [Online]. Available: http://www.microbial-earth.org [Accessed].

https://seer.cancer.gov/statfacts/html/pancreas.html.

AGUIRRE, A. J., BARDEESY, N., SINHA, M., LOPEZ, L., TUVESON, D. A., HORNER, J., REDSTON, M. S. & DEPINHO, R. A. 2003. Activated Kras and Ink4a/Arf deficiency cooperate to produce metastatic pancreatic ductal adenocarcinoma. *Genes Dev,* 17**,** 3112-26.

ALLEN, P. J., KUK, D., CASTILLO, C. F., BASTURK, O., WOLFGANG, C. L., CAMERON, J. L., LILLEMOE, K. D., FERRONE, C. R., MORALES-OYARVIDE, V., HE, J., WEISS, M. J., HRUBAN, R. H., GONEN, M., KLIMSTRA, D. S. & MINO-KENUDSON, M. 2017. Multi-institutional Validation Study of the American Joint Commission on Cancer (8th Edition) Changes for T and N Staging in Patients With Pancreatic Adenocarcinoma. *Ann Surg,* 265**,** 185-191.

BARDEESY, N., CHENG, K. H., BERGER, J. H., CHU, G. C., PAHLER, J., OLSON, P., HEZEL, A. F., HORNER, J., LAUWERS, G. Y., HANAHAN, D. & DEPINHO, R. A. 2006. Smad4 is dispensable for normal pancreas development yet critical in progression and tumor biology of pancreas cancer. *Genes Dev,* 20**,** 3130-46.

BLANDO, J., SHARMA, A., HIGA, M. G., ZHAO, H., VENCE, L., YADAV, S. S., KIM, J., SEPULVEDA, A. M., SHARP, M., MAITRA, A., WARGO, J., TETZLAFF, M., BROADDUS, R., KATZ, M. H. G., VARADHACHARY, G. R., OVERMAN, M., WANG, H., YEE, C., BERNATCHEZ, C., IACOBUZIO-DONAHUE, C., BASU, S., ALLISON, J. P. & SHARMA, P. 2019. Comparison of immune infiltrates in melanoma and pancreatic cancer highlights VISTA as a potential target in pancreatic cancer. *Proc Natl Acad Sci U S A,* 116**,** 1692-1697.

CAPORASO, J. G., LAUBER, C. L., WALTERS, W. A., BERG-LYONS, D., HUNTLEY, J., FIERER, N., OWENS, S. M., BETLEY, J., FRASER, L., BAUER, M., GORMLEY, N., GILBERT, J. A., SMITH, G. & KNIGHT, R. 2012. Ultra-high-throughput microbial community analysis on the Illumina HiSeq and MiSeq platforms. *ISME J,* 6**,** 1621-4.

CARSTENS, J. L., CORREA DE SAMPAIO, P., YANG, D., BARUA, S., WANG, H., RAO, A., ALLISON, J. P., LEBLEU, V. S. & KALLURI, R. 2017. Spatial computation of intratumoral T cells correlates with survival of patients with pancreatic cancer. *Nat Commun,* 8**,** 15095.

CHAO, M. P., WEISSMAN, I. L. & MAJETI, R. 2012. The CD47-SIRPalpha pathway in cancer immune evasion and potential therapeutic implications. *Curr Opin Immunol,* 24**,** 225-32.

CHYTIL, A., MAGNUSON, M. A., WRIGHT, C. V. & MOSES, H. L. 2002. Conditional inactivation of the TGF-beta type II receptor using Cre:Lox. *Genesis,* 32**,** 73-5.

COLLINS, M. A., BEDNAR, F., ZHANG, Y., BRISSET, J. C., GALBAN, S., GALBAN, C. J., RAKSHIT, S., FLANNAGAN, K. S., ADSAY, N. V. & PASCA DI MAGLIANO, M. 2012. Oncogenic Kras is required for both the initiation and maintenance of pancreatic cancer in mice. *J Clin Invest,* 122**,** 639-53.

COMMISSO, C., DAVIDSON, S. M., SOYDANER-AZELOGLU, R. G., PARKER, S. J., KAMPHORST, J. J., HACKETT, S., GRABOCKA, E., NOFAL, M., DREBIN, J. A., THOMPSON, C. B., RABINOWITZ, J. D., METALLO, C. M., VANDER HEIDEN, M. G. & BAR-SAGI, D. 2013. Macropinocytosis of protein is an amino acid supply route in Ras-transformed cells. *Nature,* 497**,** 633-7.

CONROY, T., DESSEIGNE, F., YCHOU, M., BOUCHE, O., GUIMBAUD, R., BECOUARN, Y., ADENIS, A., RAOUL, J. L., GOURGOU-BOURGADE, S., DE LA FOUCHARDIERE, C., BENNOUNA, J.,

BACHET, J. B., KHEMISSA-AKOUZ, F., PERE-VERGE, D., DELBALDO, C., ASSENAT, E., CHAUFFERT, B., MICHEL, P., MONTOTO-GRILLOT, C., DUCREUX, M., GROUPE TUMEURS DIGESTIVES OF, U. & INTERGROUP, P. 2011. FOLFIRINOX versus gemcitabine for metastatic pancreatic cancer. *N Engl J Med,* 364**,** 1817-25.

CONROY, T., HAMMEL, P., HEBBAR, M., BEN ABDELGHANI, M., WEI, A. C., RAOUL, J. L., CHONE, L., FRANCOIS, E., ARTRU, P., BIAGI, J. J., LECOMTE, T., ASSENAT, E., FAROUX, R., YCHOU, M., VOLET, J., SAUVANET, A., BREYSACHER, G., DI FIORE, F., CRIPPS, C., KAVAN, P., TEXEREAU, P., BOUHIER-LEPORRIER, K., KHEMISSA-AKOUZ, F., LEGOUX, J. L., JUZYNA, B., GOURGOU, S., O'CALLAGHAN, C. J., JOUFFROY-ZELLER, C., RAT, P., MALKA, D., CASTAN, F., BACHET, J. B., CANADIAN CANCER TRIALS, G. & THE UNICANCER, G. I. P. G. 2018. FOLFIRINOX or Gemcitabine as Adjuvant Therapy for Pancreatic Cancer. *N Engl J Med,* 379**,** 2395-2406.

COX, A. D., FESIK, S. W., KIMMELMAN, A. C., LUO, J. & DER, C. J. 2014. Drugging the undruggable RAS: Mission possible? *Nat Rev Drug Discov,* 13**,** 828-51.

DALEY, D., ZAMBIRINIS, C. P., SEIFERT, L., AKKAD, N., MOHAN, N., WERBA, G., BARILLA, R., TORRES-HERNANDEZ, A., HUNDEYIN, M., MANI, V. R. K., AVANZI, A., TIPPENS, D., NARAYANAN, R., JANG, J. E., NEWMAN, E., PILLARISETTY, V. G., DUSTIN, M. L., BAR-SAGI, D., HAJDU, C. & MILLER, G. 2016. gammadelta T Cells Support Pancreatic Oncogenesis by Restraining alphabeta T Cell Activation. *Cell,* 166**,** 1485-1499 e15.

DENARDO, D. G., BARRETO, J. B., ANDREU, P., VASQUEZ, L., TAWFIK, D., KOLHATKAR, N. & COUSSENS, L. M. 2009. CD4(+) T cells regulate pulmonary metastasis of mammary carcinomas by enhancing protumor properties of macrophages. *Cancer Cell,* 16**,** 91-102.

DEY, P., LI, J., ZHANG, J., CHAURASIYA, S., STROM, A., WANG, H., LIAO, W. T., CAVALLARO, F., DENZ, P., BERNARD, V., YEN, E. Y., GENOVESE, G., GULHATI, P., LIU, J., CHAKRAVARTI, D., DENG, P., ZHANG, T., CARBONE, F., CHANG, Q., YING, H., SHANG, X., SPRING, D. J., GHOSH, B., PUTLURI, N., MAITRA, A., WANG, Y. A. & DEPINHO, R. A. 2020. Oncogenic KRAS-Driven Metabolic Reprogramming in Pancreatic Cancer Cells Utilizes Cytokines from the Tumor Microenvironment. *Cancer Discov,* 10**,** 608-625.

EL-ANDALOUSSI, S., LEE, Y., LAKHAL-LITTLETON, S., LI, J., SEOW, Y., GARDINER, C., ALVAREZ-ERVITI, L., SARGENT, I. L. & WOOD, M. J. 2012. Exosome-mediated delivery of siRNA in vitro and in vivo. *Nat Protoc,* 7**,** 2112-26.

ENGLE, D. D., TIRIAC, H., RIVERA, K. D., POMMIER, A., WHALEN, S., ONI, T. E., ALAGESAN, B., LEE, E. J., YAO, M. A., LUCITO, M. S., SPIELMAN, B., DA SILVA, B., SCHOEPFER, C., WRIGHT, K., CREIGHTON, B., AFINOWICZ, L., YU, K. H., GRUTZMANN, R., AUST, D., GIMOTTY, P. A., POLLARD, K. S., HRUBAN, R. H., GOGGINS, M. G., PILARSKY, C., PARK, Y., PAPPIN, D. J., HOLLINGSWORTH, M. A. & TUVESON, D. A. 2019. The glycan CA19-9 promotes pancreatitis and pancreatic cancer in mice. *Science,* 364**,** 1156-1162.

EVANS, R. A., DIAMOND, M. S., RECH, A. J., CHAO, T., RICHARDSON, M. W., LIN, J. H., BAJOR, D. L., BYRNE, K. T., STANGER, B. Z., RILEY, J. L., MARKOSYAN, N., WINOGRAD, R. & VONDERHEIDE, R. H. 2016. Lack of immunoediting in murine pancreatic cancer reversed with neoantigen. *JCI Insight,* 1.

FUNG-LEUNG, W. P., SCHILHAM, M. W., RAHEMTULLA, A., KUNDIG, T. M., VOLLENWEIDER, M., POTTER, J., VAN EWIJK, W. & MAK, T. W. 1991. CD8 is needed for development of cytotoxic T cells but not helper T cells. *Cell,* 65**,** 443-9.

GELLER, L. T., BARZILY-ROKNI, M., DANINO, T., JONAS, O. H., SHENTAL, N., NEJMAN, D., GAVERT, N., ZWANG, Y., COOPER, Z. A., SHEE, K., THAISS, C. A., REUBEN, A., LIVNY, J., AVRAHAM, R., FREDERICK, D. T., LIGORIO, M., CHATMAN, K., JOHNSTON, S. E., MOSHER, C. M., BRANDIS, A., FUKS, G., GURBATRI, C., GOPALAKRISHNAN, V., KIM, M., HURD, M. W., KATZ, M., FLEMING, J., MAITRA, A., SMITH, D. A., SKALAK, M., BU, J., MICHAUD, M., TRAUGER, S. A., BARSHACK, I., GOLAN, T., SANDBANK, J., FLAHERTY, K. T., MANDINOVA, A., GARRETT, W. S., THAYER, S. P., FERRONE, C. R., HUTTENHOWER, C., BHATIA, S. N., GEVERS, D., WARGO, J. A., GOLUB, T. R. & STRAUSSMAN, R. 2017. Potential role of intratumor bacteria in mediating tumor resistance to the chemotherapeutic drug gemcitabine. *Science,* 357**,** 1156-1160.

GOPALAKRISHNAN, V., SPENCER, C. N., NEZI, L., REUBEN, A., ANDREWS, M. C., KARPINETS, T. V., PRIETO, P. A., VICENTE, D., HOFFMAN, K., WEI, S. C., COGDILL, A. P., ZHAO, L., HUDGENS, C. W., HUTCHINSON, D. S., MANZO, T., PETACCIA DE MACEDO, M., COTECHINI, T., KUMAR, T., CHEN, W. S., REDDY, S. M., SZCZEPANIAK SLOANE, R., GALLOWAY-PENA, J., JIANG, H., CHEN, P. L., SHPALL, E. J., REZVANI, K., ALOUSI, A. M., CHEMALY, R. F., SHELBURNE, S., VENCE, L. M., OKHUYSEN, P. C., JENSEN, V. B., SWENNES, A. G., MCALLISTER, F., MARCELO RIQUELME SANCHEZ, E., ZHANG, Y., LE CHATELIER, E., ZITVOGEL, L., PONS, N., AUSTIN-BRENEMAN, J. L., HAYDU, L. E., BURTON, E. M., GARDNER, J. M., SIRMANS, E., HU, J., LAZAR, A. J., TSUJIKAWA, T., DIAB, A., TAWBI, H., GLITZA, I. C., HWU, W. J., PATEL, S. P., WOODMAN, S. E., AMARIA, R. N., DAVIES, M. A., GERSHENWALD, J. E., HWU, P., LEE, J. E., ZHANG, J., COUSSENS, L. M., COOPER, Z. A., FUTREAL, P. A., DANIEL, C. R., AJAMI, N. J., PETROSINO, J. F., TETZLAFF, M. T., SHARMA, P., ALLISON, J. P., JENQ, R. R. & WARGO, J. A. 2018. Gut microbiome

modulates response to anti-PD-1 immunotherapy in melanoma patients. *Science,* 359**,** 97-103.

HABBE, N., SHI, G., MEGUID, R. A., FENDRICH, V., ESNI, F., CHEN, H., FELDMANN, G., STOFFERS, D. A., KONIECZNY, S. F., LEACH, S. D. & MAITRA, A. 2008. Spontaneous induction of murine pancreatic intraepithelial neoplasia (mPanIN) by acinar cell targeting of oncogenic Kras in adult mice. *Proc Natl Acad Sci U S A,* 105**,** 18913-8.

HINGORANI, S. R., WANG, L., MULTANI, A. S., COMBS, C., DERAMAUDT, T. B., HRUBAN, R. H., RUSTGI, A. K., CHANG, S. & TUVESON, D. A. 2005. Trp53R172H and KrasG12D cooperate to promote chromosomal instability and widely metastatic pancreatic ductal adenocarcinoma in mice. *Cancer Cell,* 7**,** 469-83.

HODI, F. S., O'DAY, S. J., MCDERMOTT, D. F., WEBER, R. W., SOSMAN, J. A., HAANEN, J. B., GONZALEZ, R., ROBERT, C., SCHADENDORF, D., HASSEL, J. C., AKERLEY, W., VAN DEN EERTWEGH, A. J., LUTZKY, J., LORIGAN, P., VAUBEL, J. M., LINETTE, G. P., HOGG, D., OTTENSMEIER, C. H., LEBBE, C., PESCHEL, C., QUIRT, I., CLARK, J. I., WOLCHOK, J. D., WEBER, J. S., TIAN, J., YELLIN, M. J., NICHOL, G. M., HOOS, A. & URBA, W. J. 2010. Improved survival with ipilimumab in patients with metastatic melanoma. *N Engl J Med,* 363**,** 711-23.

HRUBAN, R. H. & FUKUSHIMA, N. 2007. Pancreatic adenocarcinoma: update on the surgical pathology of carcinomas of ductal origin and PanINs. *Mod Pathol,* 20 Suppl 1**,** S61-70.

HTTPS://SEER.CANCER.GOV/STATFACTS/HTML/PANCREAS.HTML.

JANG, J. E., HAJDU, C. H., LIOT, C., MILLER, G., DUSTIN, M. L. & BAR-SAGI, D. 2017. Crosstalk between Regulatory T Cells and Tumor-Associated Dendritic Cells Negates Anti-tumor Immunity in Pancreatic Cancer. *Cell Rep,* 20**,** 558-571.

KAMERKAR, S., LEBLEU, V. S., SUGIMOTO, H., YANG, S., RUIVO, C. F., MELO, S. A., LEE, J. J. & KALLURI, R. 2017. Exosomes facilitate therapeutic targeting of oncogenic KRAS in pancreatic cancer. *Nature,* 546**,** 498-503.

LAMM, D. L., BLUMENSTEIN, B. A., CRAWFORD, E. D., MONTIE, J. E., SCARDINO, P., GROSSMAN, H. B., STANISIC, T. H., SMITH, J. A., JR., SULLIVAN, J., SAROSDY, M. F. & ET AL. 1991. A randomized trial of intravesical doxorubicin and immunotherapy with bacille Calmette-Guerin for transitional-cell carcinoma of the bladder. *N Engl J Med,* 325**,** 1205-9.

LE, D. T., LUTZ, E., URAM, J. N., SUGAR, E. A., ONNERS, B., SOLT, S., ZHENG, L., DIAZ, L. A., JR., DONEHOWER, R. C., JAFFEE, E. M. & LAHERU, D. A. 2013. Evaluation of ipilimumab in combination with allogeneic pancreatic tumor cells transfected with a GM-CSF gene in previously treated pancreatic cancer. *J Immunother,* 36**,** 382-9.

LIAO, W., OVERMAN, M. J., BOUTIN, A. T., SHANG, X., ZHAO, D., DEY, P., LI, J., WANG, G., LAN, Z., LI, J., TANG, M., JIANG, S., MA, X., CHEN, P., KATKHUDA, R., KORPHAISARN, K., CHAKRAVARTI, D., CHANG, A., SPRING, D. J., CHANG, Q., ZHANG, J., MARU, D. M., MAEDA, D. Y., ZEBALA, J. A., KOPETZ, S., WANG, Y. A. & DEPINHO, R. A. 2019. KRAS-IRF2 Axis Drives Immune Suppression and Immune Therapy Resistance in Colorectal Cancer. *Cancer Cell,* 35**,** 559-572 e7.

LIU, C., ZHENG, S., JIN, R., WANG, X., WANG, F., ZANG, R., XU, H., LU, Z., HUANG, J., LEI, Y., MAO, S., WANG, Y., FENG, X., SUN, N., WANG, Y. & HE, J. 2020. The superior efficacy of anti-PD-1/PD-L1 immunotherapy in KRAS-mutant non-small cell lung cancer that correlates with an inflammatory phenotype and increased immunogenicity. *Cancer Lett,* 470**,** 95-105.

MCALLISTER, F., BAILEY, J. M., ALSINA, J., NIRSCHL, C. J., SHARMA, R., FAN, H., RATTIGAN, Y., ROESER, J. C., LANKAPALLI, R. H., ZHANG, H., JAFFEE, E. M., DRAKE, C. G., HOUSSEAU, F., MAITRA, A., KOLLS, J. K., SEARS, C. L., PARDOLL, D. M. & LEACH, S. D. 2014. Oncogenic Kras activates a hematopoietic-to-epithelial IL-17 signaling axis in preinvasive pancreatic neoplasia. *Cancer Cell,* 25**,** 621-37.

MENDT, M., KAMERKAR, S., SUGIMOTO, H., MCANDREWS, K. M., WU, C. C., GAGEA, M., YANG, S., BLANKO, E. V. R., PENG, Q., MA, X., MARSZALEK, J. R., MAITRA, A., YEE, C., REZVANI, K., SHPALL, E., LEBLEU, V. S. & KALLURI, R. 2018. Generation and testing of clinical-grade exosomes for pancreatic cancer. *JCI Insight,* 3.

NEOPTOLEMOS, J. P., STOCKEN, D. D., FRIESS, H., BASSI, C., DUNN, J. A., HICKEY, H., BEGER, H., FERNANDEZ-CRUZ, L., DERVENIS, C., LACAINE, F., FALCONI, M., PEDERZOLI, P., PAP, A., SPOONER, D., KERR, D. J., BUCHLER, M. W. & EUROPEAN STUDY GROUP FOR PANCREATIC, C. 2004. A randomized trial of chemoradiotherapy and chemotherapy after resection of pancreatic cancer. *N Engl J Med,* 350**,** 1200-10.

OLIVE, K. P., JACOBETZ, M. A., DAVIDSON, C. J., GOPINATHAN, A., MCINTYRE, D., HONESS, D., MADHU, B., GOLDGRABEN, M. A., CALDWELL, M. E., ALLARD, D., FRESE, K. K., DENICOLA, G., FEIG, C., COMBS, C., WINTER, S. P., IRELAND-ZECCHINI, H., REICHELT, S., HOWAT, W. J., CHANG, A., DHARA, M., WANG, L., RUCKERT, F., GRUTZMANN, R., PILARSKY, C., IZERADJENE, K., HINGORANI, S. R., HUANG, P., DAVIES, S. E., PLUNKETT, W., EGORIN, M., HRUBAN, R. H., WHITEBREAD, N., MCGOVERN, K., ADAMS, J., IACOBUZIO-DONAHUE, C., GRIFFITHS, J. & TUVESON, D. A. 2009. Inhibition of Hedgehog signaling enhances delivery of chemotherapy in a mouse model of pancreatic cancer. *Science,* 324**,** 1457-61.

OSTREM, J. M., PETERS, U., SOS, M. L., WELLS, J. A. & SHOKAT, K. M. 2013. K-Ras(G12C) inhibitors allosterically control GTP affinity and effector interactions. *Nature,* 503**,** 548-51.

POUR, P. M., PANDEY, K. K. & BATRA, S. K. 2003. What is the origin of pancreatic adenocarcinoma? *Mol Cancer,* 2**,** 13.

PROVENZANO, P. P., CUEVAS, C., CHANG, A. E., GOEL, V. K., VON HOFF, D. D. & HINGORANI, S. R. 2012. Enzymatic targeting of the stroma ablates physical barriers to treatment of pancreatic ductal adenocarcinoma. *Cancer Cell,* 21**,** 418-29.

PUSHALKAR, S., HUNDEYIN, M., DALEY, D., ZAMBIRINIS, C. P., KURZ, E., MISHRA, A., MOHAN, N., AYKUT, B., USYK, M., TORRES, L. E., WERBA, G., ZHANG, K., GUO, Y., LI, Q., AKKAD, N., LALL, S., WADOWSKI, B., GUTIERREZ, J., KOCHEN ROSSI, J. A., HERZOG, J. W., DISKIN, B., TORRES-HERNANDEZ, A., LEINWAND, J., WANG, W., TAUNK, P. S., SAVADKAR, S., JANAL, M., SAXENA, A., LI, X., COHEN, D., SARTOR, R. B., SAXENA, D. & MILLER, G. 2018. The Pancreatic Cancer Microbiome Promotes Oncogenesis by Induction of Innate and Adaptive Immune Suppression. *Cancer Discov,* 8**,** 403-416.

RAHEMTULLA, A., FUNG-LEUNG, W. P., SCHILHAM, M. W., KUNDIG, T. M., SAMBHARA, S. R., NARENDRAN, A., ARABIAN, A., WAKEHAM, A., PAIGE, C. J., ZINKERNAGEL, R. M. & ET AL. 1991. Normal development and function of CD8+ cells but markedly decreased helper cell activity in mice lacking CD4. *Nature,* 353**,** 180-4.

RIQUELME, E., ZHANG, Y., ZHANG, L., MONTIEL, M., ZOLTAN, M., DONG, W., QUESADA, P., SAHIN, I., CHANDRA, V., SAN LUCAS, A., SCHEET, P., XU, H., HANASH, S. M., FENG, L., BURKS, J. K., DO, K. A., PETERSON, C. B., NEJMAN, D., TZENG, C. D., KIM, M. P., SEARS, C. L., AJAMI, N., PETROSINO, J., WOOD, L. D., MAITRA, A., STRAUSSMAN, R., KATZ, M.,

WHITE, J. R., JENQ, R., WARGO, J. & MCALLISTER, F. 2019. Tumor Microbiome Diversity and Composition Influence Pancreatic Cancer Outcomes. *Cell,* 178**,** 795-806 e12.

ROUTY, B., LE CHATELIER, E., DEROSA, L., DUONG, C. P. M., ALOU, M. T., DAILLERE, R., FLUCKIGER, A., MESSAOUDENE, M., RAUBER, C., ROBERTI, M. P., FIDELLE, M., FLAMENT, C., POIRIER-COLAME, V., OPOLON, P., KLEIN, C., IRIBARREN, K., MONDRAGON, L., JACQUELOT, N., QU, B., FERRERE, G., CLEMENSON, C., MEZQUITA, L., MASIP, J. R., NALTET, C., BROSSEAU, S., KADERBHAI, C., RICHARD, C., RIZVI, H., LEVENEZ, F., GALLERON, N., QUINQUIS, B., PONS, N., RYFFEL, B., MINARD-COLIN, V., GONIN, P., SORIA, J. C., DEUTSCH, E., LORIOT, Y., GHIRINGHELLI, F., ZALCMAN, G., GOLDWASSER, F., ESCUDIER, B., HELLMANN, M. D., EGGERMONT, A., RAOULT, D., ALBIGES, L., KROEMER, G. & ZITVOGEL, L. 2018. Gut microbiome influences efficacy of PD-1-based immunotherapy against epithelial tumors. *Science,* 359**,** 91-97.

ROYAL, R. E., LEVY, C., TURNER, K., MATHUR, A., HUGHES, M., KAMMULA, U. S., SHERRY, R. M., TOPALIAN, S. L., YANG, J. C., LOWY, I. & ROSENBERG, S. A. 2010. Phase 2 trial of single agent Ipilimumab (anti-CTLA-4) for locally advanced or metastatic pancreatic adenocarcinoma. *J Immunother,* 33**,** 828-33.

RYAN, D. P., HONG, T. S. & BARDEESY, N. 2014. Pancreatic adenocarcinoma. *N Engl J Med,* 371**,** 1039-49.

SHONO, Y., DOCAMPO, M. D., PELED, J. U., PEROBELLI, S. M., VELARDI, E., TSAI, J. J., SLINGERLAND, A. E., SMITH, O. M., YOUNG, L. F., GUPTA, J., LIEBERMAN, S. R., JAY, H. V., AHR, K. F., POROSNICU RODRIGUEZ, K. A., XU, K., CALARFIORE, M., POECK, H., CABALLERO, S., DEVLIN, S. M., RAPAPORT, F., DUDAKOV, J. A., HANASH, A. M., GYURKOCZA, B., MURPHY, G. F., GOMES, C., LIU, C., MOSS, E. L., FALCONER, S. B.,

BHATT, A. S., TAUR, Y., PAMER, E. G., VAN DEN BRINK, M. R. M. & JENQ, R. R. 2016. Increased GVHD-related mortality with broad-spectrum antibiotic use after allogeneic hematopoietic stem cell transplantation in human patients and mice. *Sci Transl Med,* 8**,** 339ra71.

SIVAN, A., CORRALES, L., HUBERT, N., WILLIAMS, J. B., AQUINO-MICHAELS, K., EARLEY, Z. M., BENYAMIN, F. W., LEI, Y. M., JABRI, B., ALEGRE, M. L., CHANG, E. B. & GAJEWSKI, T. F. 2015. Commensal Bifidobacterium promotes antitumor immunity and facilitates anti-PD-L1 efficacy. *Science,* 350**,** 1084-9.

STOFFEL, E. M., MCKERNIN, S. E., BRAND, R., CANTO, M., GOGGINS, M., MORAVEK, C., NAGARAJAN, A., PETERSEN, G. M., SIMEONE, D. M., YURGELUN, M. & KHORANA, A. A. 2019. Evaluating Susceptibility to Pancreatic Cancer: ASCO Provisional Clinical Opinion. *J Clin Oncol,* 37**,** 153-164.

STROMNES, I. M., BROCKENBROUGH, J. S., IZERADJENE, K., CARLSON, M. A., CUEVAS, C., SIMMONS, R. M., GREENBERG, P. D. & HINGORANI, S. R. 2014. Targeted depletion of an MDSC subset unmasks pancreatic ductal adenocarcinoma to adaptive immunity. *Gut,* 63**,** 1769-81.

SWIDNICKA-SIERGIEJKO, A. K., GOMEZ-CHOU, S. B., CRUZ-MONSERRATE, Z., DENG, D., LIU, Y., HUANG, H., JI, B., AZIZIAN, N., DANILUK, J., LU, W., WANG, H., MAITRA, A. & LOGSDON, C. D. 2017. Chronic inflammation initiates multiple forms of K-Ras-independent mouse pancreatic cancer in the absence of TP53. *Oncogene,* 36**,** 3149-3158.

TAKAORI, K., HRUBAN, R. H., MAITRA, A. & TANIGAWA, N. 2004. Pancreatic intraepithelial neoplasia. *Pancreas,* 28**,** 257-62.

VON HOFF, D. D., ERVIN, T., ARENA, F. P., CHIOREAN, E. G., INFANTE, J., MOORE, M., SEAY, T., TJULANDIN, S. A., MA, W. W., SALEH, M. N., HARRIS, M., RENI, M., DOWDEN, S., LAHERU, D., BAHARY, N., RAMANATHAN, R. K., TABERNERO, J., HIDALGO, M., GOLDSTEIN, D., VAN CUTSEM, E., WEI, X., IGLESIAS, J. & RENSCHLER, M. F. 2013. Increased survival in pancreatic cancer with nab-paclitaxel plus gemcitabine. *N Engl J Med,* 369**,** 1691-703.

WANG, Y., WIESNOSKI, D. H., HELMINK, B. A., GOPALAKRISHNAN, V., CHOI, K., DUPONT, H. L., JIANG, Z. D., ABU-SBEIH, H., SANCHEZ, C. A., CHANG, C. C., PARRA, E. R., FRANCISCO-CRUZ, A., RAJU, G. S., STROEHLEIN, J. R., CAMPBELL, M. T., GAO, J., SUBUDHI, S. K., MARU, D. M., BLANDO, J. M., LAZAR, A. J., ALLISON, J. P., SHARMA, P., TETZLAFF, M. T., WARGO, J. A. & JENQ, R. R. 2018. Fecal microbiota transplantation for refractory immune checkpoint inhibitor-associated colitis. *Nat Med,* 24**,** 1804-1808.

WEI, D., WANG, L., YAN, Y., JIA, Z., GAGEA, M., LI, Z., ZUO, X., KONG, X., HUANG, S. & XIE, K. 2016. KLF4 Is Essential for Induction of Cellular Identity Change and Acinar-to-Ductal Reprogramming during Early Pancreatic Carcinogenesis. *Cancer Cell,* 29**,** 324-338.

WINOGRAD, R., BYRNE, K. T., EVANS, R. A., ODORIZZI, P. M., MEYER, A. R., BAJOR, D. L., CLENDENIN, C., STANGER, B. Z., FURTH, E. E., WHERRY, E. J. & VONDERHEIDE, R. H. 2015. Induction of T-cell Immunity Overcomes Complete Resistance to PD-1 and CTLA-4 Blockade and Improves Survival in Pancreatic Carcinoma. *Cancer Immunol Res,* 3**,** 399-411.

YING, H., KIMMELMAN, A. C., LYSSIOTIS, C. A., HUA, S., CHU, G. C., FLETCHER-SANANIKONE, E., LOCASALE, J. W., SON, J., ZHANG, H., COLOFF, J. L., YAN, H., WANG, W., CHEN, S., VIALE, A., ZHENG, H., PAIK, J. H., LIM, C., GUIMARAES, A. R., MARTIN, E. S., CHANG, J., HEZEL,

A. F., PERRY, S. R., HU, J., GAN, B., XIAO, Y., ASARA, J. M., WEISSLEDER, R., WANG, Y. A., CHIN, L., CANTLEY, L. C. & DEPINHO, R. A. 2012. Oncogenic Kras maintains pancreatic tumors through regulation of anabolic glucose metabolism. *Cell,* 149**,** 656-70.

ZHANG, Y., VELEZ-DELGADO, A., MATHEW, E., LI, D., MENDEZ, F. M., FLANNAGAN, K., RHIM, A. D., SIMEONE, D. M., BEATTY, G. L. & PASCA DI MAGLIANO, M. 2017. Myeloid cells are required for PD-1/PD-L1 checkpoint activation and the establishment of an immunosuppressive environment in pancreatic cancer. *Gut,* 66**,** 124-136.

ZHANG, Y., YAN, W., MATHEW, E., BEDNAR, F., WAN, S., COLLINS, M. A., EVANS, R. A., WELLING, T. H., VONDERHEIDE, R. H. & DI MAGLIANO, M. P. 2014. CD4+ T lymphocyte ablation prevents pancreatic carcinogenesis in mice. *Cancer Immunol Res,* 2**,** 423-35.

VITA

Krishnan K. Mahadevan was born in Chennai, India in March 1990. After completing high school in 2007 from St. Patrick higher secondary school, he pursued his medical degree from Jawaharlal institute of post graduate medical training and research (JIPMER). Krishnan graduated with honors from his medical school and subsequently worked as a research fellow at Massachusetts General Hospital in Boston before joining The University of Texas MD Anderson Cancer Center UTHealth Graduate School of Biomedical Sciences. Krishnan joined the lab of Dr. Raghu Kalluri to pursue his PhD dissertation project to understand the role of immune system and pancreatitis in pancreatic cancer progression.